CHANNEL AVULSION PROCESSES ON THE LOWER BRAZOS RIVER, TEXAS

TWDB Final Report 0904830968

İnci Güneralp[1], Billy U. Hales[2], Anthony M. Filippi[1]

[1] Associate Professor, Department of Geography, Texas A&M University

[2] Ph.D. Student, Department of Geography, Texas A&M University

CHANNEL AVULSION PROCESSES ON THE LOWER BRAZOS RIVER, TEXAS

TWDB Final Report 0904830968

İnci Güneralp[1], Billy U. Hales[2], Anthony M. Filippi[1]

[1] Associate Professor, Department of Geography, Texas A&M University

[2] Ph.D. Student, Department of Geography, Texas A&M University

CONTENT **Page**

1. BACKGROUND

An avulsion is a process that results in relatively sudden abandonment of a river channel for a new course at a lower level in the floodplain (Allan 1965; Knighton, 1998). Avulsions differ in their size and frequency (Figure 1.1). The governing physical processes of different type of avulsions can be different. They may result from either abrupt channel shifts or gradual channel migration; nevertheless, these processes are often intertwined (Knighton, 1998). Thus, all avulsion types need be considered together under the overall process of channel change.

Valley-scale—also called *large-scale*—avulsions create new channels that extend over large distances downstream on the floodplain. These avulsions are also called '*regional*' avulsions, as discussed by Slingerland and Smith (2004). Valley-scale avulsions tend to occur at intervals of hundreds to thousands of years and typically and form alluvial ridges that create steep gradients away from the channel (Makaske et al. 2002; Slingerland and Smith 2004; Tooth et al. 2007). Geomorphologic and geologic history of a floodplain are important factors influencing the occurrence of valley-scale avulsions (Collins and Montgomery 2011). For example, deltas and alluvial fans form as a result of many avulsions through time.

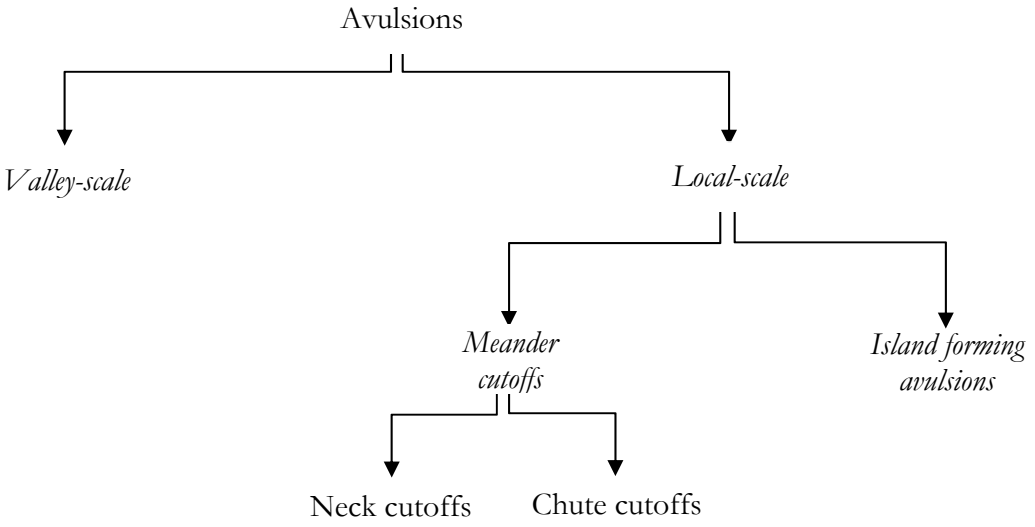

Figure 1.1. Different types of channel avulsion (Stouthamer 2001)

Due to their association with abrupt changes in the course of the river, valley-scale avulsions have hydrologic, geomorphic, ecological, and engineering implications. Avulsions play an essential role in floodplain evolution, alluvial stratigraphy and architecture as well as river channel planform evolution. The stratigraphy and alluvial architecture in southeast Texas point

to the dominancy of avulsions throughout the Quaternary (Waters and Nordt 1995, Aslan and Blum 1999, Aslan et al. 2005, Blum and Aslan 2006, Taha and Anderson 2008). Avulsion have been increasingly seen as one of the dominant processes of the evolution of alluvial deposits including those in the floodplains and deltas (Aslan et al. 2005, Jones and Schumm1999, Hudson et al. 2008, Slingerland and Smith 2004, Blum and Aslan 2006). Nevertheless, valley-scale avulsions have also important implications on the surface morphology and on current forms, processes, and evolution via modifications on the water and sediment fluxes (Blum and Aslan 2006, Sylvia and Galloway 2006).

Island-forming avulsions tend to be at local-scale and can occur regularly during floods and on forested islands in floodplains. On the other hand, *meander cutoffs* are a form of local avulsions that create new river channels relatively small in size. These types of avulsions are a direct result of gradual bend migration. They are spatially and temporally common in actively-migrating meandering rivers. They occur as natural and regular responses to lengthening of the channel and decreasing channel slope resulting from river-channel migration (Allen 1965, Hickin and Nanson 1975, Hooke 1995, Erskine et al. 1992, Bridge et al. 1986). These types of avulsions are classified as neck and chute cutoffs. Neck and chute cutoffs create channels between adjacent meander bends, and as a result, they have a local impact via modification of a relatively small area of the floodplain. Meander cutoffs typically occur over years to decades. Although they are local, the impact of meander cutoffs can be significant in large streams because of the scaling of the river bends with the size of a stream (Leopold and Wolman 1960)

1.1. Valley-scale avulsions

Valley-scale avulsions are also called regional- or floodplain-scale avulsions (Figure 1.1). In spite of their role in channel change and floodplain evolution, and thus, their importance for river hazards and management, the conditions necessary and sufficient for causing river avulsions are not fully understand and are still under much debate (Aslan et al. 2005; Phillips 2009; Slingerland and Smith 1998).

Large-scale avulsions occur in two steps. First, the conditions develop towards an avulsion threshold. Then, a triggering event such as a flood forces the river towards a stability threshold (Jones and Schumm 1999). In Figure 1.2, Line 1 shows increasing propensity of a channel to avulse as it approaches the avulsion threshold, which indicates certainty of avulsion at time B. This trajectory is governed by both system instability and time. Superimposed on line 1 are vertical lines representing flood magnitude, which could be construed as an expression of

system instability. The large flood at time A causes avulsion; had it not occurred, smaller floods would lead to avulsion between times A and B. Note that even large floods do not cause avulsion until the line representing channel instability approaches the avulsion threshold. This makes the idiom, *'The straw that broke the camel's back…'*, an appropriate simplification when describing avulsion. This idea is general, and not tailored to an environment. The shape, curvature and slope of line 1 will vary for different rivers, as well the magnitude and number of floods required. The concept is based on Schumm (1977).

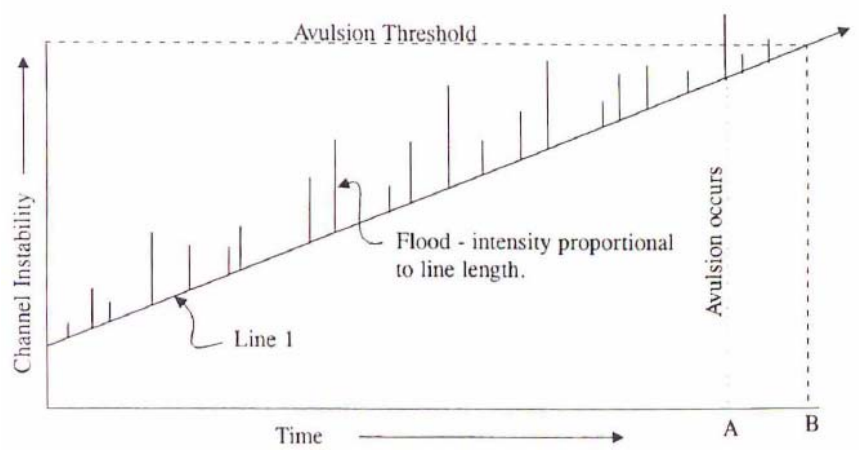

Figure 1.2. Approach to avulsion threshold. Probability of the occurrence of avulsions increases over time (*after* Jones and Schumm 1999).

Branching off from the idea of stability discussed in Jones and Schumm (1999), Phillips (2007a) takes a nonlinear dynamical systems approach to explain the occurrence of valley-scale avulsions and considers them as local perturbations to a fluvial system. The effects of such local perturbations depend on the dynamical stability of the system as it determines whether the effects of small disturbances are going to be damped or not. If they are damped the state before the disturbance will be recovered, a hallmark of a stable system. Alternatively, the effects may be amplified, and the system will change states, a hallmark of system instability. However, Phillips (2007b) adds that another condition, system metastability, is possible. In this case, the effects of a perturbation persist without significant amplification, but the system tends to evolve to a new stable state. This approach, in agreement with Jones and Schumm (1999), shows that the probability of the occurrence for avulsions increases over time (Figure 1.2).

Determining large-scale avulsion thresholds and the factors leading to avulsions will help mitigation of river hazards associated with avulsions. Three general factors are considered to

contribute to the process of avulsion: gradient advantage, channel capacity limitations, and channel blockages (Aslan 2005). Most studies highlight gradient advantages as one of the most important underlying driving mechanisms for avulsion (Slingerland and Smith 1998). Extreme peak discharges, ice jams, etc. are considered as critical factors for initiating an avulsion (Smith et al., 1989; Jones and Schumm, 1999; Törnqvist and Bridge, 2002). However, the prediction of avulsions in terms of when and where they occur is impossible due to the uncertainty involved in the process. Past research suggest that avulsions are strongly associated with aggrading floodplains (Slingerland and Smith, 2004). Fluvial aggradation, fault movement, climate change, and sea level rise are seen as conditions more useful for predicting the locations of future avulsions. These processes are also considered as the controllers of the style of avulsion (Törnqvist, 1994; Aslan and Blum, 1999; Morozovo and Smith, 1999; Peakall et al., 2000; Gibling et al., 2005; Maynard, 2006). The studies on avulsions on the Lower Brazos River, Texas (Taha and Anderson, 2008) and Rhine-Meuse delta (Stouthamer and Berendson, 2007), for example, indicate that avulsion locations are nonrandom and can be related to allogenic factors of sea level rise, climate change, and human influences.

Crevasse splays

Avulsions also leave their mark on the sedimentary configuration of a floodplain in the form of crevasse splays. Upon the triggering of an avulsion, most likely during a major flood, crevasse splays commonly form as consequence of a breach in the natural levee or alluvial ridge surrounding a river (Slingerland and Smith 2004). Defined by a coarsening upward sequence of suspended load to bed load per breaching event, the sandy crevasse splay evolves in multiple stages and forms a complex network of channels that advance the coverage of the deposit by hydrologic and sediment transport contributions from the main stream (Smith et al. 1989) (Figure 1.3).

Figure 1.3. Example crevasse splay from the LBR.

Smith et al. (1989) recorded three distinctive stages in the evolution of a crevasse splay, and these stages of evolution are contingent on the amount of hydrologic and sediment contribution from the avulsed trunk (crevasse) at the main channel. Stages I and II represent an increase in complexity for the geometry of a crevasse splay, and Stage III represents a simplification of that structure. The case of the crevasse splay is a microcosm of the process of avulsion itself, as they evolve by a continuous process of avulsing and reoccupation of micro-channels within the splay itself (Smith et al. 1989).

The presence of crevasse splays on the landscape can indicate two things: that the given channel has—or has recently lost—the competence to carry sand-sized particles as bedload and is susceptible to avulsion by annexation (Slingerland and Smith 2004). Often viewed a failed avulsion, a crevasse splay, over time, can mature and build its own natural levees—becoming an ideal alternate channel in case the crevasse or trunk of the splay is opened again (Slingerland and Smith 2004). However, the often-times case is that the presence of crevasse splays actually can reduce the probability of avulsions because their geometries often create a lower cross-valley slope (Aslan et al. 2005, Slingerland and Smith 2004). A repeated successful rejoining of a crevasse-splay channel to its parent channel is often considered a sign of anastomosis (Slingerland and Smith 2004). Here, we will map crevasse splays with the intent of assessing setup for avulsion as well as a historical record of past avulsions.

1.2. Local-scale avulsions

Island forming (anabranching) avulsions

Anabranching river systems and avulsions are closely related. Anastomosing rivers often form in low-energy conditions near a local base level. Avulsions are the mechanism for creating anastomosing channels (Makaske, 2001). Avulsions create bypasses; however, the by-passed older channel segment still persists. Alternatively, diverted avulsive flow bifurcates, resulting in formation of multiple channels in the floodplain. Sometimes both bifurcated avulsive flow and the by-passed channel segment may be present in the same system (Makaske, 2001). Nanson and Knighton (1996) classify the processes that produce multiple-channel, anabranching patterns as avulsion-based processes and accretion-based ones. Avulsion-based anabranching channels occur when a river scours new channels into the floodplain or reoccupy relict channels (i.e., paleo-channels, floodplain sloughs) and switch back and forth between them and reconnect with the main channel farther downstream (Collins et al. 2003, Collins et al. 2012). These processes typically create forested islands between channels. The accretion-based anabranching patterns include channel extension into floodbasins that represents one of the avulsion styles recognized by other workers (Slingerland and Smith, 2004; Blum and Aslan, 2006). Island-forming avulsions are relatively common in watersheds and floodplains dominated by aged forests. These aged forests can generate large log jams that induce avulsions (Abbe and Montgomery 1996, Collins et al. 2012, Phillips 2012).

Channel migration and meander cutoffs

Meander cutoffs are bend-to-multi-bend scale avulsions on the channel. Meander cutoffs include neck and chute cutoffs. Although both are related to the gradual migration of river planforms (Figure 1.1), avulsion processes resulting in neck and chute cutoffs are different from each other; thus, development of neck and chute cutoffs depends on different factors and spatial and environmental conditions. Both strongly affect the planimetric morphology and the spatiotemporal evolution of this morphology. Cutoffs determine the formation of side channel (also called secondary channels) complexes, abandoned channels, oxbow lakes, also called horseshoe lakes, and chute channels on floodplains. The cutoff channels created by the dynamics of meandering rivers help maintain the morphological complexity of meandering river channels and floodplain landscapes (Amoros and Bornette, 2002; Ward et al., 2002).

Gradual migration of meander bends results from the erosion of the banks on the outside of meander bends. Lateral accretion or deposition of sediment occurs simultaneously on the

inside of channel bends (Figure 1.1). Channel migration is dependent on the stream flow and the erodibility of soils on the meander cutbanks (Nanson and Croke, 1992). Bank erosion rate typically increases with increasing discharge, velocity and duration of stream flows exceeding a threshold condition. For instance, channel migration rates are generally greatest during floods (Konrad, 2012).

The knowledge on the physical processes leading to the occurrence of meander cutoffs is limited due to their infrequent nature and the wide range of hydro-geomorphic conditions governing the patterns and processes of meandering-river floodplains (Hooke 1995; 2004). During meander migration, meander bends elongate and increase their amplitude and sinuosity. The neck of an elongated meander may become increasingly narrower due to progressive migration of the upstream and downstream bends and double-back upon itself, leading to the formation of a *neck cutoff* (Figures 1.4-1.5).

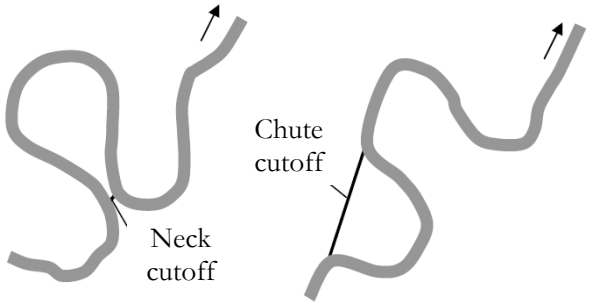

Figure 1.4. Neck and chute cutoffs (*after* Crosato, 2008)

Two major processes govern the formation of neck cutoffs:

1) Progressive migration of an elongated bend via bank erosion leading to a breach and final breaching can occur in a low-magnitude event (Hooke 1995); and
2) Incision of a very narrow meander neck during a high flow (Allen 1965; Erskine *et al.* 1992). Cutoff process is generally defined as a neck cutoff when the meander neck is shorter than one channel width.

Figure 1.5. The formation of a neck cutoff and an oxbow lake on the Lower Brazos River (LBR), Texas [29°15'38.03"N, 95°34'5.88"W].

Neck-cutoff processes are influenced by:

1) The evolutionary stage of a meandering channel.
2) The spatial structure of the upstream and downstream channel morphology, i.e., spatially-distributed planimetric geometry or curvature, (Constantine and Dunne, 2010). Planimetric morphology of meander bends play an important role on the spatial and temporal characteristics of the migration rates, and thus the location and the timing of the cutoffs.
3) Migration pattern characteristics both in *bend scale* and *meander-series scale*. Particularly, the spatial distribution of the migration rates is critical (Güneralp and Rhoads 2009, 2010, Howard 1992, 1996, Camporeale et al. 2005, Sun et al. 1996).
4) Floodplain environment (i.e., spatial and temporal heterogeneity in land use-land cover, soil characteristics, presence of clay plugs (Hudson and Kesel 2000, Güneralp and Rhoads 2011), presence and frequency of channel confluences and their orientation, etc.).

On the other hand, a *chute cutoff* develops through the incision of a new channel across the neck of a meander bend (Figures 1.4, 1.6). Chute cutoffs occur due to one of the three major mechanisms. *Firstly*, chute cutoffs commonly develop in meander bends with scroll bar (ridge and swale) topography (Bridge *et al.* 1986; Hickin and Nanson 1975) or in the presence of remnants of old abandoned channels on the floodplain. During very high flows, where the local water heights exceed bank elevations (i.e., overbank flows), swales and remnants of old channels can provide flow-routing paths and channelize the overbank flow. The swale or the old channel providing a flow-routing path may gradually enlarge due to water erosion, and it may eventually capture most of the main channel flow and form a chute channel.

Secondly, chute cutoffs can also develop during overbank flows that are sufficient enough to concentrate a boundary shear stress capable of cutting a new shallow side channel across the neck of a meander bend (Hooke 1995; Lewis and Lewin 1983). In this case, cutoff channels develop through the gradual enlargement of an initially shallow area. High flows can cause an increase in the water stage upstream of a meander bend leading to a steepened water-surface gradient between the upstream and downstream ends of the bend. The steepened water-surface gradient may result from a temporal lag in the adjustment of the channel bed to the increases in water height (Joglekar 1971). Alternatively, a steepened water-surface gradient may also be achieved by an unexpected obstacle at the river bed such as large channel bars, masses of bank failures or woody debris (Johnson and Paynter 1967). The steepened water gradient directs the river flow across the lowest parts of the floodplain or to the remnants of old channels. High flow velocities may be reached at the confluence of the main-channel flow and the flow concentrated in the depressions at the downstream end of the bend leading to headcutting (i.e., progression up-river direction) (Gay et al. 1998; Joglekar 1971). There may be multiple headcuts at the beginning; however, over time, one headcut becomes dominant, likely because of suitable erodibility conditions resulting from the variability in soil type and vegetation cover (Gay et al. 1998). This new channel may grow and start capturing the river flow. When it is large enough to capture the entire river flow, the new chute channel across the neck becomes the main channel by short-circuiting the primary channel and links the upstream and downstream portions of the meander bend. Chute cutoff-dominated meandering rivers have lower sinuosity than do neck cutoff-dominated rivers.

Thirdly, chute cutoffs may occur along large rivers with uniform floodplain topography via the downstream extension of an embayment at the upstream part of a meander bend (Constantine et al. 2010). Embayments on meander bends seem develop as a result of localized bank erosion along the cutbanks of the channel subject to chute cutoff. Valley slope, the structure of floodplain vegetation, and the nature and quantity of sediment in transport during a flood all strongly influence the occurrence of this type of chute cutoff. Embayments seem to have a tendency to form just upstream of the inflection point of the meander undergoing cutoff (Constantine et al. 2010), at a location where channel curvature is greatest. An embayment can develop and extend by erosion during high flows sufficient to entrain the floodplain sediment until it fully cuts through the meander neck and forms a chute channel.

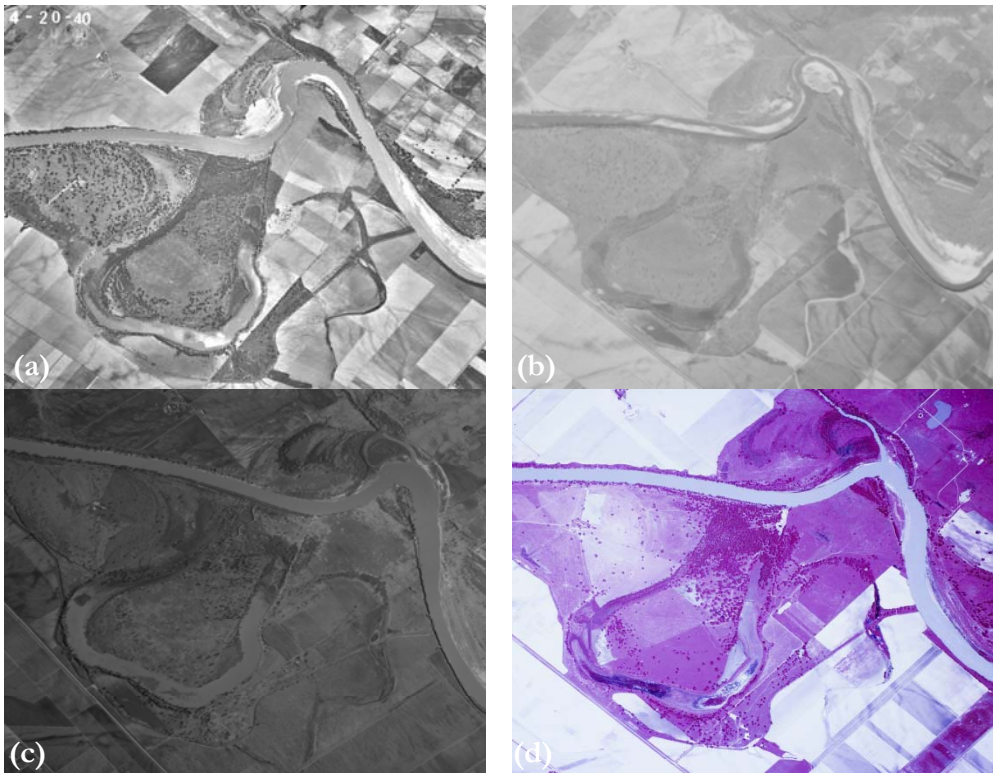

Figure 1.6. Spatiotemporal evolution of a chute-cutoff channel on the LBR: (a) 1940, (b) 1953, (c) 1960, (d) 1973 aerial photographs.

Cutoffs are often the result of flow encountering more resistant material or shear stress reduction due to flattening of energy slope. Recent laboratory experiments demonstrated that channel bars may initiate chute cutoffs (Peakall et al., 2007). Within a heterogeneous floodplain, sedimentological differences in the resistance of bank sediment to erosion are also going to distort meander shapes. Ikeda (1989) thus found channel-planform migration rates to be strongly influenced by the presence and distribution of cohesive bank sediments. Similarly, Hooke (1980) noted the importance of the silt and clay fraction in bank resistance. Friedkin (1945) for instance, working on the Mississippi River, noted the importance of the high silt/clay fraction within old channels in resisting erosion. Meander directions are also likely to be deflected where freely-meandering bends meet valley sides. Also, rate of migration varies along a river in the presence of an increase or a decrease in stream power. Hooke (1980) obtained a regression equation between migration rate of meander loops and upstream drainage area.

In terms of cutoff processes, avulsions occur generally at bends, forming as a result of superelevation on the outside of banks during flood conditions, and there areas are the first point of overspilling onto the floodplain. There is a tendency for avulsions to exploit minor

channels, or old courses, which enter the main channel upstream or downstream of meander apex where floodplain elevation is lower.

A cutoff meander bend, produced by either neck- or chute-cutoff processes, is not abandoned immediately; it stays connected to the main channel fully or partially until sediment deposition closes off its entrance and exit creating an oxbow lake (Figure 1.5). The infilling of a cut-off channel is controlled by the character of the sediment transported during high flows, the magnitude and frequency of these flows, and the distance between the abandoned and present channels (Erskine et al. 1992). Oxbow lakes are generally filled with mostly fine-sediment deposits and form sediment plugs (also called clay plugs due to the higher content of fine material in deposits), which are highly resistant to erosion (Hooke 2004). Sediment plugs leave the signature of a former channel position on the floodplain, and, that is why they are also called meander scars. Meander scars are generally discernable due to their distinct soil characteristics and the patterns of colonized vegetation around them.

Fully or partially abandoned channels formed by cutoff processes, the remnants of old channels, and meander scars are important components of low-land alluvial floodplains. They create a segregated and complicated sedimentary floodplain environment. Heterogeneous mosaics of differential floodplain erodibility also result from the interactions between the processes of river meandering and other landscape patterns and processes such as vegetation dynamics and human activities (Gilvear et al. 2000, Micheli et al. 2004; Micheli and Larsen 2011). Degree of this heterogeneity influences the spatial patterns of planform evolution by causing variability in migration rates as well as by affecting spatial and temporal occurrence of cutoffs (Gilvear et al. 2000, Hudson and Kesel 2006, Güneralp and Rhoads 2011). Certain spatial scales and magnitudes of erosional heterogeneity promote the occurrence of neck cutoffs in shorter time scales and a higher degree of irregularity in planform morphology compared to homogeneous floodplain environments (Güneralp and Rhoads, 2011).

1.3. Avulsions as river hazards

Both valley- and local-scale avulsions pose an important concern for river hazards and thus river management. They are difficult to predict and pose a hazard to regions developed in a floodplain, making the implementation of successful floodplain management difficult to achieve (Phillips 2009). Understanding the avulsion hazards and the natural processes leading to these hazards are necessary to protect people, biodiversity, and infrastructure and develop sustainable floodplain management practices (Arnaud-Fassetta et al. 2009).

One of the biggest concerns—with valley-scale avulsions especially—is flooding. Typically, to assess flood hazards, FEMA's flood zones and floodways are used. However, these maps do not characterize areas susceptible to avulsions and bank erosion and channel migration either within or outside of the areas prone to flooding. Thus, many flood-zone and floodway boundaries are not reliable for long periods of time, and they fall short in taking into account the river hazards associated with abrupt and gradual changes in the river courses. Given that the projections of climate change and population in Texas, U.S.A. predict significant changes in hydrologic regime with more extreme events of flooding and an 82%-increase in population by 2060 (TWDB 2012), understanding the potential changes in the rivers of Texas draining the coastal plains becomes critical.

The channel migration is a hazardous process. It also raises societal concerns due to the hazards associated with bank erosion and channel change. Migrating channels pose a threat to infrastructure, homes, etc. Nevertheless, there are beneficial consequences of channel migration. The migration process crates new habitats (oxbow lakes, fresh sediment deposits on the point bars, woody debris in the channel recruited during cutbank erosion) by migration processes.

The patterns of historical channel migration may not predict the spatial extent of the channel migration in the future. For example, channel migration can occur in areas on the floodplain that the channel had not occupied historically (O'Connor et al. 2003). In addition, environmental changes are likely to influence the patterns of channel migrations. Channels may migrate outside the historical migration zones in response to the changes in the environmental conditions. These changes can result from human activities such as agriculture, urbanization and various types of water- and land-management practices (e.g., damming, irrigation, riparian forest management) as well as climatic conditions (Meybeck et al. 2003, Karl et al. 2009, Vörösmarty et al. 2010). These environmental stressors are predicted to cause rapid changes in flow and sediment regimes, and then change the dynamics of river channels, and pose profound threats to these river systems and ecosystems (Richter et al. 1997; Palmer et al. 2009; Pinter et al. 2010).

2. PURPOSE OF THE STUDY

The purpose of this study is to examine the avulsion potential on the Lower Brazos River (LBR). For this purpose, we examine the setup potential of both the valley-scale and local-scale avulsions. In examining the potential of valley-scale avulsions, which will result in the formation of new channels and/or reoccupation of relict channels, floodplain sloughs, or paleo channels, we focus on the concept of gradient advantage. In examining the local-scale avulsions, namely, meander cutoffs and those that can results from channel migration, we analyze the migration of the channel over a period of 1910-2010. We examine historical and future potential channel changes with the aim of determining both gradual changes in the river channel course due to channel migration and abrupt changes due to chute and neck cutoffs.

3. STUDY REACH

3.1. The Lower Brazos River (LBR)

We examine the avulsions on the LBR, Texas (Figure 3.1). The Brazos River is the largest river in Texas with a length of >1900 km. It extends from its headwaters in New Mexico to the Gulf of Mexico at Freeport and has a drainage area of ~118,000 km^2. The LBR is located in the coastal plains of Texas, which are characterized by a humid subtropical climate. The mean annual precipitation ranges from 750 to 1300 mm/yr. Watersheds in the region are dominated by agricultural land uses, mainly grazing (Phillips, 2007b).

The LBR experienced several episodes of cutting, filling, channel migration, extension, and contraction related to Quaternary sea level and climate changes (Alford and Holmes, 1985; Blum et al., 1995; Waters and Nordt, 1995; Morton et al., 1996). Most of the LBR is incised and has a larger channel capacity relative to its discharge, accounting for the less frequent overbank flow. Nevertheless, mean daily flows at or above flood stage occur, on average, more than three days per year (Phillips, 2011). The Brazos River is a mixed load system (Schumm 1977) and, on average, yields 9.9 ha m^3/yr of suspended load and 0.9 ha m^3/yr of bedload to the Gulf of Mexico (Paine and Morton 1989). This makes it the river with the second-highest sediment yield of all rivers in Texas and the highest yield in terms of suspended load (Milliman and Syvitski 1992)..

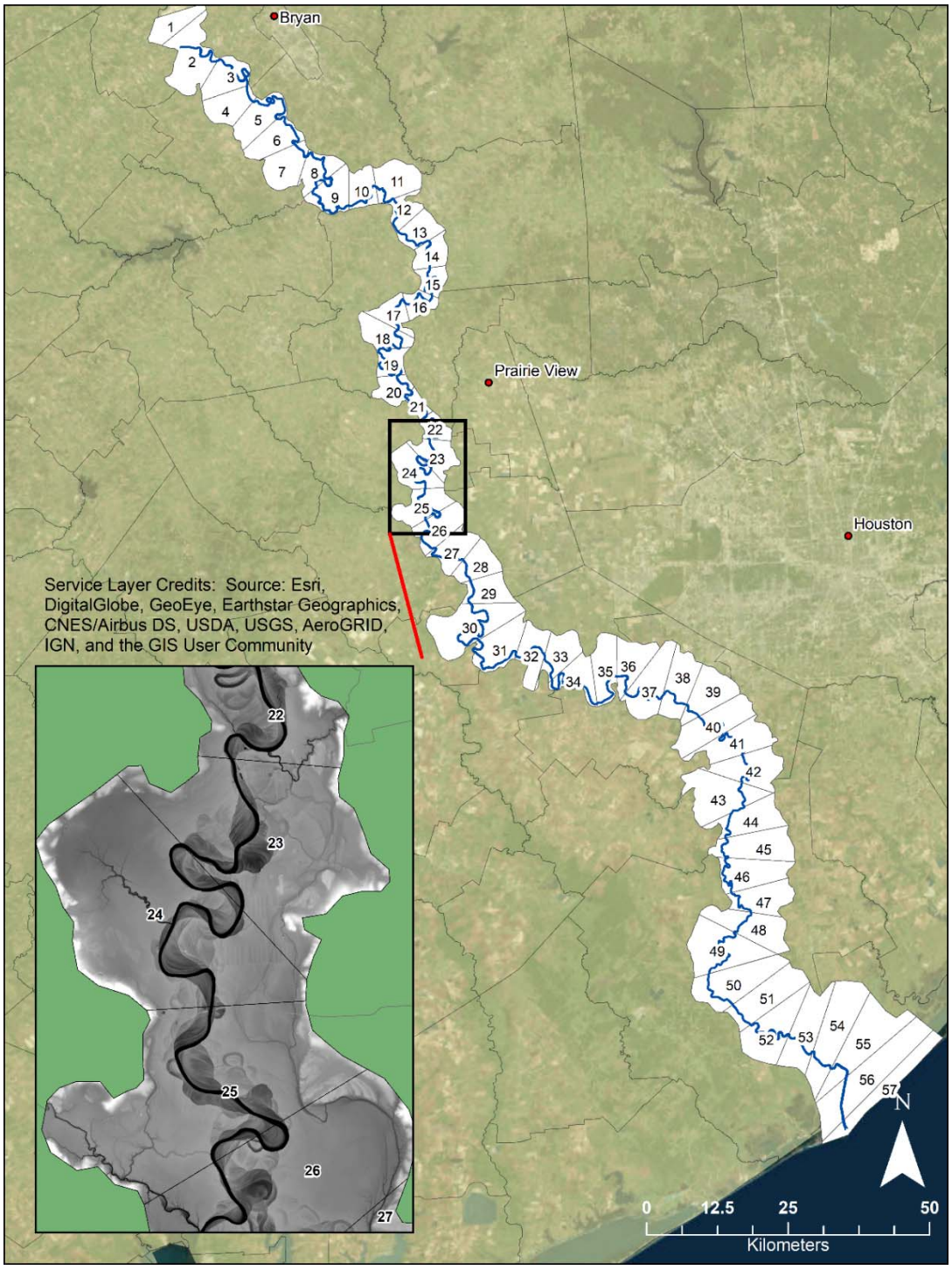

Figure 3.1. The study area on the Lower Brazos River (LBR), Texas. The LBR is characterized by a single-thread channel with many oxbow lakes, paleo-channels, sloughs, tributary avulsive channels. The study area begins at the bridge on the State Highway (SH) 21 near Bryan/College Station and ends at the SH 36 close the Gulf of Mexico.

The dominant planform pattern of the LBR is meandering. The LBR is characterized by both historical and recent channel migrations on relatively wide floodplains with varying degrees of connectivity between the river channel and the floodplain (Phillips, 2007b). Floodplain presents geomorphic landforms typical of dynamic meandering channels, including oxbow lakes resulting from neck cutoffs, chute cutoffs, meander scars, and scrolls and a range of avulsive channels (Figure 3.2). The average floodplain width is ~8.7 km and ranges approximately between 2.3 km and 24 km. Initially, the valley width decreases slightly and then gradually increases starting at approximately midway from the Gulf of Mexico, and reaches to its widest form toward the Gulf (Figure 3.3).

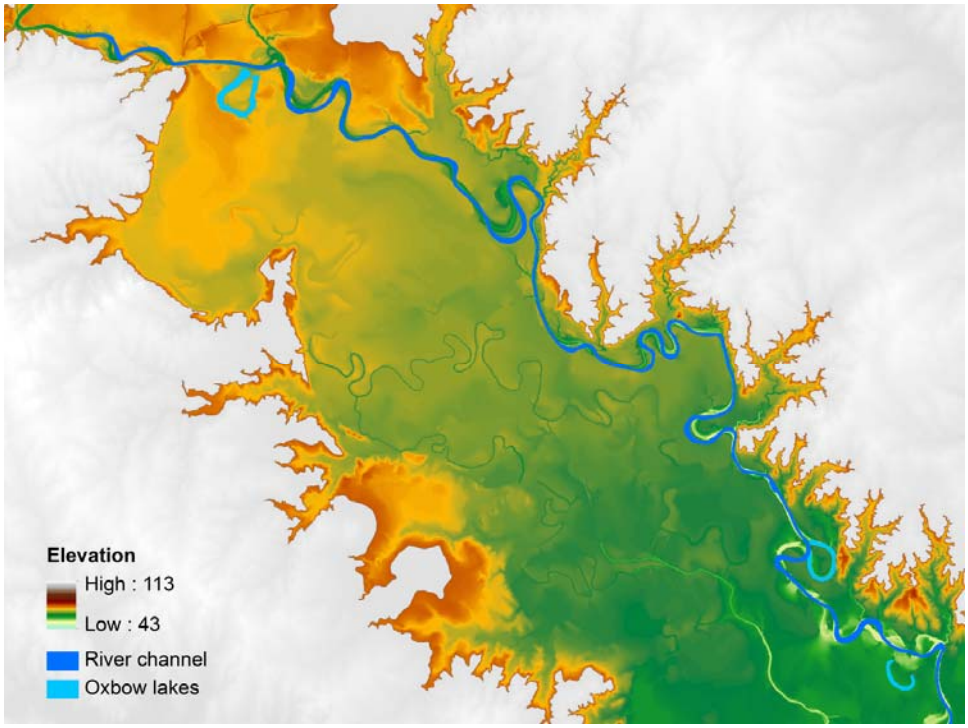

Figure 3.2. A section of the floodplain on the LBR. Floodplain boundary of this section is located within meandering incised valley fill zone on the LBR, Texas. The river is characterized by a single-thread channel; many oxbow lakes and relic channels are present. Elevation data shown are obtained from the U.S. Geological Survey (USGS) National Elevation Dataset (NED) (cell size = 10 m).

The average channel width (W) is 126 m, with a range from 75 m to 375 m. The average meander bend length is about 1100 m (corresponds to ~10W). The channel substrate ranges from sandy to muddy (Phillips, 2007b). The bed material is highly mobile; however, in certain areas, bedrock, which is typically composed of cohesive clayey pre-Quaternary sediments, is exposed or covered by a thin (<1 m) alluvial sediment layer (Phillips 2007b)

In this study, we focus on the section of the LBR between the bridge on the State Highway (SH) 21 near Bryan/College Station and the SH 36 close the Gulf of Mexico (Figure 3.1).

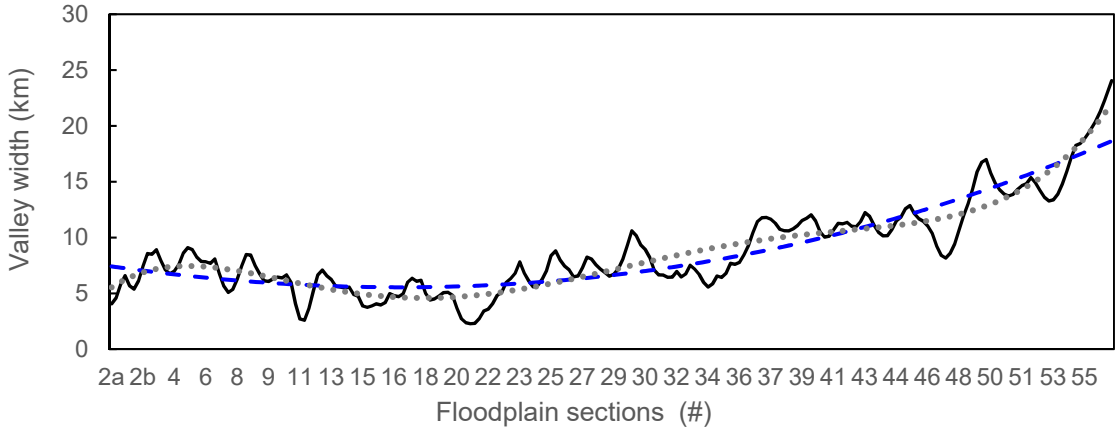

Figure 3.2. Variability of valley width in the LBR, Texas. The river is characterized by a single-thread channel; many oxbow lakes and relic channels are present. Horizontal axis presents the floodplain sections from #2a (the most upstream) to #56 (the closest to the Gulf of Mexico). The gray dotted line show a six-order polynomial fit ($y = -2E\text{-}12x^6 + 3E\text{-}09x^5 - 1E\text{-}06x^4 + 0.0002x^3 - 0.0119x^2 + 0.2872x + 5.2575$, $R^2 = 0.8728$) and blue dashed lines shows the third-order polynomial fit ($y = 3E\text{-}07x^3 + 0.0004x^2 - 0.0576x + 7.4722$, $R^2 = 0.823$) to the valley width distribution.

3.2. Zonation of the LBR based on River Styles

Phillips (2007b) examined the LBR based on the *River Styles* framework developed by Brierly and Fryirs (2005) (Table 3.1). The *River Styles* framework is not a classification, rather it is dynamic approach to river characterization. As opposed to a classical a categorical classification scheme, which only considers static conditions, thus, assumes a stable system, this framework aims to incorporate evolutionary characteristics of the river system under study. Therefore, it allows for assessing the linkages of multiple processes governing in a spatial and temporal and holistic context (Brierly et al., 2002). Phillips (2007b) adapted the River Styles framework to examine the LBR as stable, steady-state equilibrium assumptions are problematic both in general and in the Texas context.

Zonation based on channel pattern and historical avulsions

Phillips (2006, 2007b) identified the zones on the LBR based on channel pattern (e.g., single-thread vs. multi-thread or anabranching channel patterns) and the presence or absence of abandoned historical river channels (avulsion channels) that are still with a flow in non-flood

conditions (Table 3.1, Figure 3.4.). He further subdivided these abandoned channels according to whether they are currently tributaries to the modern LBR or a part of the avulsive Bessie's Creek/Oyster Creek system. This system still maintains partial connections to the LBR although it has an independent path to the Gulf of Mexico.

Phillips (2006, 2007b) also identified the regions which might represent past avulsions utilizing DOQQs and satellite imagery. The sites with possible avulsions were determined based on the following criteria: 1) Anabranches, tributaries, distributaries, or linear channel-like depressions which join (or appear to have once joined) the modern river at a non-acute angle; 2) Channel width and meander amplitude and wavelength consistent with the Brazos or Navasota River rather than lower-order streams (Table 3.1, Figure 3.4).

Zonation based on channel-floodplain connectivity

Zonation based on channel-floodplain connectivity was performed assessing the frequency of overbank flooding using stage-discharge relationships to estimate the discharge associated with flood stages at each USGS gage site in the study area. The analysis shows that overbank flooding is relatively rare at the Bryan station and very rare at Hempstead (Phillips 2006, 2007b). This is the result of the incised nature of the LBR channel. In addition, at Hempstead station, geological constriction inhibits floodplain development and confines most of the flows in a relatively deep, narrow channel. Mean daily flows of bankfull or above occur annually, on average, at Richmond, and more often at Rosharon (Table 11 in Phillips 2007b).

Although major overbank flooding is relatively rare in the Bryan station, the sub-bankfull flows can cause significant backwater flooding in tributaries (e.g., the Little Brazos River), resulting in significant hydrologic connectivity. At Hempstead, the very rare flood stage produces only minor overbank flooding, however less than 1 m increase in stage can result in a widespread floodplain inundation in the area. At Richmond, stages about 1.5 m below flood stage can trigger backwater flooding and flow toward Oyster Creek, while stages at or just below flood stage initiate cross floodplain flow into Oyster Creek. Flood stage and above can trigger significant inundation and cross-valley flows. Similarly, the Rosharon gage site also experiences cross-valley flows at higher flood stages (Table 12 in Phillips 2007b). Phillips (2007b), following the analysis briefly presented above, generated the channel-floodplain connectivity zones on the LBR ranging from low to high connectivity (Table 3.1, Figure 3.5).

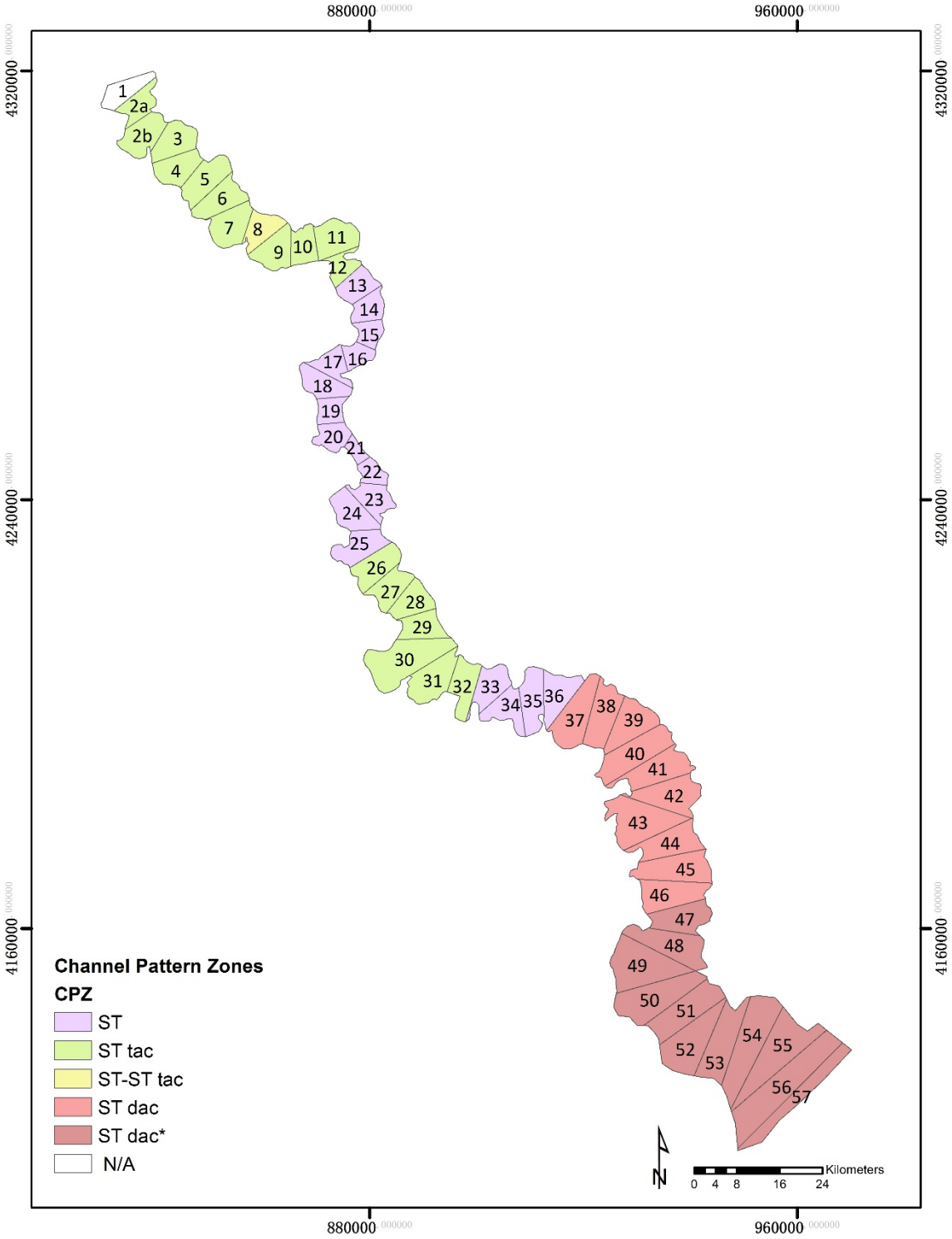

Figure 3.4. The zonation of the LBR and its floodplain based on channel pattern (Phillips, 2007b), with channel pattern classes of ST, ST tac, ST-ST tac, ST dac, and ST dac*. ST =single thread; tac =with tributaries occupying avulsion channels; dac = with distributaries occupying avulsion channels; and dac* = with distributaries occupying avulsion channels with coastal backwater or tidal influence. The boundaries represent the floodplain sections 1–57.

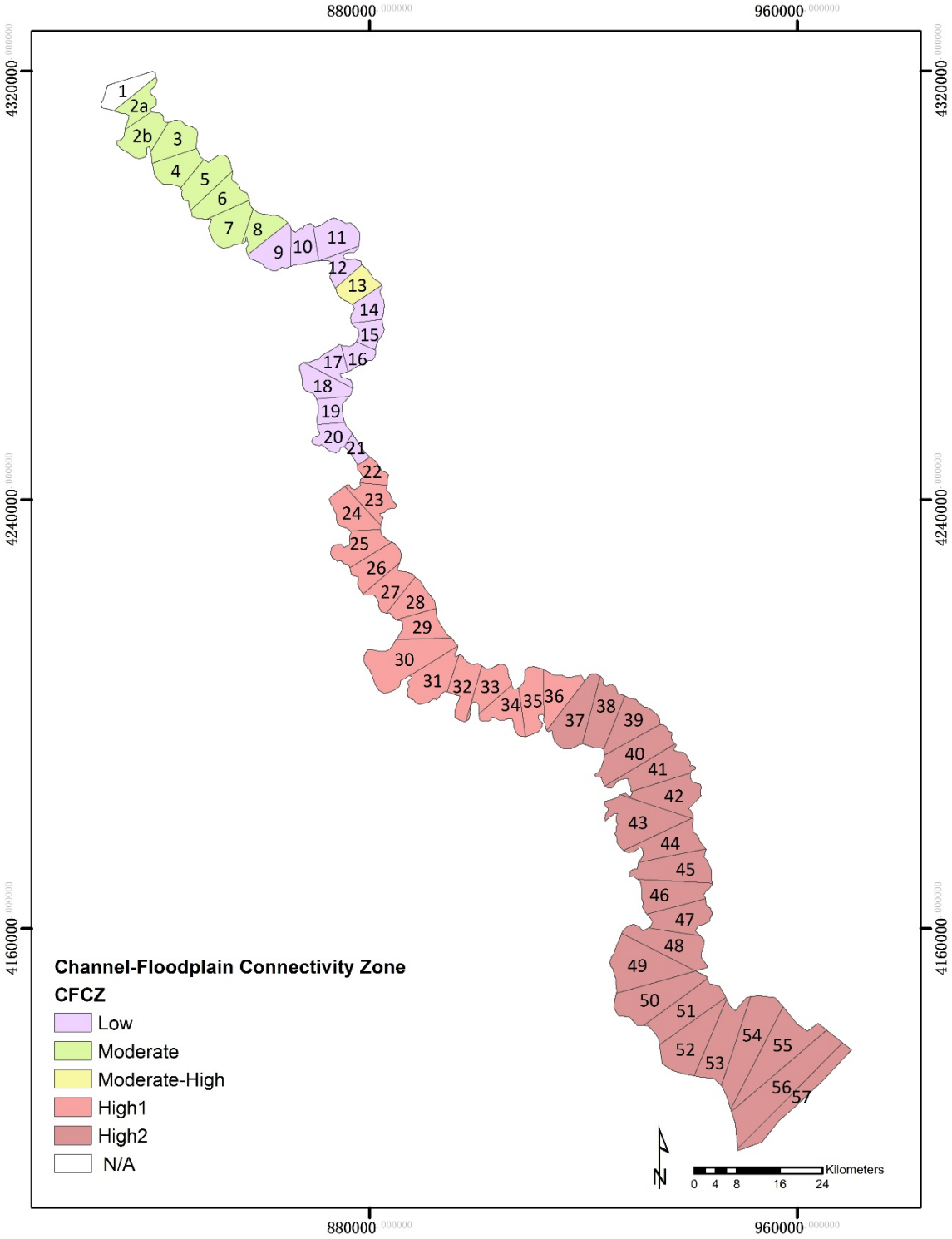

Figure 3.5. The zonation of the LBR and its floodplain based on channel-floodplain connectivity (Phillips, 2007b), with connectivity classes of low, moderate, moderate to high, high 1 and high 2. High 1 refers to high connectivity primarily due to flooding of oxbows, sloughs, and flood basins, high 2 refers to high connectivity primarily due to cross-floodplain flow. The boundaries represent the floodplain sections 1–57.

Table 3.1. The LBR Zones based on River styles (Brierly and Fryirs, 2005) by Phillips (2007b).

Zones	Floodplain sections	Location	River style	Valley confinement	Mean channel slope	Sinuosity	Channel-floodplain connectivity	Channel pattern	Sediment bars
		State Highway (SH) 21 bridge	*(upstream end of study area)*						
1	2a-2b	Thompson's Creek	Steeply Incised Valley (IV) Fill	Unconfined	0.020459	Low sinuosity		ST tac	Many
2	3	Upstream of SH 60 bridge	Meandering IV Fill	Unconfined	0.000164	Meandering	Moderate	ST tac	Many
3	4-7, 8	Boggy Creek	Meandering Confined IV Fill	Confined	0.000164	Meandering	Moderate	ST tac	Many
4	8	Yegua Creek	Strongly Meandering IV Fill	Unconfined	0.000164	Strongly meandering	Moderate	ST	All
5	9-10	Hidalgo Falls	Confined Strongly Meandering IV Fill	Confined	0.000164	Strongly meandering	Moderate	ST tac	Few/No
6	11-12	Navasota River	Hidalgo Falls	Confined	0.000183	Strongly meandering	Low	ST tac	Few/No
7	13	Rocky Creek	Confined Strongly Meandering IV Fill II	Confined	0.000183	Strongly meandering	Low	ST	Few/No
8	14-18	New Year Creek	Partly Confined Strongly Meandering IV Fill	Partially confined	0.000183	Strongly meandering	Moderate/High	ST	All
9	19	Austin Branch Road	Bedrock Confined Valley	Confined	0.000183	Strongly meandering	Low	ST	All
10	20-21	Clear Creek	Bedrock Confined Valley	Confined	0.000077	Strongly meandering	Low	ST	All
11	22-24	SH 529 bridge	Unconfined Alluvial Valley	Unconfined	0.000077	Strongly meandering	Low	ST	All
12	25	Hannay and Palmer Lakes	Unconfined Alluvial Valley	Unconfined	0.000077	Meandering	High 1	ST	Mixed
13	25	Garrett Lake	Unconfined Wide Alluvial Valley	Unconfined	0.000077	Meandering	High 1	ST	Mixed
14	26-27	Irons Creek	Avulsed Alluvial Valley	Partially confined	0.000077	Meandering	High 1	ST tac	Mixed
15	28-29	Buckintin Road	Avulsed Alluvial Valley	Partially confined	0.000251	Meandering	High 1	ST tac	Mixed
16	30-32	Allens Creek	Avulsed Alluvial Valley	Partially confined	0.000251	Tortuous	High 1	ST tac	Mixed
17	33	Dyer Moore Ranch Road	Confined Avulsed Alluvial Valley	Confined	0.000251	Meandering	High 1	ST	Mixed
18	34	Houston Street bridge, Rosenberg	Confined Avulsed Alluvial Valley	Confined	0.000111	Meandering	High 1	ST	Mixed
19	35-36	US 90A bridge, Richmond	Confined Avulsed Alluvial Valley	Confined	0.000111	Strongly meandering	High 1	ST	Mixed
20	37-40	Thompson Ferry Road	Unconfined Low-Sinuousity	Unconfined	0.000111	Low sinuosity	High 1	ST dac	Mixed
21	41	Rabbs Ridge oil field	Avulsed Alluvial Valley II	Unconfined	0.000111	Strongly meandering	High 2	ST dac	Mixed
22	42-43, 44	Big Creek	Avulsed Alluvial Valley II	Unconfined	0.000138	Strongly meandering	High 2	ST dac	Mixed
23	44, 45	Cow Creek	Unconfined Low-Sinuousity	Unconfined	0.000138	Low sinuosity	High 2	ST dac	Mixed
24	45-46	Otey	Partly Confined Low-Sinuousity	Partially confined	0.000138	Low sinuosity	High 2	ST dac	Mixed
25	46	Harris Reservoir north	Partly Confined Low-Sinuousity II	Partially confined	0.000031	Low sinuosity	High 2	ST dac	Few/No
26	47	Harris Reservoir south	Lower Coastal Plain	Partially confined	0.000031	Meandering	High 2	ST dac*	Few/No
27	48-50	Middle Bayou	Lower Coastal Plain	Partially confined	0.000031	Meandering	High 2	ST dac*	Few/No
28	51	Cutoff Lake	Low-Sinuousity Lower Coastal Plain	Partially confined	0.000031	Strongly meandering	High 2	ST dac*	Few/No
29	52-55	Freeport ship channel	Low-Sinuousity Lower Coastal Plain	Unconfined	0.000031	Low sinuosity	High 2	ST dac*	Few/No
30	56	Gulf of Mexico	Low-Sinuousity Lower Coastal Plain	Unconfined	0.000031	Straight	High 2	ST dac*	Few/No

ST = single thread; tac = tributaries occupying avulsion channels; dac = distributaries occupying avulsion channels; *coastal backwater or tidal influence; Sediment bars: presence of active sandy point bars at meander bends; High = high connectivity primarily due to flooding of oxbows, sloughs, and flood basins, High = high connectivity primarily due to cross-floodplain flow. Sinuosity: 1.0–1.25: straight; 1.25-1.49: low sinuosity: 1.50–1.99, meandering: 2.0–3.0, strongly meandering: >3.0, tortuous.

3.3. The history of the LBR and past valley-scale avulsions

Similar to many other environments, valley-scale avulsions are an important processes in floodplain construction and alluvial architecture in southeast Texas coastal plain rivers (Waters and Nordt 1995; Blum and Price 1998, Aslan and Blum 1999, Blum and Aslan 2006, Taha and Anderson 2008). Reoccupation of former channels, and diversion into flood basins are the two major styles of avulsions in the Gulf coastal plain rivers undergo two distinct styles of avulsion (Aslan and Blum 1999, Sylvia and Galloway 2006, Phillips 2009).

The LBR is commonly characterized by an infilled incised valley (Waters and Nordt 1995, Phillips 2007b). From 18,000 to 8, 5000 years ago, the meandering LBR was able to leave thick coarse deposits via vertical accretion as it migrated across its floodplain. Approximately at 9, 000 to 9.400 years ago, it transitioned to an underfit river that was incised into its vertically accreted deposits (Waters and Nordt 1995).

In the LBR floodplain, avulsions are common. The valley filling is the major control over the avulsions of the LBR (Aslan and Blum, 1999; Blum and Aslan, 2006). Although valley-scale avulsions on the LBR had important implications on the surface morphology and on current forms, processes, and evolution as via modifications on the water and sediment fluxes (Blum and Aslan 2006, Sylvia and Galloway, 2006), the controls over the timing and specific location of avulsions are poorly understood (Taha and Anderson, 2008). The frequency of occurrence of avulsions show that floodplain-scale avulsions in the LBR occur over time scales of decades to a few thousand years (Taha and Anderson, 2008). Over the past few centuries, the LBR has experienced no regional or valley-scale avulsions; Waters and Nordt (1995) found evidence of Brazos River avulsions as recently as 300 and 500 years BP.

Taha and Anderson (2008) studied the Holocene avulsion history of the lower Brazos alluvial valley of east Texas, USA, using drill cores, radiocarbon dates, aerial photos, and a digital elevation model. The findings of this study indicate that the LBR has experienced avulsions that delivered large volumes of sediment to the floodplain and led to rapid valley alluviation. Historical avulsion locations on the LBR are nonrandom and can be related to allogenic factors of sea level rise, climate change, and human influences (Taha and Anderson 2008).

In the same study, Taha and Anderson (2008) identify three historical avulsions (Figure 3.6) and attribute these avulsions on the paleo-LBR to the long-term process of valley aggradation. Avulsion #1 is the oldest and closest to the Gulf of Mexico, about 40 km inward of the current

shoreline (Figure 3.6). Avulsion #2 is located approximately 70 km inward from the coast, where a prominent crevasse splay complex exists. Taha and Anderson (2008) identified avulsion #2 as initiated from the Big Slough channel around ~4.0 ka and led to the creation of Oyster Creek. Avulsion #2 is associated with a crevasse splay complex with a size approximately 25 to 50 times larger in area than a nonavulsion-related crevasse splay. Most of the other crevasse splays observed along the modern LBR have areas of 1/4 km^2 or less. Avulsion #3 is located 140 km inward from the current shoreline. It outlines of former bifurcating and coalescing streams preserved on the floodplain and initiated from the Oyster Creek ~1.5 ka led to the formation of contemporary the LBR (Figure 3.6). The crevasse splay associated with it is of similar size of that associated with avulsion #2 and covers the western half of floodplain.

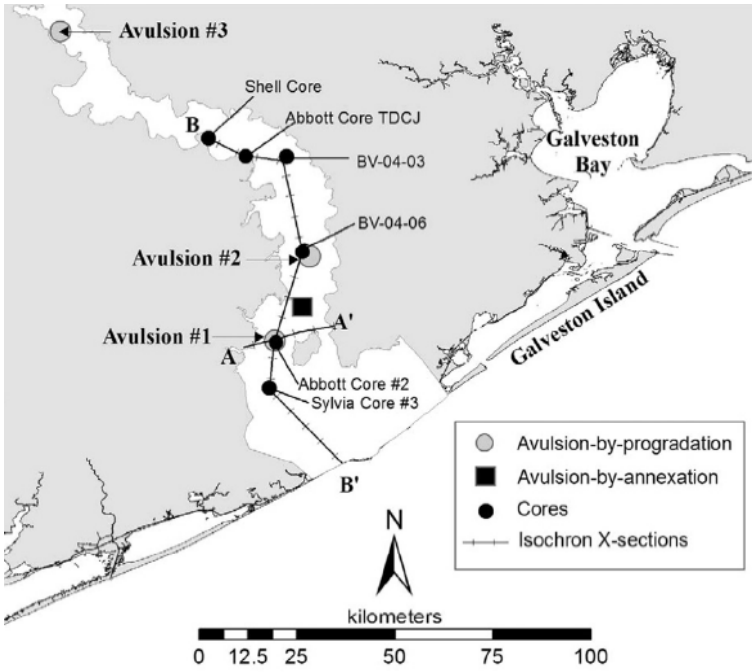

Figure 3.6. Location map of the past major avulsions on the lower Brazos valley marked as Avulsion #1–3 *after* Taha and Anderson (2008).

Much of the research on the avulsions in the LBR and the coastal plains in Texas in general has focused on the sedimentary record with the aim of developing a better understanding of the role of avulsions in floodplain evolution and alluvial architecture (Aslan and Blum 1999, 2006, Taha and Anderson 2008, Taha 2007). Recently, taking a different approach, Phillips (2007a) examined the effect of channel shifts on the contemporary river channel and

floodplain morphology, and on their role on internal adjustments of the fluvial system on the lower reaches of five rivers in southeast Texas.

Phillips (2007a) identifies nine historical avulsions and indicates that relocations or distributaries are dominant in the LBR. Specifically, he points out that eight of nine avulsions were relocations, one distributary and none were anastomoses. Six of these nine avulsions are infilled and the rest are occupied by tributaries. The avulsion by progradation into flood basins associated with the infilling is more likely to lead to relocation and distributary avulsions vs. anastomoses. Phillips (2007a) also shows that the LBR has a watershed fragmentation avulsion, where the tributary occupying the abandoned channel (Oyster Creek) is not hydraulically connected with the Brazos and maintains an independent path to the Gulf of Mexico. According to Phillips (2007a), crevasse splays are more common than avulsions and cutoffs in the LBR; there were a total of 46 of them. Cutoffs are more numerous than avulsions in the LBR; Phillips (2007a) identified a total of 17 cutoffs, where 14 of them were neck and 3 of them chute cutoffs.

3.4. Gradient advantages on the LBR

Using 10-m NED Digital elevation data, Phillips (2007a) calculated gradient advantages (the ratio of cross-valley slope to down-valley slope) at multiple LBR test cross-sections and found that three of six sites had gradient advantages relative to downstream slopes. One of these has a gradient advantage was of only 2.54. In the other two cases, however, the gradient advantages were immense, with ratios >65. He also noted that at both of these sites cross-valley flow paths led to floodplain depressions or flood basins. At the other three test sections, alluvial ridges were far from the channel edges, so flow was routed back into the river in the same general vicinity. These finding confirms the suggestion that cross-valley gradient advantages are more common than avulsions (Aslan et al. 2005)

3.5. Channel change on the LBR

Past studies on the historical channel migrations after the river control provides contradicting results. Gillespie and Giardino (1997) showed although lateral migration rates on the LBR are still high, they decreases substantially after the flow regulation. On the other hand, other studies by Hudson and Mossa (1997) and Dunn and Raines (2001) indicated that effects of flow control on the LBR are minimal and therefore, the cause of the observed decrease in the channel dynamics is not clear.

4. METHODS

4.1. Analysis of gradient advantages

Conceptual framework

Avulsions are associated with floods or threshold discharges required for breaching levees or alluvial ridges. Gradient advantages have been found to be a necessary condition for the breaching to occur (Jones and Schumm 1999). One such application of this idea is the in the work of Mackey and Bridge (1995), where they model alluvial stratigraphy such that the probability of an avulsion at a certain cross-valley transect is defined as

$$P(a) = (Q_f/Q_a)^{eQ} (kS_{cv}/S_{dv})^{eS} \quad \text{(Eq. 1)}$$

Where Q_f is maximum flood discharge for a given time period, Q_a is the threshold discharge for an avulsion to occur, S_{cv} is cross-valley slope at the edge of the channel belt, and S_{dv} the local downvalley slope of the channel belt. The variable, k, is the slope probability constant (0.1 to 0.5), and the variables, eQ and eS, are discharge and slope exponents, respectively. The eQ, eS are model coefficients to tune the model to produce realistic avulsion frequencies (Mackey and Bridge 1995).

Taken together, in Eq. (1), the k, eQ, and eS incorporate stochastically the local, contingent factors that are critical in triggering avulsions—in which a number of smaller floods and local factors play a role (Slingerland and Smith 2004). This also fits into the scheme of Slingerland and Smith (2004), where they describe avulsions as a setup and trigger process. In all, the avulsion process is one that involves a trajectory to stability or instability and the small factors that cause the process to occur (Jones and Schumm 1999) (Figure 1.2).

Gradient advantage calculations

Attempts to quantify the risk or instability of a riverine system with respect to avulsion comes in the form of the gradient advantage (Jones and Schumm 1999; Mackey and Bridge 1995, Slingerland and Smith 2004). Gradient advantage is calculated within the domain of a transect through a ratio of the cross-valley dimensionless slope to the along-channel dimensionless slope. In order to properly assess gradient advantages for highly sinuous reaches, topography of the flood plain and river channel is evaluated to determine cross-valley to down-valley dimensionless slopes (Aslan et al. 2005). An avulsion is theorized to

occur when an increase when cross-valley slope reaches some multiple of the down-channel slope (Slingerland and Smith 1998; Jones and Schumm 1999).

The gradient advantage covers a component the setup mechanism (Slingerland and Smith 2004). This gradient advantage is triggered into an avulsion during a flood event and other locally-operating factors, allowing flood waters to irreversibly enlarge and open a preexisting crevasse or random topographic low in the levee (Slingerland and Smith 1998). This often results in the abandonment of the river channel for a new or preexisting channel, changing the course of the river (Schumm 2005). The channel-capacity-limited models of avulsion (Makaske 2001) attribute avulsions to a decrease of sediment transport capacity, which lead to a building up of sediment and an avulsion (Schumm et al. 1996). While this viewpoint highlights a series of contributing factors, it is still not independent of gradient advantage, and it is unknown what the ultimate driving force behind the avulsion process actually is. Several other examples of avulsion due to channel blockage also exist (King and Martini 1984, Schumann 1989, McCarthy et al. 1992, Harwood and Brown 1993, Ethridge et al. 1999), but ruling out gradient advantage as the driving force is still not clear. The question that arises is: does gradient advantage lead to avulsion, or is it a necessary prerequisite for the other factors to drive an avulsion?

To assess the role of gradient advantage in the potential for avulsion setup, our goal is to calculate the gradient advantage as described by Jones and Schumm (1999) and Aslan et al. (2005). Throughout the literature, this is either measured via topographic maps or digital elevation models (DEMs). For our study, gradient advantage analysis is conducted with DEMs produced with Light Detection and Ranging (LiDAR) measurements.

DEMs produced through LiDAR measurements enable a researcher with detailed understanding of channels flows and their connections with the floodplain the ability to identify and quantify critical morphometric parameters for measuring avulsion setup. This is because LiDAR DEMs provide a greater vertical and horizontal accuracy over other methods (Overton et al. 2009). In addition, these DEMs allow for the study of these processes over large areas. Detailed elevations of river floodplains can help determine the importance of gradient advantage and improve our understating of the avulsion process.

Towards this goal, we produce a LiDAR DEM that covers the LBR Floodplain. To do this task, we conduct a fusion of three different LiDAR datasets that were obtained from the

Texas Natural Resources Institute (TNRIS) in the form of bare-earth DEMs. These different LiDAR datasets represent the Stratmap 2011 Austin, Grimes, Walker collection, the Stratmap 2014 Fort Bend collection, and the FEMA 2006 Coastal Counties collection (Table 4.1).

Table 4.1. Description of LiDAR Data used in the analysis.

	Stratmap 2011	**Stratmap 2014**	**FEMA 2006**
Resolution	1 meter	3 feet	1.4 meters
Projection	NAD 1983 UTM Zone 14N	NAD 1983 Texas State Plane 4104	NAD 1983 UTM Zone 14N+15N

Bare earth DEMs are processed by the LiDAR data provider and have vegetation removed as well as select urban features—such as residential installations and most buildings. Features that still remain are larger buildings, roads, and man-made levees. To facilitate hydrologic modeling, overpasses are removed so that flow can be objectively modeled (https://tnris.org/news/2015-05-12/central-texas-fort-bend-county-lidar).

These data, originally in the format of USGS DEMs, were converted to GeoTIFF raster datasets and projected into a common coordinate system of North American Datum 1983 Texas State Plane-South Central (4104). The data are then resampled with a common resolution of 5 meters via Bilinear Interpolation, and then mosaicked with a 'First' mosaicking operator using ArcGIS Desktop® software—with DEMs further from the coast being first. Then, the data are clipped to our study area—which is an outline of the LBR floodplain (Figure 4.1).

Using a LiDAR DEM, we frame our analysis in the form of systematically spaced transects that branch out from the channel in terms of left and right bank—with the perspective of downstream flow going down the river toward the ocean. The upstream portion of this study is approximately 17 kilometers west of Prairie View, Texas and between zones 11–30 of Phillips (2007b). Within these zones, he considered the LBR to be conducive to avulsion. Although theory dictates that the each transect should be perpendicular to the channel (Jones and Schumm 1999), we opt for a different orientation that is perpendicular to the valley axis to facilitate a systematic analysis of the channel and floodplain (Figure 4.1). This analysis is conducted via sections that are spaced at 4800 meters (22–56 of 56 zones with a spacing of 40 average river widths) along the valley axis. Within each floodplain section, there are 4 transects that are spaced at 1200 meters (total of 140 transects at 10 average river

widths) and branch out to the edge of the floodplain. Each of these transects intersect the channel, and are then split in terms of left bank and right bank (now, 280 transects total). At certain highly sinuous reaches, there may be multiple intersections from a transect. These are resolved in a manner where the analysis can yield the most discernable results.

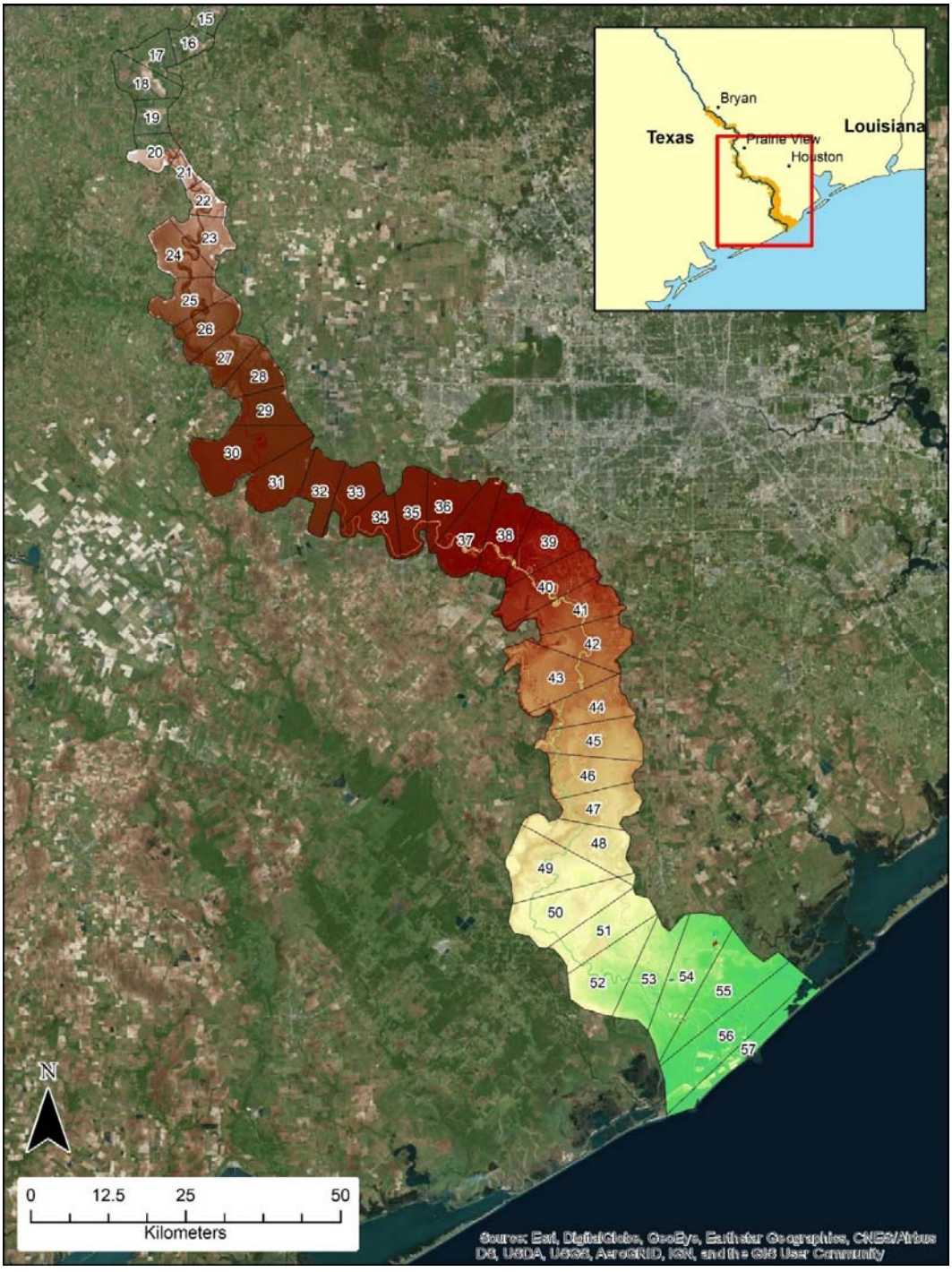

Figure 4.1. Study area on the LBR with floodplain sections #15–57 presented.

Cross-valley slope measurements

At each transect, the cross-valley slope is calculated for each transect on each side of the channel. This slope ratio, being a component of the setup for river avulsion (Phillips 2007a), is measured or described differently by different researchers (Mackey and Bridge 1995, Phillips 2007b, Aslan et al. 2005, Jones and Schumm 1999). The main reason for this difference is that they are studying different types of rivers in different environments (Mackey and Bridge 1995, Aslan et al. 2005, Jones and Schumm 1999). Therefore, there are logistical questions that must be answered before doing such an analysis for the LBR floodplain.

To accommodate this knowledge and resolve other questions, we make a series of considerations to determine where the slope should end. Even with a clarity given of where one should start or end a slope measurement, the real world offers a level of complexity in which a simple understanding of a system is not adequate. Hence, there are other considerations. One such consideration involves nearby features such as urban structures or floodplain depressions and streams. How does the researcher assess the valley slope when the transect encapsulates a floodplain feature—such as an abandoned channel—near the alluvial ridge or if that feature is within the confines of a basin? In this study, the slope is measured by pouring into such a feature, as we consider the possibility of avulsion by annexation should be viewed as important.

These considerations for identifying the ending point of a cross-valley slope calculation are:

- Slope should decrease to near zero OR slope should start to point toward the channel—in the case of a basin.
- Spikes that are perturbations closer than a half channel width to the centerline are ignored, as these can be errors or digital dams inherent in a LiDAR DEM that is not hydro-flattened or hydro-enforced *(https://www.usgs.gov/media/videos/digital-elevation-models-hydro-flattening-and-hydro-enforcement)*.
- Commonly, there are small pits that represent abandoned channels or tributaries/distributaries that are bounded by small levees or alluvial ridges. These alluvial ridges, if they are lower in height than the main channel alluvial ridge and monotonically decrease from the alluvial ridge are ignored, in addition to the small pit, and do not stop slope calculation.

- Small spikes (inverted pits) that are lower in height and monotonically decrease from the channel ridge are ignored and do not stop slope calculation.
- Isolated spikes and pits, regardless of size, that are not prismatic along the channel length are ignored and do not stop slope calculation.
- If the general trend of the levee or alluvial ridge is back into the channel, then the calculation never occurs.

Using these considerations, an analyst observed each of the derived profiles to quantify a cross valley slope by identifying the beginning point for the slope, the ending point for the slope, and their respective heights. While conducting the analysis, we recognized that different features within the floodplain seem to influence our slope ratios. With this observation, we then identified each transect as being influenced by a point bar, human structures or activities, and a nearby avulsion.

Down-valley slope measurements

The down-valley slope measurement is also variable among different studies (Phillips 2007b, Aslan et al. 2005; Jones and Schum, 1999). Some consider the down-valley slope as going down the valley axis or some surrogate for the valley axis (Aslan et al., 2005), and others measure along-channel slope from the perspective of water surface level with the channel (Phillips 2007b). As Aslan et al. (2005) found, highly meandering reaches can be biased because their slope is often much less than the valley axis—which would serve to bias the slope ratio measurements. Being that much of our study reach is meandering, we opt to use the valley axis as our measure of down-valley slope (Figure 4.2).

However, the down-valley slope profile (Figure 4.2) shows that there are regions have distinct slopes. With this observation in mind, we calculate two different classes of slope ratios—those with a global slope and those with a local slope. We calculate local slopes with a series of steps. First, we obtain a valley trend raster by smoothing the down-valley profile and applying methods of deriving Digital Relative Elevation Models (Jones 2006). Once this raster is generated, we use Jenk's Natural Breaks criteria with the ArcGIS Desktop® software to identify slope regions (Figure 4.2). These slope regions are then used to identify transects within each slope class. Once this is known, down-valley slopes are defined for each transect. The breakdown of slopes are described in Figure 4.2 and Table 4.2.

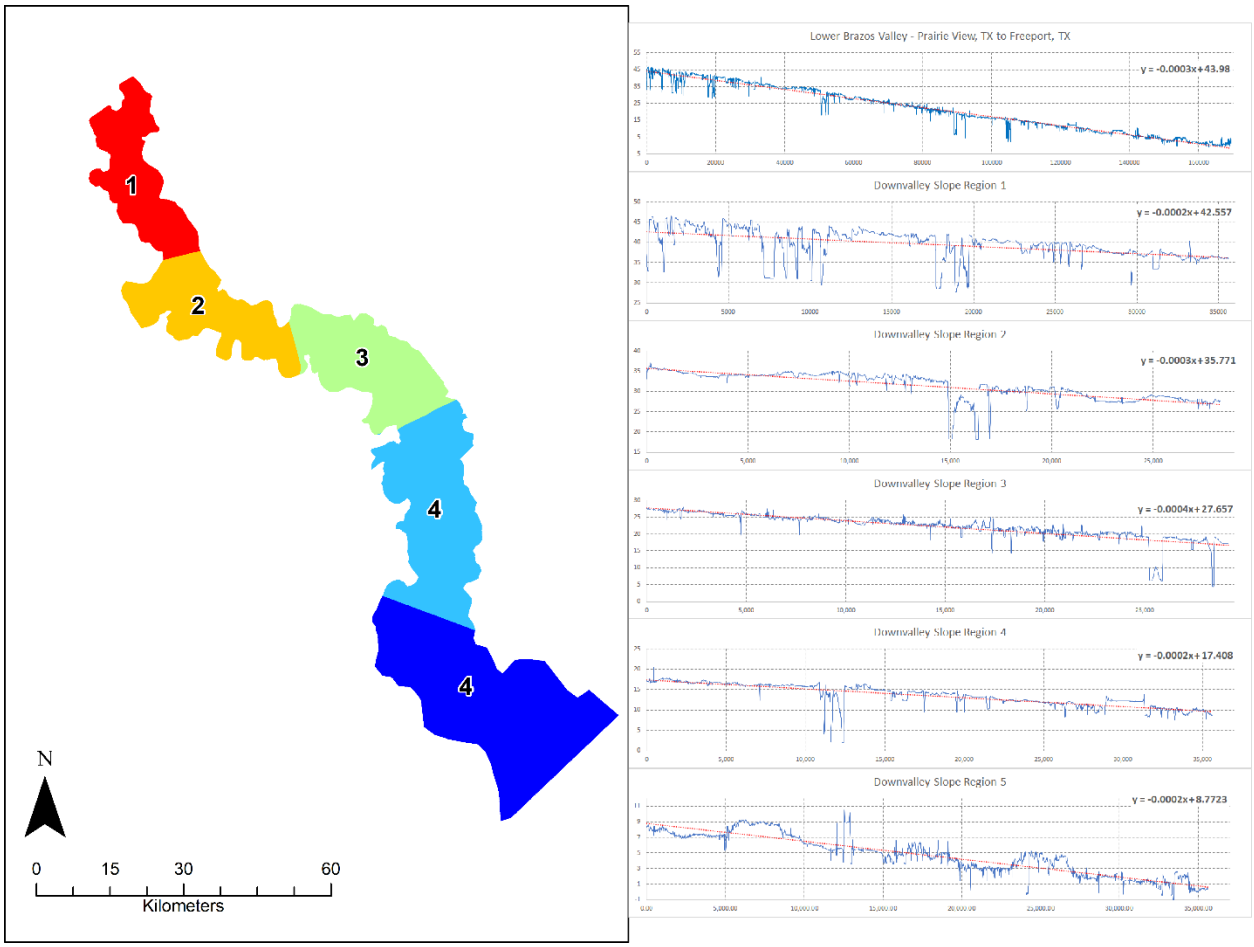

Figure 4.2. Down-valley slope classes with the following colors. Outline is the LBR floodplain.

Table 4.2. Slopes assigned to each along-slope class.

Class	Dimensionless Slope
Class 1	0.0002
Class 2	0.0003
Class 3	0.0004
Class 4	0.0002
Class 5	0.0002

With cross- and down-valley slopes defined, the only task left to derive gradient advantages is to divide the cross-valley by the down-valley slope for each transect (280 in total). To further analyze the statistical and spatial distribution of slope ratios, we aggregate these transect measurements into floodplain sections 22-56. For each section, we derive summary statistics (range, mean, standard deviation). To help us understand the effects of urban and floodplain connectivity features on the derivation of gradient advantages, we successively

remove them, and observe summary statistics.

4.2. Identification of Crevasse Splays

LiDAR DEMs provide an ability to assess the detailed topography of a landscape, and their utility is not lost on crevasse splays. Crevasse splays have a complicated geometry of several active and abandoned channels that results in complex arrangements of sheet sands as well as sand fingers (Phillips 2011, Smith et al. 1989, Taha and Anderson 2008) (Figure 4.3).

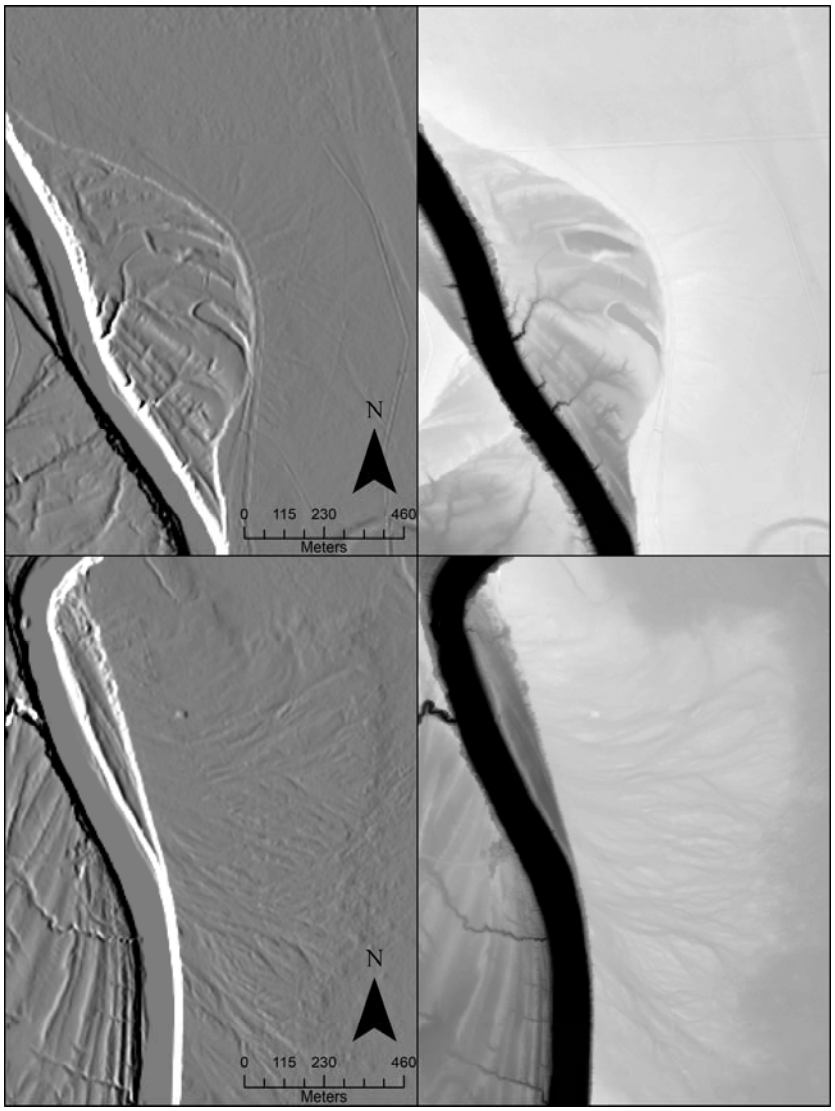

Figure 4.3. Extant crevasse splay identified along the LBR. Sobel-Filtered DREM (upper left) and 5m LiDAR DEM (upper right) that features crevasse splay highlighted in Taha and Anderson (2008); Sobel-Filtered DREM (lower left) and 5 m DREM (lower right) that features another crevasse splay within the LBR Floodplain.

Given this geometry, we can observe the presence of crevasse splays around the main channel by a 'contrast-stretch' method that stretches the contrast of an image based on the extent that the user is viewing. This functionality is already built into ArcGIS Desktop® software. Furthermore, we derived a technique to create a digital relative elevation model (Jones, 2006) based on the water stage during a 1.5 year flood. With that DREM, we then implemented a a Sobel nonlinear filter (Jensen 2016) that helped to further identify crevasse splays by texture and orientation of texture with respect to the channel. Also, aerial photography via Google Earth® were utilized to support these identifications.

4.3. Analysis of historical channel migration

Historical river channel change

Historical analysis of channel migration can help understand the amounts and rate of channel change and floodplain area reworked by the river. It will also help determining, at least historically, the most active sections of the river, thus, may provide clues for migration patterns to the future.

The overall methodology in this study included the following steps. First, we gathered historical topographic maps (topomaps), scanned from hard-copy paper maps, geotopomaps, scanned/digital historical aerial photographs, and recent Digital OrthoPhoto Quadrangles (DOQQs) to produce data on the spatial and temporal extent of the channel changes in the LBR over a 100-year period (1910–2010). The intervals between the available spatial data varied over the available data period. Second, we produced digital data pertaining to river-channel features, including channel boundaries and polygons bounding the river boundaries. Then, we combined the river-channel data obtained from different years using the capabilities of a GIS to yield a quantitative analysis of the channel migration.

We produced river-channel polyline boundaries for the left and right banks, respectively, and channel polygons bounding the river boundaries via two methods: 1) on-screen, heads-up digitization; and 2) automated extraction of channel features from topographic maps and aerial photographic image mosaics in a geographic information system (GIS)/digital image-processing environment. For the present analysis, we ultimately opted for generating channel polyline boundaries and polygons by manual image interpretation and digitization. The delineation accuracy of the results accrued via the automated methods investigated are promising, but further research regarding the application of those algorithms to complex

geomorphic environments, such as the fluvial landscapes analyzed in this study, would be beneficial prior to their operational use for river avulsion studies. We expect, however, that such automated, algorithmic procedures will enable batch processing of very large data sets in future studies, which will likely, in turn, facilitate broader-scale avulsion and other fluvial landscape research. A summary of the algorithms implemented/investigated is given in Appendix A.

Based on manual map/image interpretation and digitization methods, the procedures employed to ultimately compute river channel-boundary migration rates are summarized as follows:

1. Mosaic and geometrically-rectify aerial photographs for selected river avulsion-relevant areas, for multiple years, as possible, given available images of acceptable quality;
2. Manually digitize river-channel boundaries based on the georeferenced digital aerial photograph mosaics, as well as false-color infrared (CIR) digital orthophoto quarter-quadrangles (DOQQs), available in more recent years;
3. Geometrically-rectify/georeference a series of multitemporal topographic maps;
4. Manually digitize river-channel boundaries based on the georeferenced digital topographic maps;
5. Merge the river-channel segments for the individual years within a given temporal merging envelope (e.g., segments from 1979, 1980, and 1981 were merged into one "1980" vector layer);
6. Calculate average change rate (ACR) (m/yr) and normalized average areal change (NAAC) rate ($m^2/m^2/yr$) for each floodplain section.

These processes are described in detail in Appendix B. Historical, multitemporal aerial-photograph mosaics that we processed (as well as available DOQQs) and topographic maps were used as base maps for digitization of LBR channel banks. Preprocessing of these base data sets (excluding DOQQs) is described in Appendix B, as is the channel digitization procedure.

Rates of channel migration and areal channel change

Using GIS-based methods, we then combined/jointly processed the river-channel boundaries for the different years noted above using GIS capabilities to a yield a spatially-explicit quantitative analysis of the river-channel change rates. In this analysis, these and

related computations were only performed for the first and last year pairs, based on available multitemporal river-channel boundary data, in each floodplain section. That is, we performed this year-pair analysis on a per-floodplain section basis, involving the first year for which data are available and the last year in the time series; in this case, this latter year was always 2010, as DOQQs afforded continuous spatial coverage over the entire LBR study area. Also, in general, we excluded from further analysis floodplain sections with only partial coverage of available data. The exception to this, however, was with the partial coverages in section 2; to address this partial coverage river-channel boundaries in that section, we split the section 2 floodplain section polygon into two polygons—one labeled as section 2a, with the other referred to as section 2b. This edit enabled full spatial-coverage analysis of the river-channel boundaries in those subsections. These subsetted floodplain sections were applied to all subsequent analyses.

1. Compute the *average channel length*. For the "average channel length" calculations, compute the average length based on both the left-bank (LB) and right-bank (RB) channel polylines for Years 1 and 2. That is, compute the average length of the LB and RB for Year 1 for a given section, as well as the average length of the LB and RB for Year 2 for that same section). Then average those Year 1 and Year 2 values.
2. Then, determine the *areal change* from one year to the other by intersecting the Year 1 LB polyline with the corresponding Year 2 LB polyline to generate LB "change polygons," and do the same for the RB. Then sum the areas of those LB and RB change polygons (or portions thereof) that fall within (are intersected with) a given floodplain section.
3. 3) For each floodplain section, compute: [areal change / average channel length] / time interval = $m^2/m/yr$. This *average change rate (ACR)* (m/yr) informs on the rate of historical channel change.
4. Furthermore, the *normalized average areal change (NAAC) rate* ($m^2/m^2/yr$) was also computed by dividing the average areal change/yr (m^2/yr) by the normalized floodplain section area (FSA) (m^2/m^2), where the latter is the FSA (m^2) for a given floodplain section divided by the minimum FSA across all floodplain sections (m^2).

4.4. Screening of oxbow lakes and meander scars

In the LBR, we identified historical meander cutoffs based on the presence of oxbow lakes or swamps. We classified them as neck cutoffs if the lake present as an isolated an entire loop in the form an oxbow. Alternatively, we classified them as chute cutoffs where the

cutoff seems occurred across a point bar and only a portion of the meander bend is isolated. We also conducted a screening of the digital relative elevation model (DREM) we generated to identify the meander scars and other depressions associated with paleo-channels. We defined them scars based on clearly identified infilled oxbow lakes or lakes formed by chute cutoffs (Phillips 2007b). In each of these identifications, in addition to our DREM, we also utilized ancillary data including topographic maps, historical aerial photographs, and Digital Orthophoto Quadrangles (DOQQs) and/or products derived from them. We mapped the oxbow lakes and included both the oxbows and meander scars in delineation of HCCZ.

4.5. Meander cutoffs

Lewis and Lewin (1983) identified five different types of meander cutoffs, three involving single-arc channels and two being multiloop versions of single-arc process types: Chute, neck, mobile bar, multiloop chute, and multiloop neck. They define *neck cutoffs* as those in which adjacent channel reaches were probably less than a channel width apart at the time of breaching. *Chute cutoffs* are those in which a much longer breach channel was created. We examined the meander bends with high potential for neck and/or chute cutoffs to occur using the stability conceptual framework discussed below.

Neck cutoff stability

We examined the neck cutoff stability using the rule of *one channel width*. This rule is based on the observation that neck cutoff occurs when the distance between two parts of the river channel becomes less than one channel width (Lewis and Lewin 1983). We identified the meander bends on the LBR with neck lengths close to one channel width (W).

Chute cutoff stability

Joglekar (1971) defines chute cutoff stability based on a ratio called the chute cutoff ratio λ. The λ is the ratio of the length of the channel bend to the length of the cutoff channel where λ is always > 1 (the ratio of the length ABC to the length of AB on Figure 4.4). Accomplishing $\lambda > 1$ is necessary but not sufficient. A cutoff will become increasingly probable as the λ value increases and when the other environmental conditions such as flood discharge, vegetation, bed slope and bed material are favorable (Joglekar 1971). Typical values of λ at which cutoffs occur vary among rivers from 1–3 for chute cutoff dominated rivers to 8–10 and larger for rivers like the Mississippi River in which neck cutoffs dominate.

We examined the chute cutoff stability using the chute cutoff ratio λ. Given that the LBR experiences extensive number of neck cutoffs, we identified the potential meander bend with a chute ratio that is equal to or above 6.

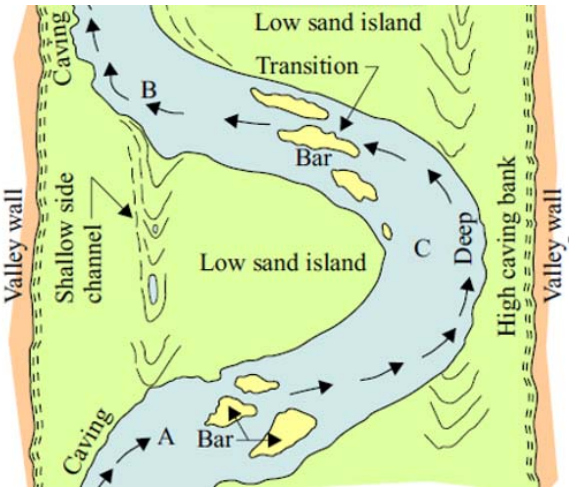

Figure 4.4. Chute cutoff stability *after* Joglekar (1971).

4.6. Insights on future channel migration patterns

Our historical analysis of channel migration included the analysis of the rates of migration and areal changes showing the reworked areas of the river change. We also examined the LBR in the context of presence of oxbows and meander scars and other types of paleo-channels. We then combined our analysis results in an end product which is a map that presents the *historical channel change zone* (HCCZ) within the floodplain in order to provide one of the inputs for evaluating future trends in channel movement (Rapp and Abbe 2003).

The analysis of HCCZ may not necessarily entirely help predict where future channel migrations will occur (O'Connor et al. 2003). The channel migrations may extend to the regions on the floodplain that was not reworked by the channel previously. To develop a better insight on the potential future migration patterns of the LBR channel, we produced another map showing the river *channel change zone* (CCZ) within the LBR floodplain. CCZ is a concept that we adapted from Rapp and Abbe (2003). Their goal is to create a formalized manner in which researchers and stakeholders can be informed of the hazards associated with fluvial migration. Here, we consider two factors, a hazard zone associated with avulsions and a hazard zone associated with bank erosion and channel migration. We analyze

these zones in two ways, by analyzing how much area and how many zones potentially are at risk by a channel migration (erosion) or local avulsion (Phillips 2007) within a floodplain section.

The CCZ map shows the channel erosion historical patterns (HCCZ) including the oxbows, meander scars, and other depressions/paleo-channels associated with river dynamics as well as the potential areas of erosion/migration due to channel migration. The potential areas include the areas where the river is anticipated to migrate gradually or via bend-to-multibend-scale avulsions (e.g., neck and chute cutoffs) and those areas with higher likelihood of other local-scale avulsions to occur. Some of these local-scale avulsions could result from high rates of connectivity during critical floods (e.g., an avulsion resulting from the connectivity of an oxbow lake to the river channel during a major flood event).

4.7. Generation of floodplain sections

To examine the results, we identified *floodplain sections* based on *floodplain transects* that we created across the floodplain at regular intervals of 40W (Figure 4.1). We digitized the floodplain transects perpendicular to the centerline of the valley bottom, which can be identified using geologic maps and LiDAR (resampled to 5 m) and NED (with a spatial resolution of 10 m) DEMs. The floodplain sections represent polygons bounded by these transects that are spaced at 40W. However, we did not start at State Highway 21. The spacing moves 40W upstream and downstream of a location ~17km west of Prairie View, TX—the upstream boundary of our section 22. This is because the initial phase of our research, for gradient advantage, takes place from sections 22-57.

We used these *floodplain sections* to, summarize, measure, and delineate broad-scale attributes such as valley width and active channel boundary. We also used them to evaluate our results from gradient advantage analysis and river migration in the LBR. We delineated a total of 58 floodplain sections (from section #1 to #57, where section #2 has to subsections, #2a and 2b). However, due to the partial coverage of data (in section #1) and the areal coverage of the sections #57, we omitted the floodplain sections #1 and #57. This resulted in a total of 57 sections (floodplain sections #2a-b to #56) used in the analysis.

4.8. Generation of digital relative elevation model (DREM)

To evaluate topography from the perspective of the river itself, we derived a digital relative elevation model (DREM) using methods adapted from Jones (2006). With a DREM, one is

able to see relative heights of features with respect to the water surface elevation within the river. This dataset has importance for identifying the historical channel change zone (HCCZ) and crevasse splays; and also evaluating the floodplain connectivity to the channel during flooding. DREM requires first a detrending procedure to remove the trend from the elevation data. We determined a trend based on channel WSE and generated a detrend surface. Detrending procedure is not straight forward, there are complications as follows. The methodology of Jones (2006) is suitable for locations where there is one LiDAR dataset generated or obtained in the study area. However, we had to utilize multiple LiDAR dataset that were acquired over weeks to months. When fusing large LiDAR datasets with temporal mismatches, the methodology needs be modified—since water surface elevation is not consistent, and refer to often over multiple days.

Therefore, our methodology differs from Jones (2006) primarily in how the water surface elevations along the channel centerline were created. For the portion of our study site that encompasses that area with available LiDAR data (i.e., *floodplain sections* 20–56), we had a total of three river gage stations with enough temporal coverage for data (Table 4.3). Using data from these gage stations, it can be possible to estimate a water surface along the channel centerline. All the stations had a vertical datum of NGVD 1929. So, they all were converted to NAVD 1988 via the National Geodetic Survey's VERTCON (https://www.ngs.noaa.gov/cgi-bin/VERTCON/vert_con.prl). Two of the stations needed additional preprocessing in order to be useful. USGS Gage Brazos Rv near Hempstead (Gage No 08111500) had inconsistent datums, so the datum had to be corrected for by 3.048 meters (10 feet) from 1941–1989, and Brazos Rv near Rosharon (Gage No 08116650) did not have a water stage height gage measurement to correspond to the discharge measurement for the year 1989. So, we constructed a rating curve to fill-in the missing value. Here, we estimate a 1.5-year recurrence interval (RI) stream flow (Leopold et al. 1964) using peak streamflow from USGS Gage data found at the following URL, http://waterdata.usgs.gov.

Table 4.3. Characteristics of USGS water gage stations used in the development of DREM.

USGS Gage Name	USGS Gage No.	Start year	End year	1.5 year recurrence interval (RI) (m)	Dist. from coast (km)
Brazos Rv near Hempstead	08111500	1941	2016	43.60	322.41
Brazos Rv near Richmond	08114000	1989	2016	19.33	154.44
Brazos Rv near Rosharon	08116650	1967	2016	10.66	93.56

We plotted the locations of each USGS water gage station in ArcGIS and found the river distance (in meters) associated with them via Linear Referencing (Nyerges 1990) in ArcGIS Desktop®. With river distances and computed water surface elevations, it is now possible to fit an equation that represents the water surface profile. We did add one value for calculation of the stream profile, and that was the height of 0 meters above sea level at the coast. For fitting the equation, we used methods that are analogous to Phillips and Lutz (2008)—where a series of logistic and polynomial equations of varying orders were tried to get an optimum fit. In this study, the data fit best to a 2nd degree polynomial (Figure 4.5). With an equation, points were located on the centerline of the river at every 5m—to match the pixel resolution of our LiDAR DEM. Using the best fit equation, the water surface elevations were associated with each location along the river. Then, the water surface elevations were associated to the closest cross-sections, and the rest of the DREM generation is similar to methods in Jones (2006).

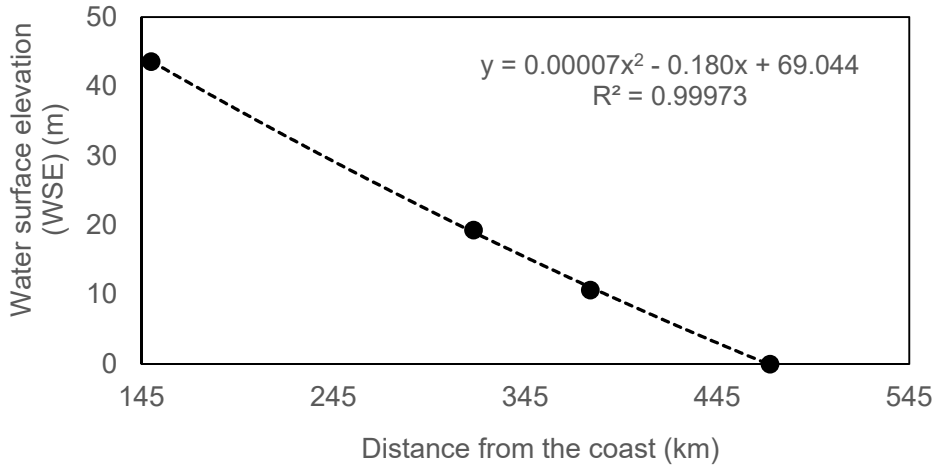

Figure 4.5. Estimated water surface elevation (WSE) for 1.5-yr recurrence interval (RI) stream flow versus distance from the USGS Gage near Bryan (Gage No 8108700).

5. RESULTS

5.1. Gradient advantages

The banks of the Lower Brazos River comprise many different alluvial environments that are distinct in river channel pattern and floodplain connectivity (Phillips, 2007b). For our study area, these environments range from sinuous, incised, urban, and straightened riverine systems. Furthermore, floodplain connectivity is considered high (Phillips 2007b), but this mode of high floodplain connectivity has two distinct regions. Sections 22–36 comprise a zone where high floodplain connectivity is primarily manifested as an exchange between floodplain features, such as oxbows and sloughs. Seconds 37–56 have exchanges of flows between channel and floodplain cross-floodplain flow. These differences in styles, but not magnitude class of floodplain connectivity gives rise to a special dynamic that is at play because of the rollover anticline.

With the consideration of multiple riverine systems and the sensitivity of the slope ratio to different environments and their features (Slingerland and Smith, 2004), we analyze the distribution of slope ratios taken within this study area in by successively omitting transects that are affected by these features. Thus, we hope to see if omitting these features can indicate to us the sensitivity of the gradient advantage to these features and help provide a clearer picture of the natural avulsive characteristics manifest in the Lower Brazos River floodplain.

For the entire study area, we defined these influential factors as Urban and Floodplain Connectivity features. Urban features that are known to influence the gradient advantage range from built structures such as human-made levees, industrial depressions or pools, roads, and ditches. In many cases, Urban features prevented flow from happening from the stream, and were thus implicitly omitted. This is especially true for the coastal region containing Freeport, TX.

Floodplain connectivity features consists of relict channels and depressions on the floodplain, such as oxbow lakes, sloughs, or abandoned streams. Floodplain connectivity features are further subdivided into spurious and non-spurious. Those immediately connected up or downstream stand a chance to be inundated before or immediately after the area of interest is inundated, and would not hold the potential for avulsion setup—through the conversion of potential energy into kinetic energy—that the geometry itself would imply. If the area to be flooded is already inundated, then there is no chance of connectivity between that feature and the area of interest—since potential energy (by height difference) will be gone.

By omitting these features, we demonstrate the effect of these features on our gradient advantages in Table 5.1. Transects whose alluvial ridge slopes capture no away-channel drainage were assessed a slope of zero, and were omitted from these statistics, they are 87 in number—out of 280 total.

Table 5.1: Summary statistics that summarize contribution of each type of channel-floodplain feature to the distribution of gradient ratios. Group A = All; Group B = Without Urban Features, Group C = Without Connectivity Features, Group D = Without Spurious Connectivity Features, Group E = Without Urban and Connectivity Features, Group F = Without Urban and Spurious Connectivity Features.

	Group A	*Group B*	*Group C*	*Group D*	*Group E*	*Group F*
Count	213	167	164	181	121	137
Range	753.86	753.41	401.09	401.09	132.32	132.32
Mean	49.65	50.63	31.48	31.36	26.16	26.72
Std. Dev.	96.36	102.3	43.96	42.16	24.86	24.16

Table 5.1 suggests that there is a large amount of variability for values of gradient advantage that can be explained as being influenced by urban features or spurious floodplain connectivity features. Without these features, the gradient advantage begins to show a range of values comparable to other published works (Aslan et al., 2005, Phillips 2007a) (Figure 5.1). To address this breakdown, we further visualize the distribution of gradient advantages in each class by using box and whiskers plots (Figure 5.1). Figure X demonstrates that the last two distributions (from left going right) have the least in terms range and number of outliers. These two distributions, transects representing potential sites with out-going flow and without urban and floodplain connectivity features and without spurious floodplain connectivity features. Here, in this work, we choose to include floodplain connectivity features and leave out spurious floodplain connectivity features—hence, the last distribution. This distribution has very similar statistical properties as the second-last distribution, and has more values in it. Overall, we discard 143 (51%) of our transects as either being no outward flow, urban features, or spurious floodplain connectivity features.

A demonstration of spurious floodplain connectivity features can be seen in Figure 5.2—where a transect intersects a tributary that is connected downstream of the channel in the immediate vicinity. Any gradient advantage enhanced by the presence of that tributary on the floodplain would most certainly be canceled in event of a flood, because of the tendency for that channel to rise nearly at a rate that is coeval with the main channel. Since our study

provides for a systematic sampling of the Brazos River at 10 river widths, these sites are identified as connecting to floodplain features as well as being spurious.

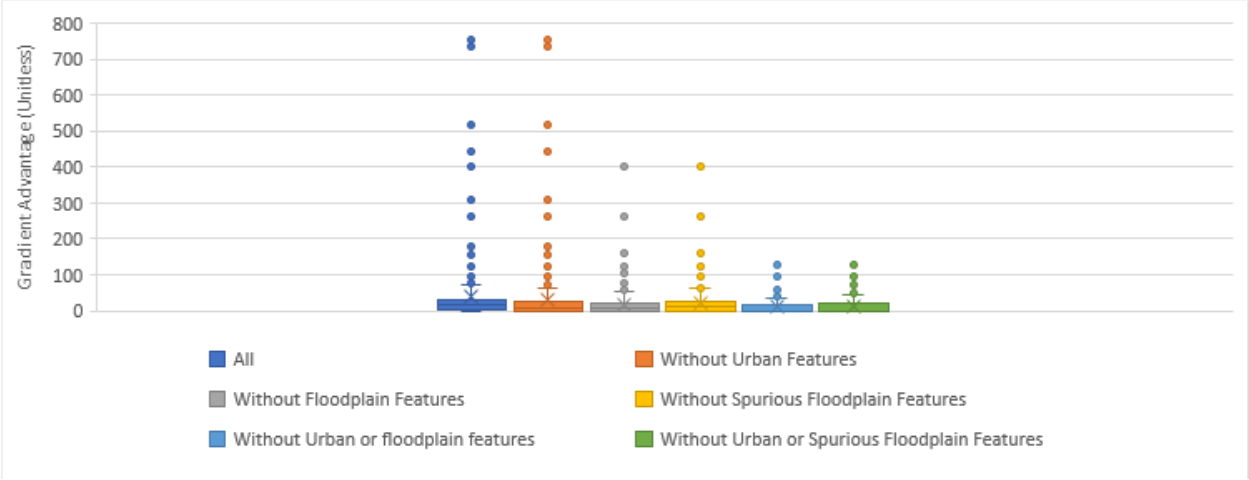

Figure 5.1. Box and whisker plot that shows distributions of gradient advantages along with statistical outliers.

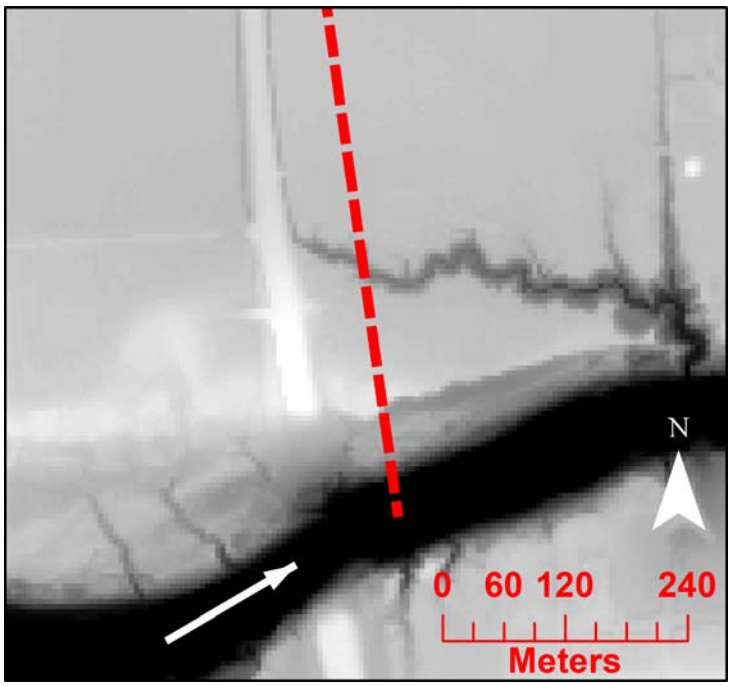

Figure 5.2. Intersection of tributary with transect. This kind of transect is considered a spurious feature—as the gradient advantage that the topography suggests would be short lived or non-existent.

The spatial arrangement of gradient advantage for the Lower Brazos River can be summarized as means standard deviations, and counts aggregated by floodplain sections (Figures 5.3–5.4). Figure 5.3 describes the spatial arrangement of aggregated mean gradient advantage for six different classes that are identified by what features they leave out. With all transects considered (Figure 5.3a), we see two loosely clustered regions identified as areas where there are sections that have large mean gradient advantages. Two of these areas align with the transitional zone between tributary to distributary-dominated channel forms and the region bracketing the Harris and Brazoria Reservoirs. These areas have elevated average gradient advantage because of several transects that are considered to have urban and spurious floodplain connectivity features. One example of such a location is next to the Brazoria Reservoir (Figure 5.5). The right bank features a small distributary (Figure 5.5, lower left) that enhances the gradient advantage, but suffers from the same problems as the transect in Figure 5.3, the small floodplain channel is directly connected to the main channel. The transect on the left bank (Figure 5.5, lower right) abuts a man-made levee that is presumably associated with the reservoir. This levee, since it is prismatic along the edge of the channel, would stop the gradient advantage calculation and we would settle for the higher angle that is composed of just the natural levee. By successively removing the effects of spurious floodplain connectivity and urban features, these two regions are no longer distinguishable from other sections. Hence, the variability of gradient advantage from the natural environment can begin to be seen (Figure 5.3e). This are still two zones that contain intermediate and high average gradient advantage, but their locations of changed. Their patterns are more closely investigated by observing Figure 5.4.

Figure 5.4 demonstrates this variability as aggregated average (a), standard deviation (b), and remaining numbers of transects (c) that show gradient advantage. In all, there appear to be three regions, although not completely distinct from each other. Hence, the borders of each group are up for interpretation. However, each region seems to have a statistical character that is distinct. The first region, which is composed of high average, variability, and count for gradient advantage are located in the northern part of the study area, floodplain sections 22–28. This particular region is the only region that has high variability, comparatively, with the rest of the study area. The reasons for this region's high variability and values of topographic advantage come in the form of local and regional controls—(Phillips, 2011; Philips, 2014). The regional control is that of valley slope. This area has a lower dimensionless slope than those adjoining regions downvalley at 0.0002—of which the other noncoastal regions have

slopes that range from 0.0003-0.0004. However, there are a combination of distinctive local factors that affect the gradient advantages as well. These are in the form of floodplain connectivity features—such as oxbow lakes. However, the most abundant and consequential floodplain connectivity feature are sloughs formed by heavily dissected meander scrolls. Furthermore, other local controls come in the form of small creeks, such as such as Irons Creek, and older, relict streams. Although present throughout the Lower Brazos Floodplain, this particular region is comparatively very narrow.

The second region is known for both low values and low variability in terms of average gradient advantage, and spans floodplain sections 29-45. Having higher down-valley slope is a regional factor that depresses values of gradient advantages. However, there are several floodplain-connected features present—just not in the clear abundance or close proximity as the other region. In contrast, other features that serve to amplify the gradient advantages in several locations throughout this region is the inclusion of urban features. Bracketing the communities of Richmond, Rosenberg, and Sugar Land, this region features locations of major urban presence. Many of these urban features often consisted of natural levees that were tall enough to not be considered monotonically moving downward with the top of the channel toward the valley—therefore, these levees often served to abort further consideration of the valley for slope calculation—hence often amplifying the gradient advantage by considering only the steepest part of the natural levee—which would be inconstant with methods of other works (Aslan et al., 2005).

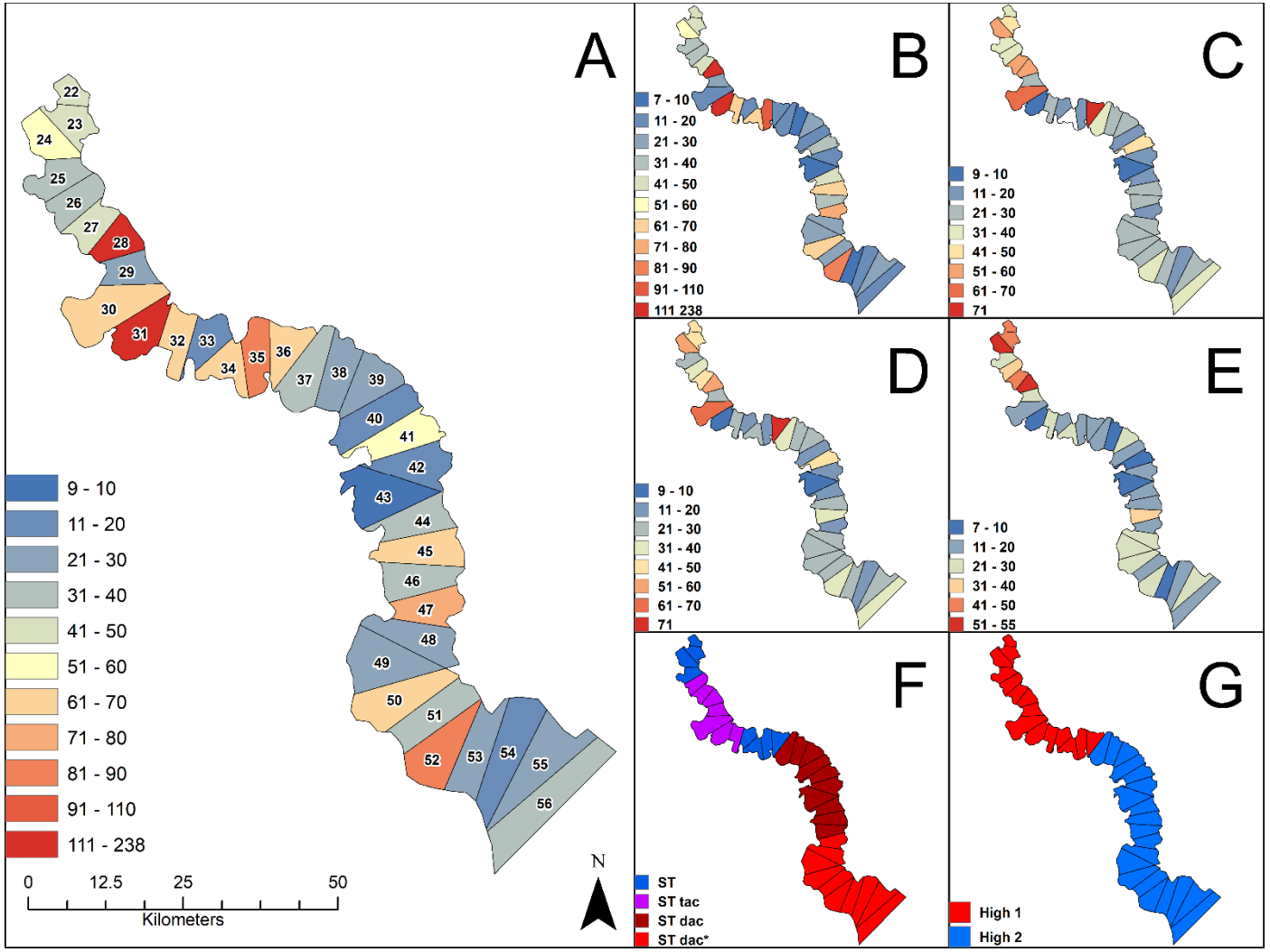

Figure 5.3. Average gradient advantage for sections 22-56 of the Lower Brazos River floodplain. Individual items are: A – All transects considered; B – Urban-affected transects removed; C – Transects affected by floodplain connectivity features removed; D – Transects only affected by spurious floodplain connectivity features removed; E – transects with both urban and spurious floodplain connectivity features removed; F – channel pattern and avulsive channels (Phillips 2007a); G – floodplain connectivity (Phillips 2007a).

The third region features intermediate values of average gradient advantage for the floodplain sections that comprise it, sections 46-56. This region is marked by a heavy urban presence near the coast in the form of Freeport, TX. However, this region is also marked by diverse natural settings. In particular, floodplain sections 48-50—just downstream of the Harris Reservoir, has a unique environment where the right bank of the Brazos is bracketed by Jones Creek, a feature that has significance in the work of Taha and Anderson (2008) for being particularly affected in its course by a normal listric fault—with the primary clue being that the both river's course is nearly parallel with the Texas coast. Jones creek is bracketed by large and wide natural levees—which implies it is has either been extant for a long time or that it undergone repeated episodes of flooding. On the right of the Brazos River, for this section, are several relict channels—such as Dry Bayou—that do not have very large natural levees. This dynamic does not permit easy avulsion by annexation in the case of Jones Creek, but does permit an easier path to avulsion by annexation in the case of those relict streams surrounding Oyster Creek. Furthermore, these floodplain sections still contain a Brazos River that has a discernable natural levee. As for the sections that comprise Freeport, TX, these environments have a large urban influence, and were thus removed—as is evidenced by the low variability and numbers of transects in sections 55-56 (Figure 5.4c).

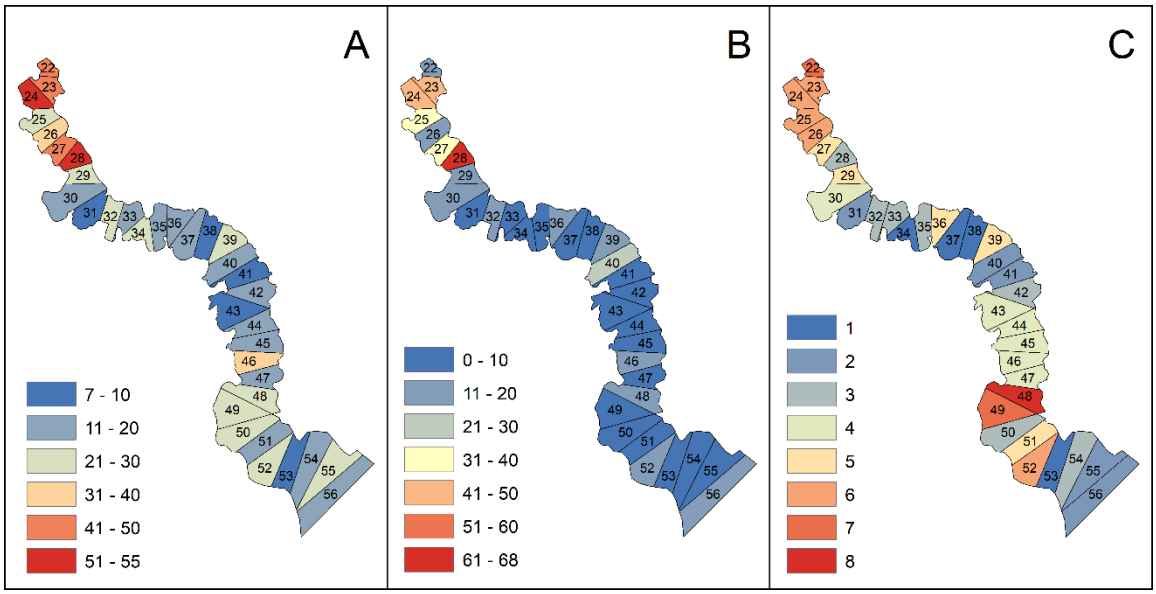

Figure 5.4. Variability of the gradient advantage with urban and spurious floodplain features removed. A – average of gradient advantage and B – standard deviation of gradient advantage, and C – number of transects left per floodplain section.

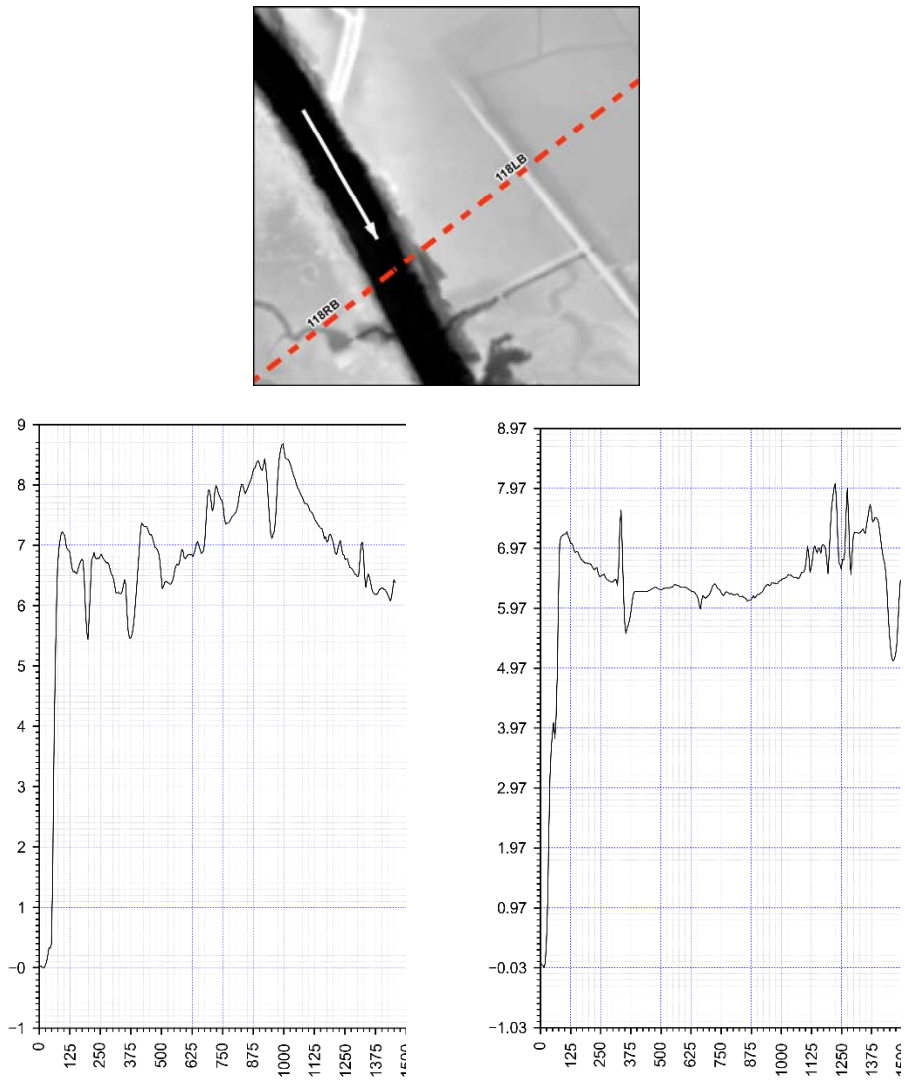

Figure 5.5. Top - Transect 118 (dashed, red) with a spurious floodplain connectivity feature along the right bank (from the perspective of the arrow) with an urban feature on the left bank; Bottom Left – First 1500m (from channel to valley) of the Right Bank profile for transect 118; Bottom Right – First 1500m (from channel to valley) of the Left Bank profile for transect 118.

5.2. Crevasse splays

Crevasse splays represents two aspects of avulsion, the past occurrence of avulsion and the current risk of avulsion. Typically, crevasse splays can represent a lower probability for avulsion, since they actively reduce the slope between the tops of alluvial ridges and the valley (Aslan et al. 2005). However, they also represent areas that have historically been prone to avulsion. By identifying features of crevasse splays, primarily based on their texture and direction of incision, we could identify 31 crevasse splays that occur in direct proximity to the

Brazos River (Figure 5.6a–c). Counts of crevasse splay in the floodplain section context (Figure 5.6b), demonstrates intermediate to high crevasse splay prevalence for all but the last 40km of floodplain that is coastal. This is not to imply that areas undergoes few avulsions, but there are noticeably less crevasse splays prevalent in this region. For comparison, the 'hot zone' of high gradient advantage (Figure 5.6a) does not feature a high incidence of crevasse splays, but the prevalence is still greater than that of the coast. It is also interesting to note that areas of high incidence for crevasse splays seem to be aligned with breaks in down-valley slope (Figure 5.6c).

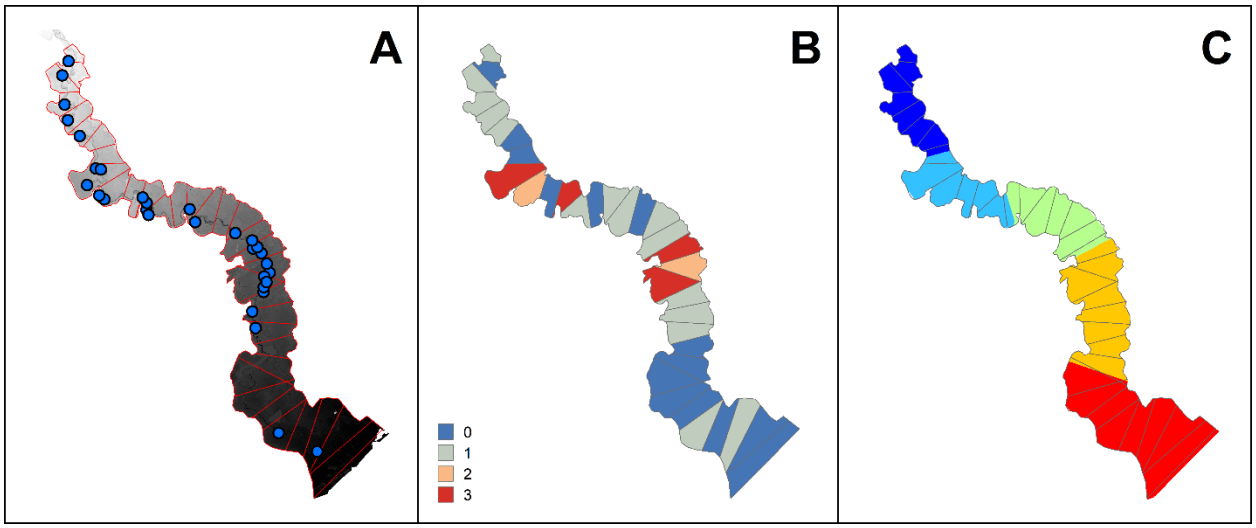

Figure 5.6. Locations of identified crevasse splays in the context of floodplain sections 22–56 and along-slope zones. A – Point locations of identified crevasse splays; B – Counts of identified crevasses plays; C – Along-slope zones with zone 1 (0.0002) being cerulean blue, zone 2 (0.0003) being cornflower blue, zone 3 (0.0004) being olivine, zone 4 (0.0002) being orange, and zone 5 (0.0002) being red.

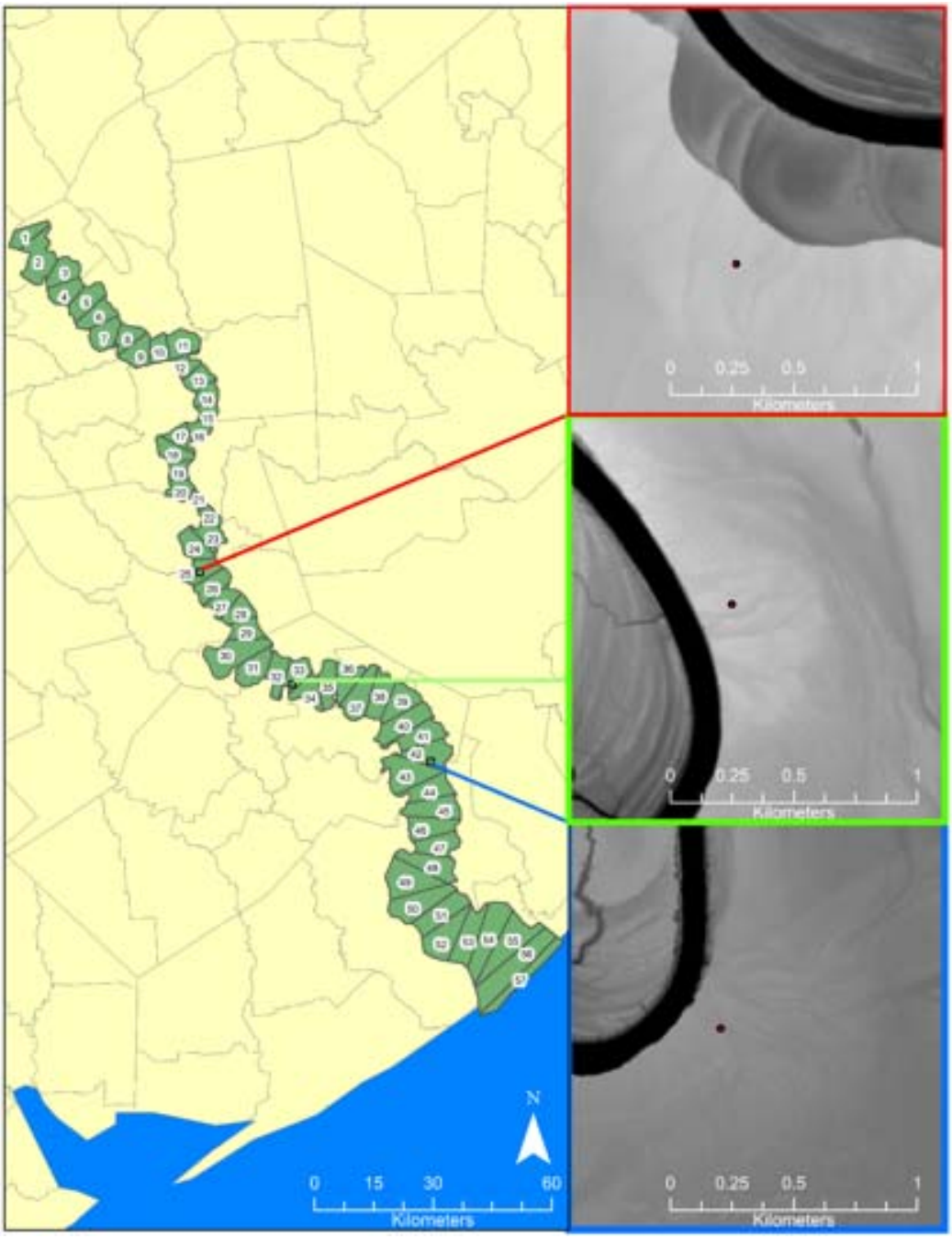

Figure 5.7. Examples of the identified crevasse splays on the LBR DREM from different floodplain sections (on the left).

5.3. Historical river channel change

We plotted river-channel polygons for multiple years (i.e., 1910, 1919, 1943, 1953, 1960, 1971, 1977, 1980, 1983, 1989, 1996, 2004, and 2010) on the same map to facilitate visualization of channel change through time. Detailed views of the multitemporal change in river-channel spatial position, focused on different, successive groups of floodplain sections, from the upstream to the downstream portions of the LBR, are given in the Appendix C (Figures C.1–C.9). Note that the existence of such data is not uniform across all floodplain sections and across all years. Therefore, care should be taken when interpreting these maps, as the lack of multitemporal coverage in a given floodplain section should not be misconstrued as minimal—or lack of—channel change in those sections.

Rate of channel migration

The average change rate (ACR) (m/yr) is particularly high in certain floodplain sections (e.g., sections 7 (4.85 m/yr), 8 (3.52 m/yr), 19 (3.57 m/yr), 21 (3.40 m/yr), 23-27 (3.47-4.72 m/yr), and 30 (3.54 m/yr)). All of these sections are located in the upstream portion (more than approximately the upper half) of the LBR study area (Figures 5.8 and 5.9). For the ACRs overall, across all floodplain sections, the minimum = 0.10; maximum = 4.85; mean = 1.84; and stdev = 1.21 m/yr.

The distribution of the higher ACRs, skewed toward the upstream ~half of the LBR floodplain, can potentially be understood in the context of simultaneously plotting the spatial distribution of these rates, as well as the valley width by floodplain section and the linear trends in valley widths for the upper and lower parts of the valley width (Figures 5.8). Given this illustration, it appears that there is a clear relationship between ACR and valley width. In the upper portion of the LBR (e.g., floodplain sections 2a~28), there is a modest-to-moderate decreasing trend in valley width with increasing floodplain section number (i.e., as a function of distance in the downstream direction). However, in the lower, or further downstream ~half of the LBR floodplain (generally, sections 29-56), there is a marked increasing linear trend in valley width progressively closer to the coastline.

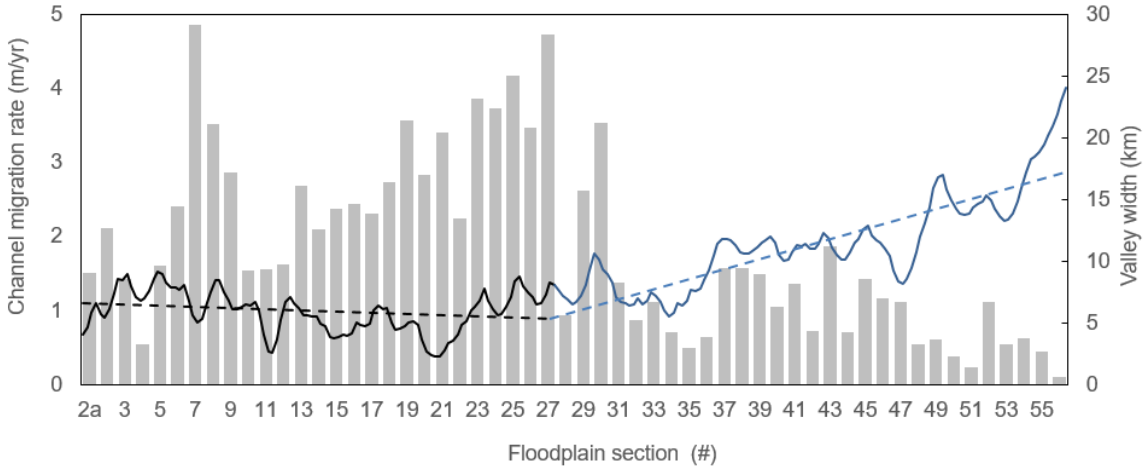

Figure 5.8. Average channel migration rate (m/yr) computed based on the first year of available river-channel planform data for a given floodplain section and that for 2010, by floodplain section. The solid lines mark the valley width and dashed lines mark the linear trends corresponding the upper and lower parts of the valley width (Figure 3.2).

In general, there are correspondences between groupings of the ACR values and the different channel-pattern classes and connectivity classes, respectively, though the relationships/patterns are not perfect nor are they always clear (Figures 3.4–3.5, 5.8–5.9). Regarding the channel-pattern classes (Figure 3.4) and ACRs (Figure 5.9), these higher-ACR floodplain sections in the upstream portion of the LBR study area generally tend to be co-located with ST tac (sections 2a/2b-7; 9-12; 26-32), ST tac-ST (section 8), and ST (sections 13-25) channel-pattern classes (Figures. 3.4, 5.8–5.9). However, ACR values in the river sections associated with the ST tac (sections 2a/2b-7; 9-12) and ST tac-ST (floodplain section 8) channel-pattern classes are quite variable (0.54-4.85 m/yr), and are more variable than such values in the sections corresponding to the ST channel-pattern class, at least in the upstream half of the LBR study area (i.e., in sections 13-25). There is a second, smaller set of floodplain sections further downstream (sections 33-36), which coincides with the ST channel-pattern class, that exhibits markedly lower ACR values (0.49-1.12 m/yr).

It is possible that the spatial position/distribution of certain channel-pattern classes (ST in this case) along the LBR floodplain may thus be related to observed ACRs. Further downstream (e.g., starting at floodplain section 37), the ST dac and ST dac* channel-pattern classes dominate (i.e., ST dac in sections 37-46; and ST dac* in sections 47-56). ACRs in sections 37-46 (ST dac) range from 0.73 to 1.87 m/yr, whereas in sections 47-56 (ST dac*), ACRs vary between 0.1-1.11 m/yr. Across the relevant floodplain sections, ACRs for the ST tac channel-

pattern class (sections 2a/2b-7; 9-12; 26-32) entail the following statistics: minimum = 0.54; maximum = 4.85; mean = 2.20; and stdev = 1.26 m/yr. Section 8 is the only section with the ST tac-ST class, with an ACR of 3.52 m/yr. Likewise, the ST class floodplain sections (sections 13-25; 33-36) the basic statistics are: minimum = 0.49; maximum = 4.17; mean = 2.43; and stdev = 1.15 m/yr, which are similar to those for the ST tac class. The mean ACR for ST is slightly higher than that of ST tac, and its stdev is lower, which agrees with variability observations noted above, although again, there are markedly different ACRs between the two spatially-disconnected groupings of ST floodplain sections. For ST dac floodplain sections (sections 37-46), minimum = 0.71; maximum = 1.87; mean = 1.30; and stdev = 0.38 m/yr. And for the ST dac* (sections 47-56), minimum = 0.10; maximum = 1.11; mean = 0.57; and stdev = 0.33 m/yr. Both ST dac and ST dac* floodplain sections exhibit markedly lower maximums, means, and stdevs relative to those for the ST tac and ST classes.

The channel-floodplain connectivity classes (Figure 3.5) include Moderate (sections 2A-8); Low (sections 9-12; 14-21); Moderate-High (section 13); High 1 (sections 22-36); and High 2 (sections 37-56) (Figures 5.8–5.9). With respect to the channel-floodplain connectivity classes and ACRs, connectivity classes with the highest ACRs are Moderate (4.85 m/yr, section 7) and High 1 (4.72 m/yr, section 27), and these sections are located in approximately upper half of the LBR study reach; and again the higher ACRs are generally observed in the upper portion of the LBR. ACRs are summarized by channel-floodplain connectivity class as follows. Moderate: min= 0.54; max = 4.85; mean = 2.24; and stdev = 1.36 m/yr. Low: min = 1.54; max = 3.57; mean =2.44; and stdev = 0.68 m/yr. Moderate-High (only one section): 2.69 m/yr. High 1: min = 0.49; maximum = 4.72; mean =2.30; and stdev = 1.50 m/yr. And High 2: min = 0.10; max = 1.87; mean =0.94; and stdev = 0.51 m/yr. Thus, Moderate, Low, and High 1 channel-floodplain connectivity classes all have similar average ACRs, though the Moderate and High 1 classes exhibit markedly higher standard deviations (which also encompass the highest ACR floodplain sections). High 2 connectivity sections—located in the lower portion of the LBR near the coast, entail the lowest minimum ACRs, the lowest maximum ACR by a good margin, by far the lowest mean ACR, and the lowest stdev (but similar to that of the Low class). Mean ACRs for the other connectivity classes (Moderate, Low, Moderate-High, and High 1) are quite similar to one another.

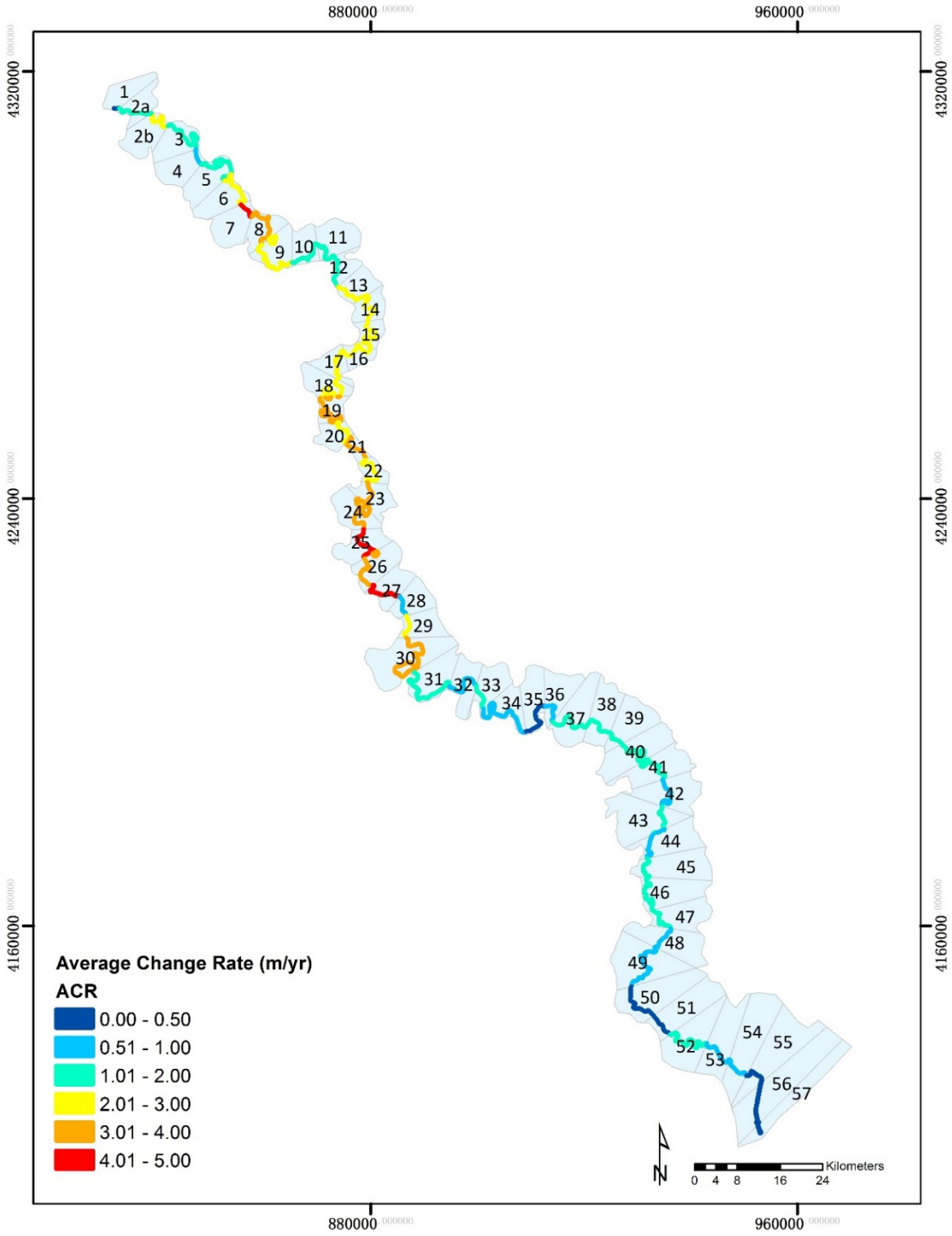

Figure 5.9. Average change rate (ACR) (m/yr), by LBR floodplain section.

Rate of areal channel change

Regarding normalized average areal change (NAAC) rates ($m^2/m^2/yr$) (Figures 5.10–5.11), the patterns of higher versus lower rates of change across the floodplain sections are broadly similar to those exhibited in the ACRs by floodplain section (Figure 5.9). That is, floodplain sections with higher NAAC values tend to agglomerate in approximately the upper half of the LBR, just as the higher ACRs did, as noted above. However, sections with the highest NAAC rates are not the same as those with the highest ACRs. The maximum NAAC rate across all sections is 29,438.15 ($m^2/m^2/yr$), which resides in section 21, and high values are also observed in sections 15 and 19 (14,074.07 and 23,362.57 $m^2/m^2/yr$, respectively) (Figures 5.10–5.11). For comparison, the sections with the highest ACRs are section 7 (4.85 m/yr) and section 27 (4.72 m/yr) (Figure 5.9). For both NAAC rates and ACRs, minimum values occur at the lower reach of LBR, near the coast, where the minimum NAAC value is at section 51, and where the minimum ACR is located in section 56. For NAAC rates overall, across all floodplain sections, the minimum = 201.26; maximum = 29,438.15; mean = 5,414.91; and stdev = 5,778.20 ($m^2/m^2/yr$) (Figures 5.10–5.11).

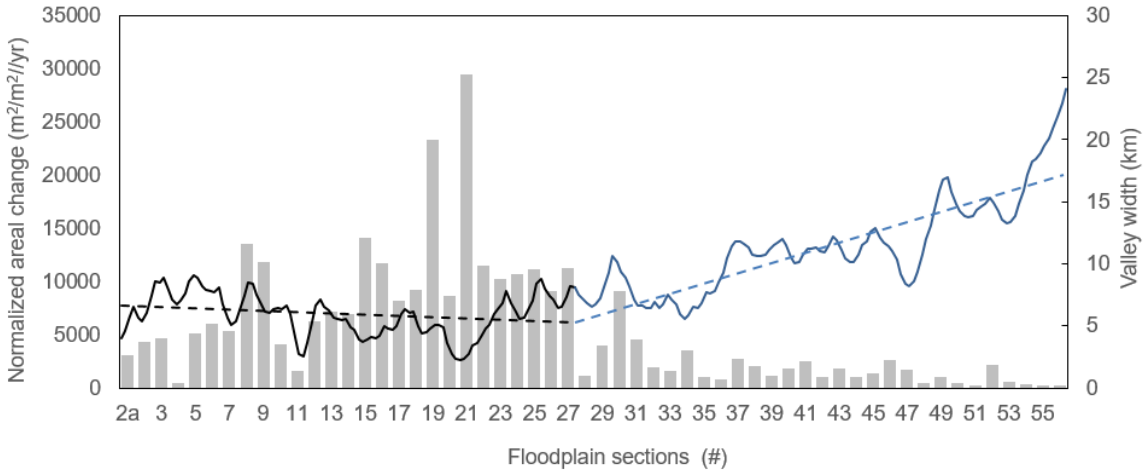

Figure 5.10. Normalized areal channel change (NAAC) rate ($m^2/m^2/yr$) computed based on the first year of available river-channel planform data for a given floodplain section and that for 2010, by floodplain section. The solid lines mark the valley width and dashed lines mark the linear trends corresponding the upper and lower parts of the valley width (Figure 3.2).

Given the general similarities in the spatial distributions of ACRs and NAAC rates, respectively, with respect to floodplain section locations (i.e., that higher values for both rates are concentrated in the upper ~half of the LBR), it is instructive to additionally generate and evaluate a plot similar to Figure 5.8. However, in this case, the valley width and the linear trends for the upper- and lower-floodplain valley width are superimposed onto the spatial distribution of NAAC rate values, by floodplain section (Figure 5.10)). Although the magnitudes and the patterns of magnitudes in NAAC rates (Figure 5.10)) versus ACRs (Figure 5.8) vary somewhat, their overall patterns from upstream to downstream are still quite similar, as are the linear trends in valley width. There is a modest/moderate declining trend from section 2a to 27, whereas further downstream from that section (from section 28-56), the linear trend markedly increases with increasing distance in the downstream direction. Thus, as with the ACRs, the spatial distribution of NAAC rates also appears to be related to that of valley width.

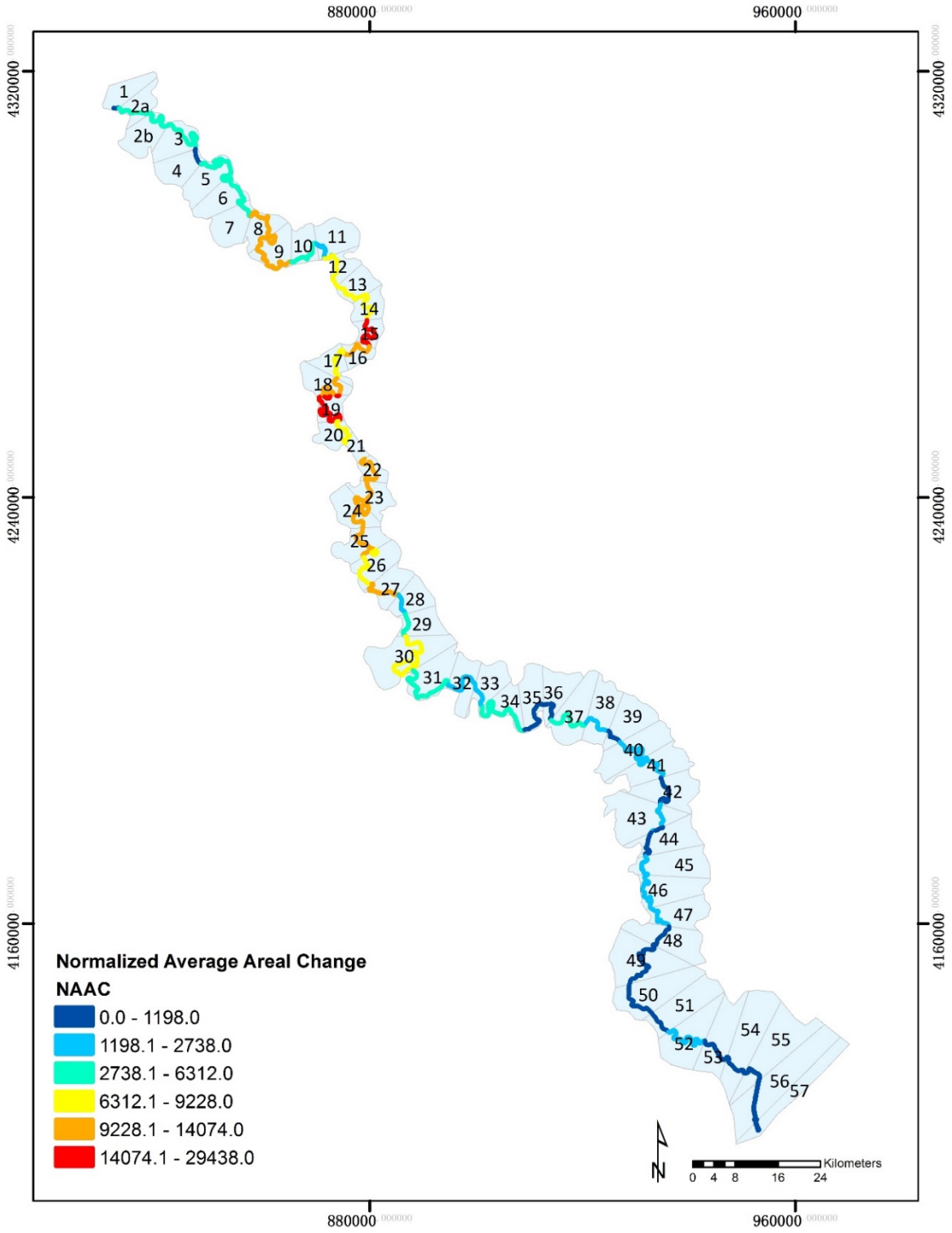

Figure 5.11. Normalized average areal change (NAAC) ($m^2/m^2/yr$), by LBR floodplain section.

5.4. Identification of oxbows

Following the criteria discussed in Section 4.4, we identified a total of 24 oxbow lakes on the LBR floodplain (Table 5.2, Figure 5.12).

Table 5.2. Oxbows identified on the LBR.

Oxbow number	Floodplain section	X coord (m)	Y coord (m)	Distance to channel (m)
1	2a	737337.00	3389880.00	200
2	7	756746.00	3374200.00	95
3	8	759419.00	3370510.00	315
4	14	779375.00	3353890.00	0
5	15	780232.00	3351560.00	180
6	17	772390.00	3342860.00	810
7	17	772754.00	3341840.00	175
8	19	773124.00	3334560.00	160
9	20	774970.00	3330230.00	335
10	21	777021.00	3329100.00	190
11	22	779302.00	3324540.00	435
12	25	777389.00	3310810.00	120
13	25	779440.00	3311110.00	1100
14	26	780185.00	3308130.00	0
15	26	780333.00	3306440.00	150
16	26	780301.00	3305080.00	735
17	27	784228.00	3300120.00	0
18	30	787620.00	3292130.00	700
19	30	789668.00	3289240.00	350
20	37	816053.00	3277810.00	325
21	37	818164.00	3277450.00	400
22	39	827233.00	3273520.00	250
23	46	833631.00	3241940.00	80
24	52	839272.00	3217550.00	400

5.5. Meander cutoff stability

Neck cutoff stability

We identified the potential meander bends to examine the neck cutoff stability. Visual evaluation of the LBR meander bends showed a total of eight meander bends to analyze the neck cutoff stability (Table 5.3). The results show that, based on one channel width rule, there is only one meander bend with a high neck cutoff potential (< 1) which is located in the

floodplain section 3 (Table 5.3, Figure 5.12–5.13). This one was followed up by two bends on the floodplain section 5 with a neck length of 1.8. The others have stability values of > 2 indicating the less likely occurrence of neck cutoffs in those due to bank erosion within a close future (Table 5.3, Figure 5.12).

Table 5.3. Stability of the potential neck cutoffs on the LBR.

Potential neck cutoff	Floodplain section	X coord (m)	Y coord (m)	Neck length (m)	Neck length/ Channel width (W)
1	3	746910.00	3386400.00	90	0.8
2	5	751110.00	3381600.00	210	1.8
3	5	751670.00	3381600.00	220	1.8
4	9	761490.00	3367300.00	350	2.9
5	24	778130.00	3317900.00	265	2.2
6	24	779100.00	3316500.00	470	3.9
7	26	780790.00	3308500.00	435	3.6
8	41	831270.00	3269000.00	270	2.3

Figure 5.12. A meander bend on the LBR with a high potential for neck cutoff (Neck length = 0.75) at floodplain section 3. On the left, the river channel is represented at the years 1960 (the most bottom boundary), 1980, 1996, 2004, 2010 (the top boundary). On the right, the meander bend is seen on the 2016 aerial photo, closer to neck cutoffs.

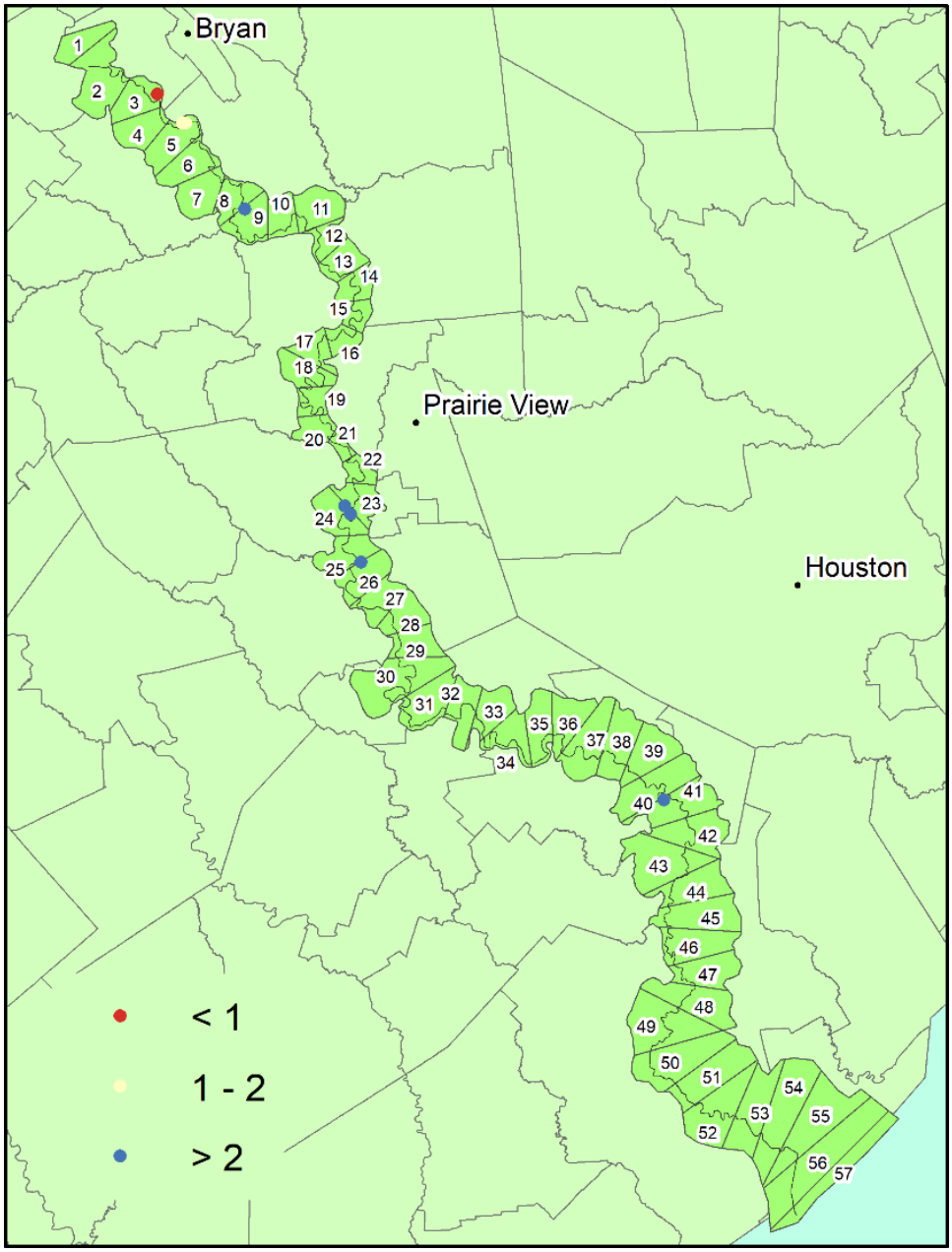

Figure 5.13. Examples of the meander bends on the LBR with a potential for neck cutoffs with stability values < 1, 1–2, and > 2.

Chute cutoff stability

Similarly, we identified the potential meander bends to examine the chute cutoff stability. Close visual evaluation of the LBR meander bends resulted in a higher number of bends than those for potential neck cutoffs; a total of 29 bends to examine (Table 5.4). Based on our chute stability rule, the results show that, there are multiple meander bends that satisfy our criteria. Among these, two have a stability ratio > 20 which are located in floodplain sections 24 and

30 (Figure 5.14). Three have a ratio of 10–20, located in floodplain sections 5, 9 and 24, and another three have a ratio of 8–10, located in floodplain sections 5, 40 and 41 (Table 5.4, Figure 5.14). In addition, these are five with a ratio of 6–8 (located in floodplain sections 5, 19, 26, 34). Considering the bends with a ratio of > 6 with a high potential, the floodplain section 5 contains the highest number of bends with a high likelihood of occurrence of chute cutoffs (Table 5.4, Figure 5.14–5. 15).

Table 5.4. Stability of the potential chute cutoffs on the LBR.

Potential chute cutoff	Floodplain section	X coord (m)	Y coord (m)	Bend length (m)	Neck length (m)	Bend length/ Neck length
1	5	751072.00	3381570.00	2198.0	210	10.5
2	5	751670.00	3381590.00	2076.0	220	9.4
3	5	752901.00	3378760.00	3142.0	421	7.5
4	8	760648.00	3371180.00	896.0	203	4.4
5	9	761420.00	3367260.00	4150.8	347	12.0
6	9	763188.00	3362740.00	1304.0	367	3.6
7	15	780206.00	3349630.00	4233.4	827	5.1
8	15	779444.00	3348490.00	3484.2	989	3.5
9	16	778978.00	3347080.00	5086.3	957	5.3
10	18	772025.00	3338690.00	3737.6	731	5.1
11	18	771813.00	3337880.00	2407.9	491	4.9
12	19	771284.00	3334680.00	3584.9	535	6.7
13	19	772945.00	3333750.00	2911.8	921	3.2
14	19	773983.00	3333670.00	3064.6	508	6.0
15	24	778216.00	3317770.00	5475.5	265	20.7
16	24	778967.00	3316600.00	5090.8	470	10.8
17	24	777941.00	3315210.00	6210.7	1144	5.4
18	26	780809.00	3308520.00	3104.9	435	7.1
19	30	788566.00	3290510.00	5394.9	1337	4.0
20	30	786175.00	3286810.00	9487.5	410	23.1
21	31	787709.00	3285640.00	5802.3	1123	5.2
22	34	802769.00	3279760.00	3969.4	576	6.9
23	40	830921.00	3271010.00	3658.4	373	9.8
24	40	830582.00	3269960.00	2321.2	453	5.1
25	41	831334.00	3268950.00	2739.0	280	9.8
26	46	832138.00	3246420.00	1590.0	337	4.7
27	46	832784.00	3243200.00	1299.9	255	5.1
28	52	840943.00	3216400.00	2046.0	504	4.1
29	52	841578.00	3216480.00	1694.0	502	3.4

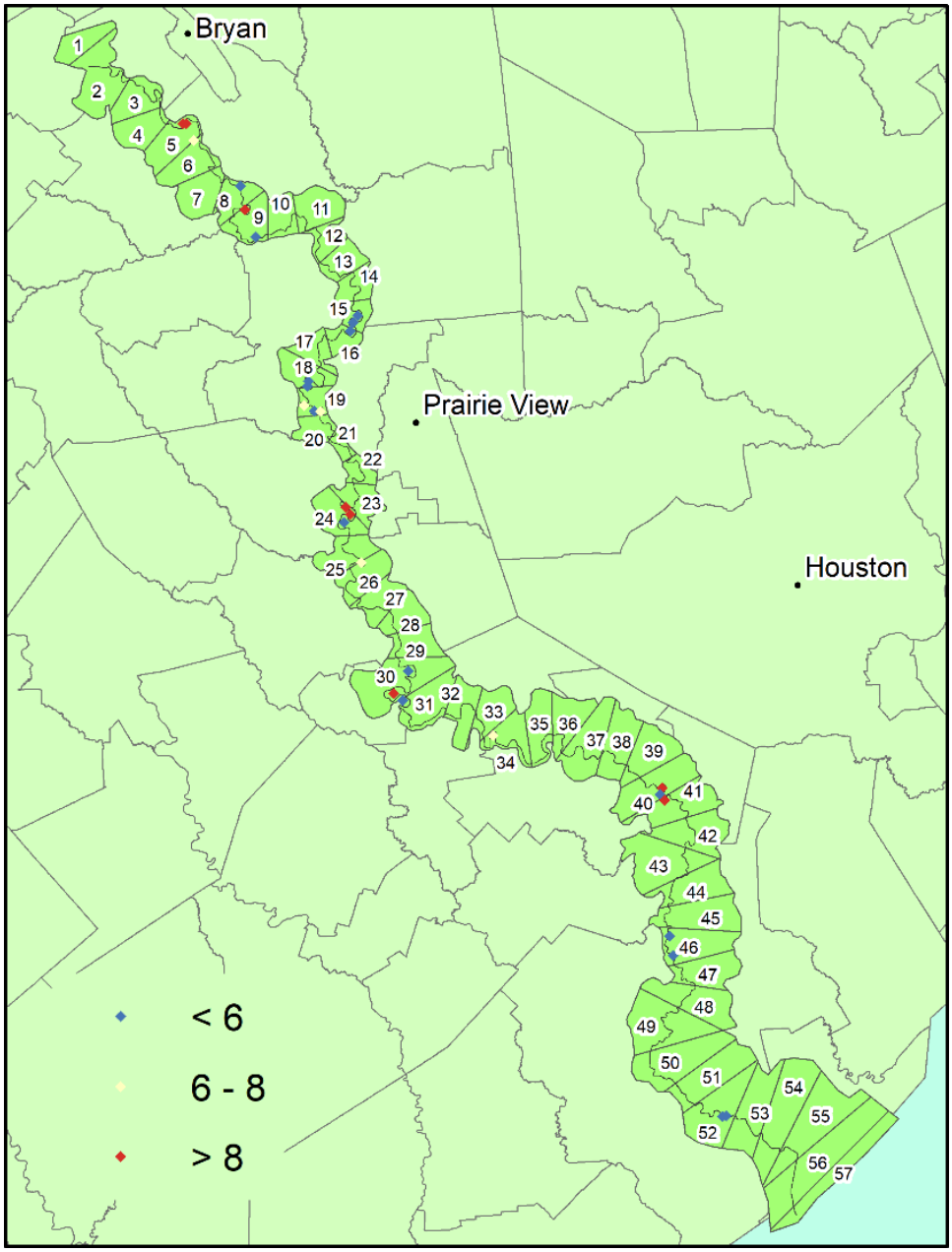

Figure 5.14. Examples of the meander bends on the LBR with a potential for chute cutoffs with stability values of < 6, 6–8, and > 8.

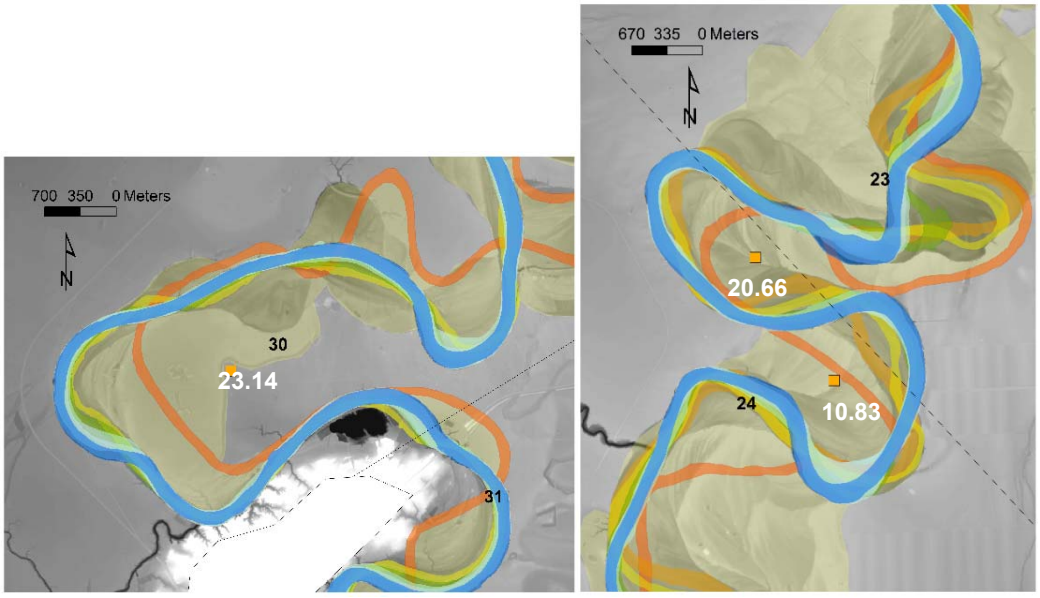

Figure 5.15. Examples of the meander bends on the LBR with a high potential for chute cutoffs at floodplain sections 30 (left) and 24 (right). the river channel is represented at the years 1960 (the most bottom boundary), 1980, 1996, 2004, 2010 (the top boundary). The numbers in white color show the chute cutoff stability ratio for the corresponding bends.

5.6. HCCZ and CZZ

Based on our results from the historical analysis of channel migration (i.e., the rates of change and areal change) in the LBR over the study period (1910–2010), and the analysis oxbows, meander scars, and other types of paleo-channels, we delineated the HCCZ (Figures 5.16–5.17).

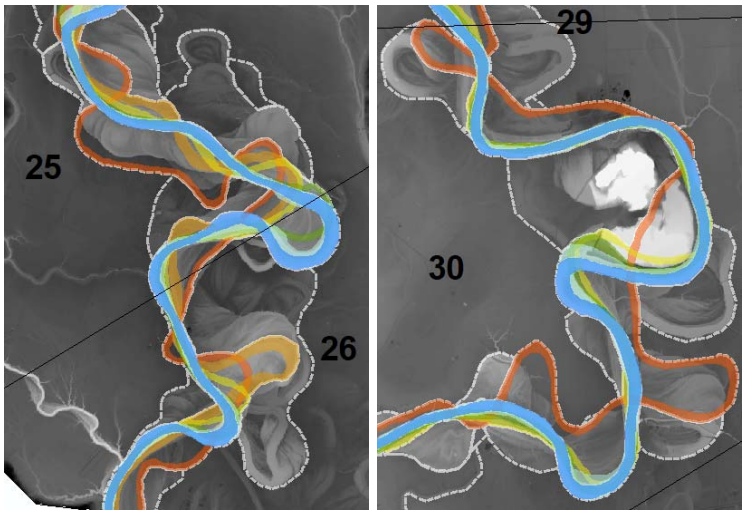

Figure 5.16. Examples of the HCCZ delineation at floodplain sections 25–26 (left) and 30 (right). The river channel is represented at the years 1919 (the most bottom), 1953, 1960, 1980, 1996, 2004, 2010 (the top).The dashed line represents the HCCZ boundary.

The width of boundaries for the historical channel change zones are directly related to the recent and ancient activity that the channel has undergone. In short, it is a snapshot of how active that channel is now and how it has been—the primary driver between speed of meander evolution is either erosional heterogeneity in the floodplain itself, human modification, or nearby channel changes—such as meander cutoffs (Hooke, 1995). The purpose of this analysis is to identify locations where there is extensive or poor channel migration for a given area. Given that, sections that have exhibited the most profound historical changes are attributed to regions comprised of floodplain sections 37-40, 29-30, and 22-27. In all of these locations, there is extensive evidence of meander scrolls and oxbow depressions that indicate past channel activity. Differences in this and locations in the northern part of the study area may be partially attributable to quality of data issues. We were able to obtain extensive LiDAR coverage for the lower part of the study area (sections 22-56). However, we only had the usage of National Elevation Dataset (NED) data for the upper part. The 10m DEM—which was mostly formed by older and more generalized DEM datasets at 30 meters resolution—could not be used to identify some of these relict channel features reliably—although we adapted texture-based methods (for image visualization) to try to infer what the texture is for a given location and maximize detection. In particular, we used the DEM along with a DEM processed with a Sobel Filter (Vincent and Folorunso, 2009) to try to highlight and pick up these textures and edges. However, there are constrained channels that are not inside the confines of the lower-quality NED dataset. Those are primarily near the coast. It is not currently understood why they do not migrate with the veracity that their northern, more incised neighbors do.

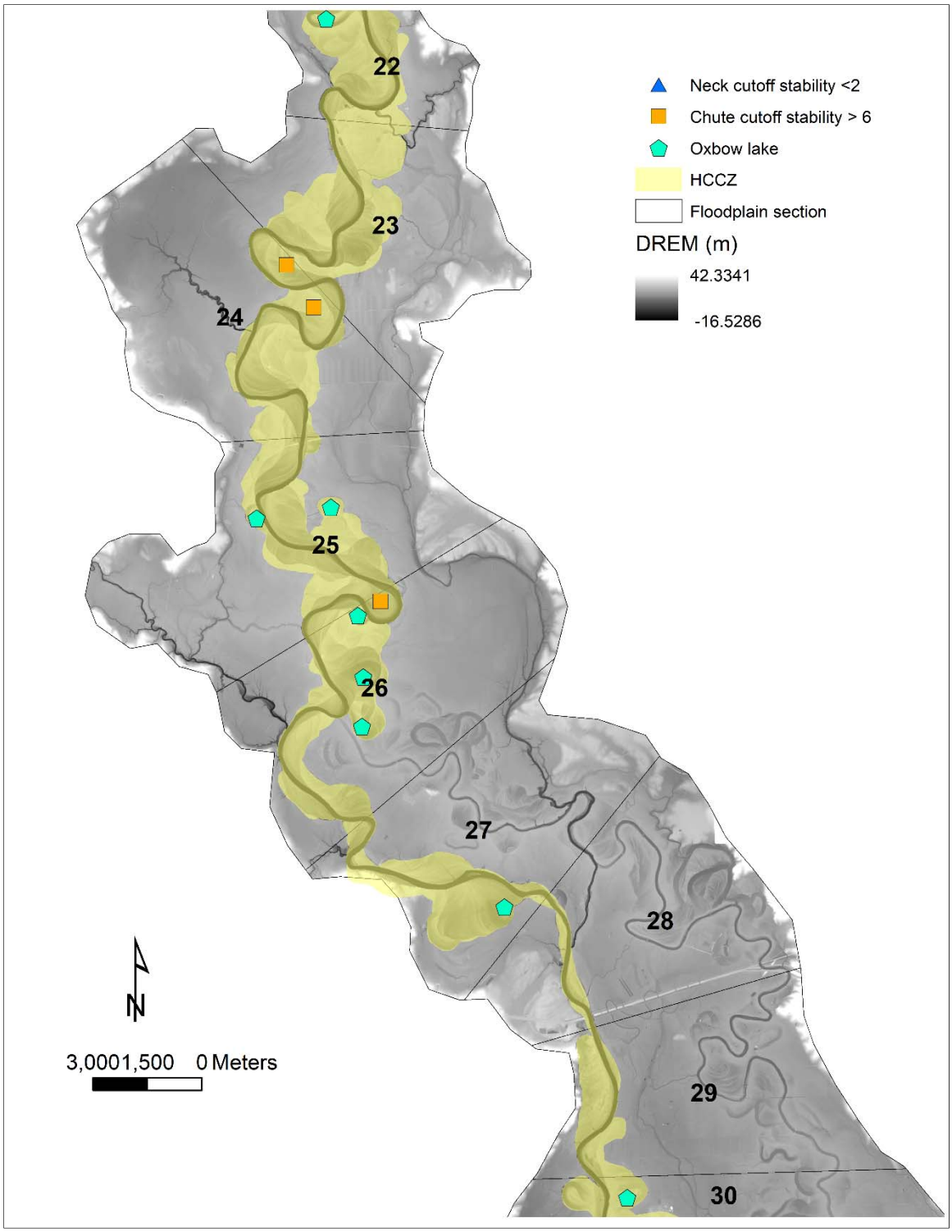

Figure 5.17. The historical channel change zone (HCCZ) on the LBR along the floodplain sections 22–29.

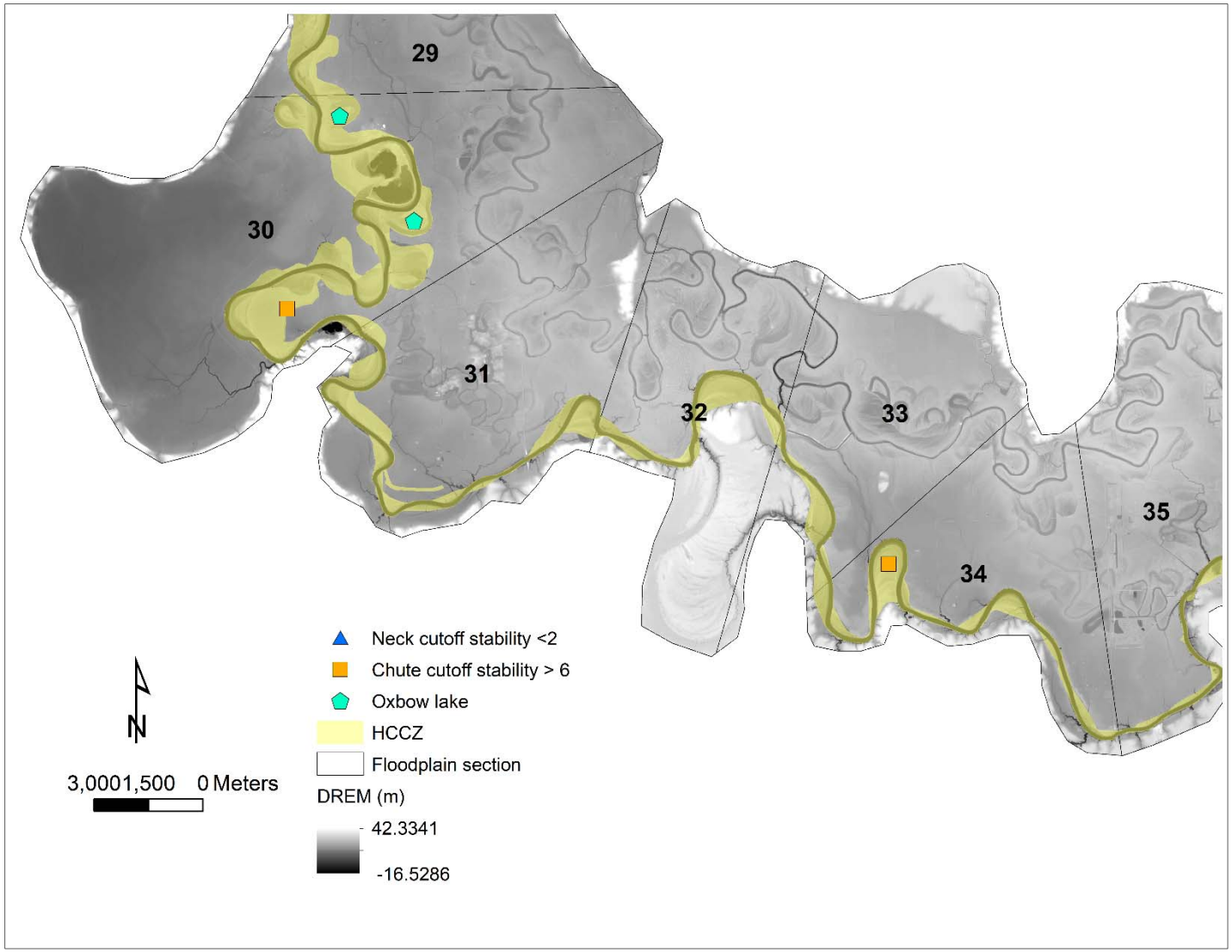

Figure 5.17 (cont'd). The historical channel change zone (HCCZ) on the LBR along the floodplain sections 30–35.

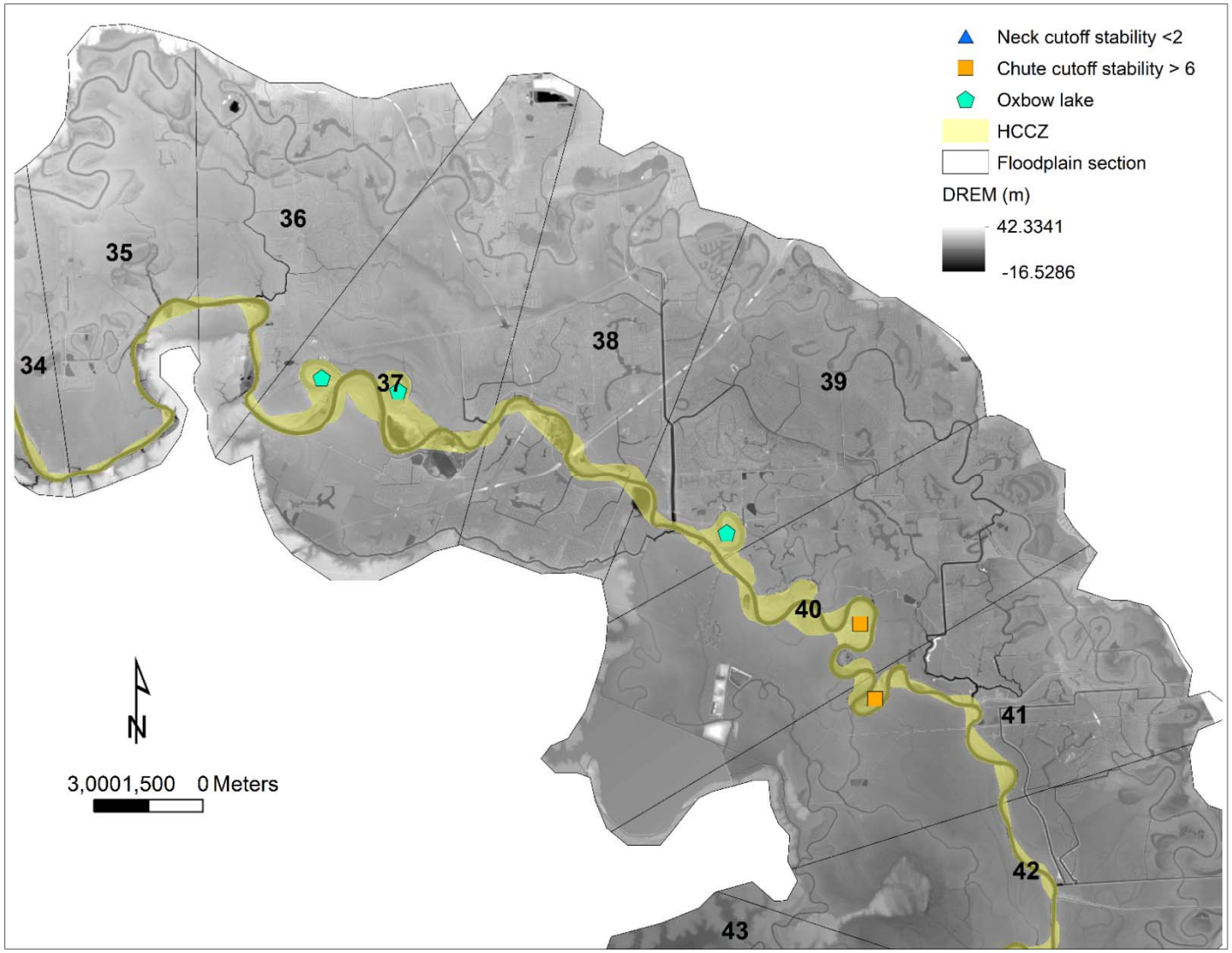

Figure 5.17 (cont'd). The historical channel change zone (HCCZ) on the LBR along the floodplain sections 35–41.

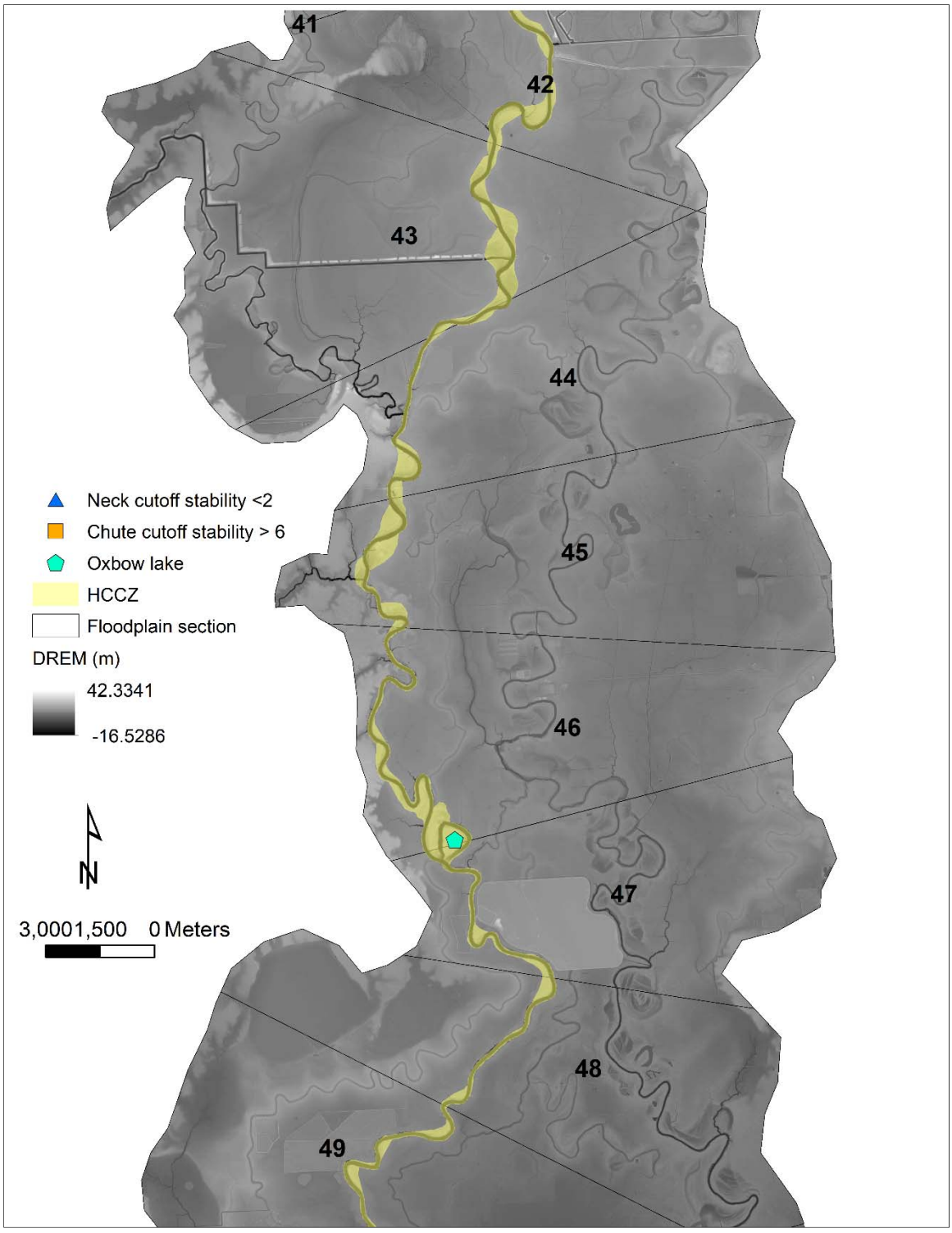

Figure 5.17 (cont'd). The historical channel change zone (HCCZ) on the LBR along the floodplain sections 42–48.

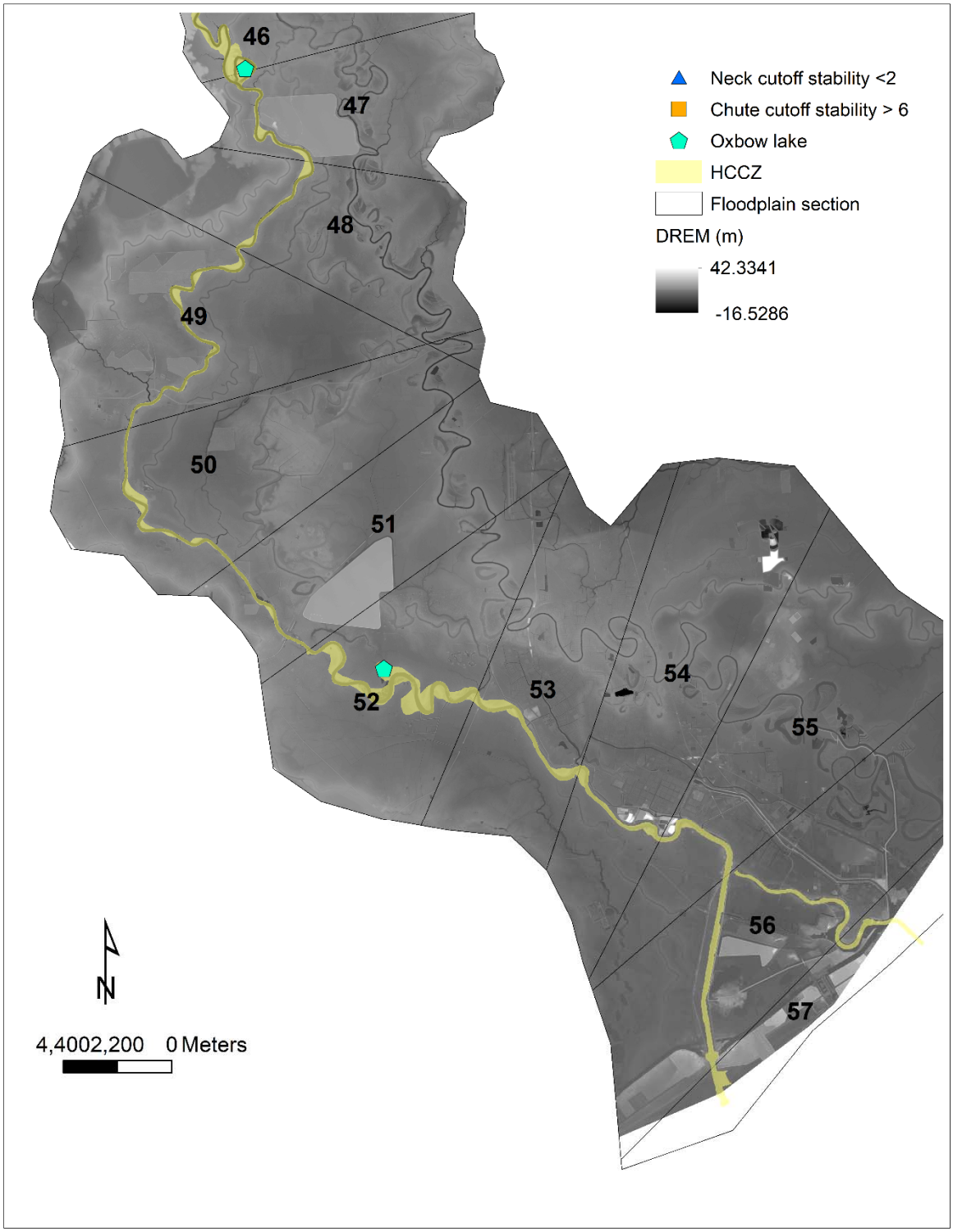

Figure 5.17 (cont'd). The historical channel change zone (HCCZ) on the LBR along the floodplain sections 47–56.

By using channel change zones (CCZ), we showed the historical channel change patterns (HCCZ) as well as the potential areas of erosion/migration due to channel migration (Figure 5.18–5.20) with the aim of providing insights into future gradual and abrupt changes that could result from high rates of connectivity during critical floods. From the summarized maps derived from the channel change zone, we consider two factors, the avulsion hazard zone (AHZ) and the erosion hazard zone (EHA). We analyze these zones in two ways, by analyzing how much area and how many zones potentially are at risk by a channel migration (erosion) or local avulsion (Phillips, 2007) within a floodplain section (Figure 5.21).

The CCZ can be seen as a *first step product* for evaluating future trends in channel change in the LBR with the aim of predicting areas at risk due to fluvial processes. Understanding of the CCZ can help decrease river hazards risks associated with bank erosion and channel migration, and potentially avulsions, by guiding infrastructure and urban development along the river and on its floodplain areas based on these risk areas. Based on the preponderance of evidence, from the CCZ and gradient advantage, the locations most susceptible to hazards from fluvial migration and avulsion would be the upper half of the study area, between floodplain sections 3-28. Within those areas, there are two hotspots. Those are sections 2 through 9 and 18 through 28. These zones, taken together, represent locations where there are extensive ancient and extant meander migration that have created floodplain depressions in the forms of oxbow lakes, sloughs, and potential for chute style avulsions. Furthermore, many of these locations feature elongate meander necks which are close to cutoff conditions.

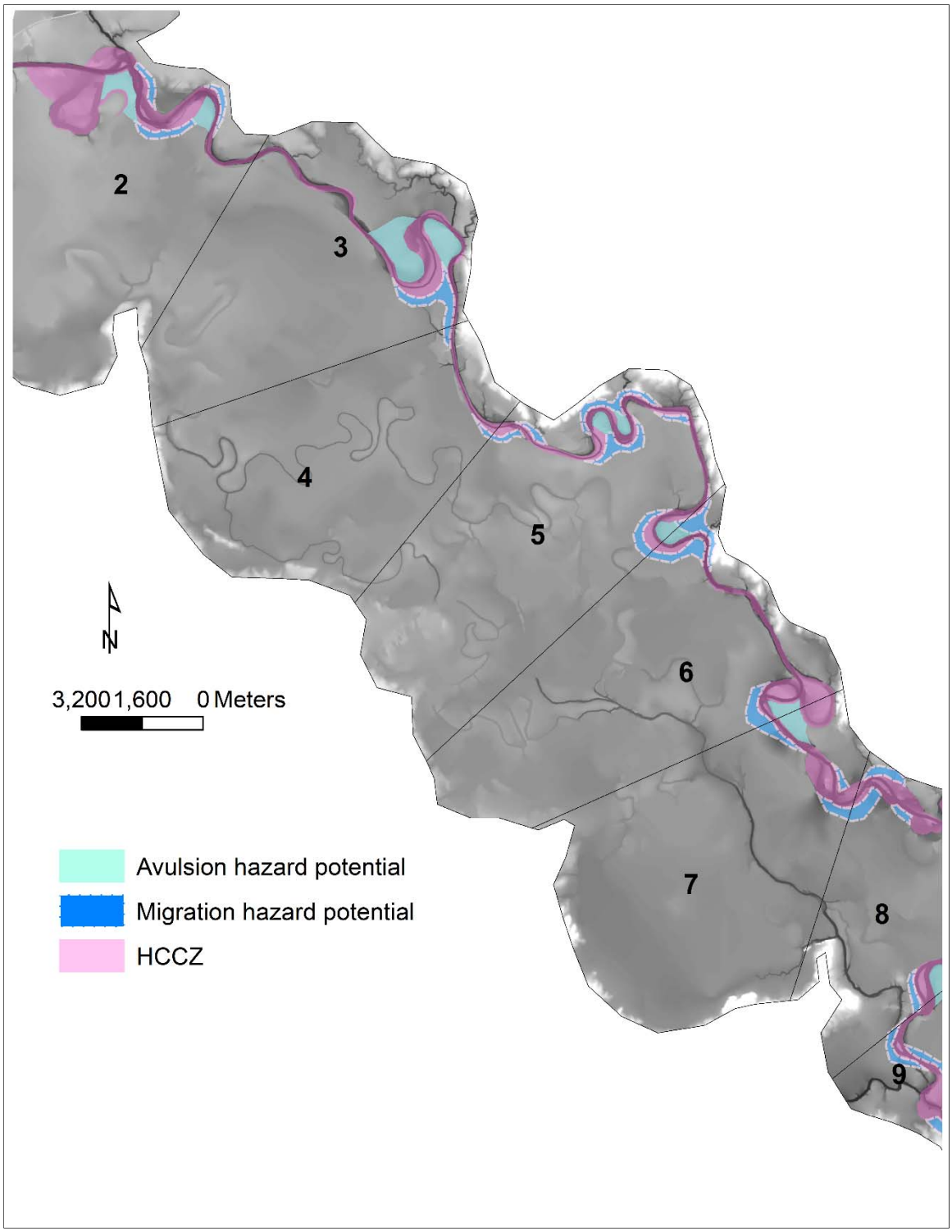

Figure 5.18. The historical channel change zone (CCZ) on the LBR along the floodplain sections 2-8.

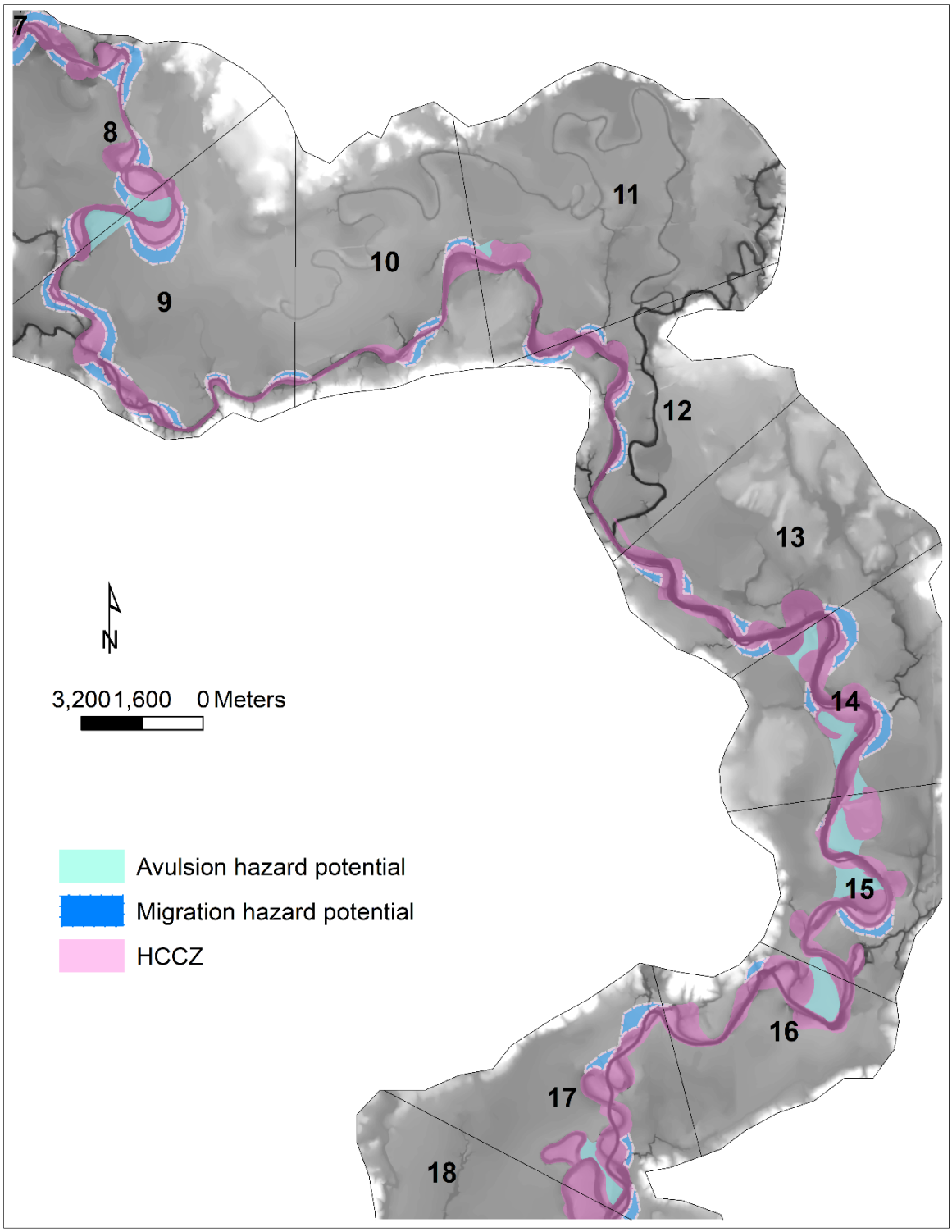

Figure 5.18 (cont'd). The historical channel change zone (HCCZ) on the LBR along the floodplain sections 8-17.

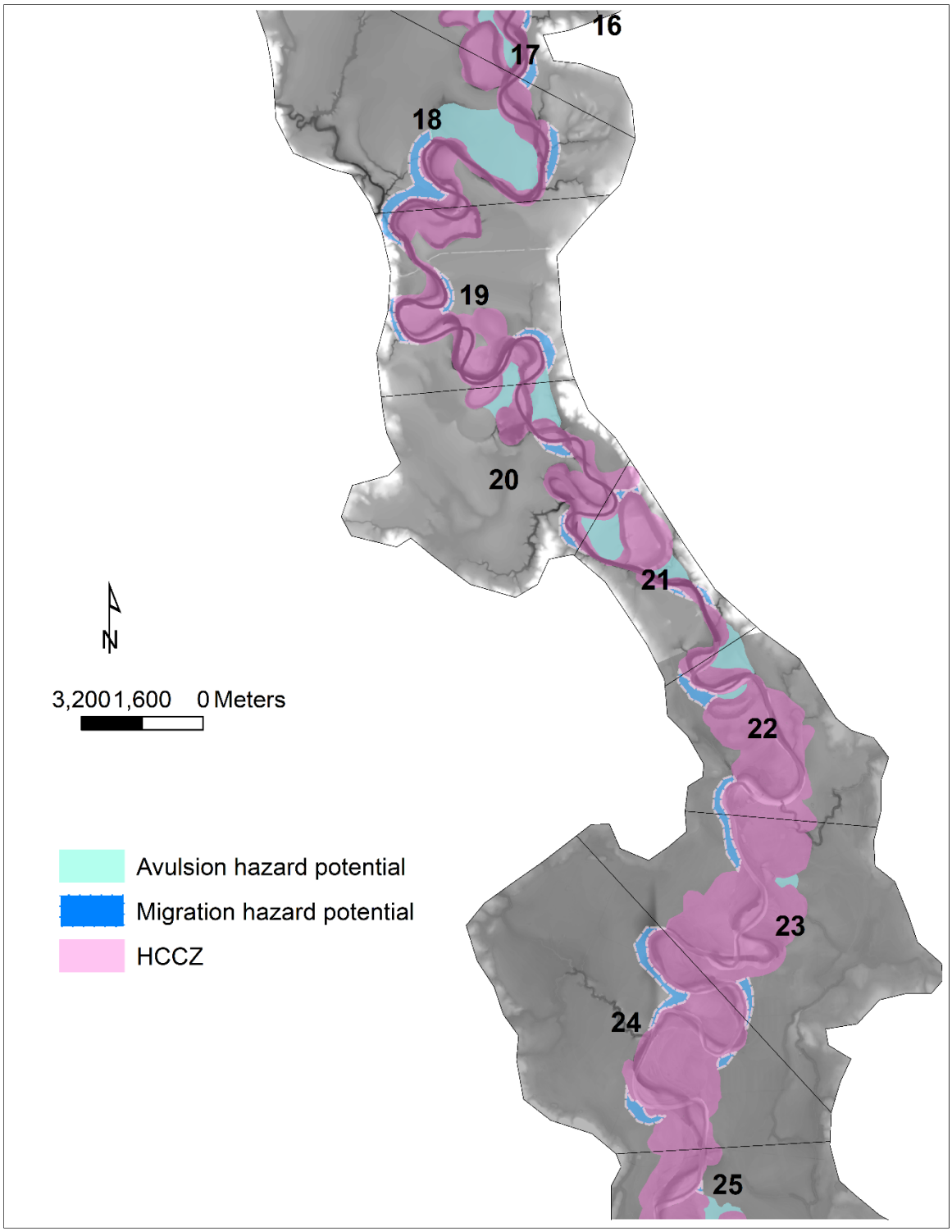

Figure 5.18 (cont'd). The historical channel change zone (HCCZ) on the LBR along the floodplain sections 18–24.

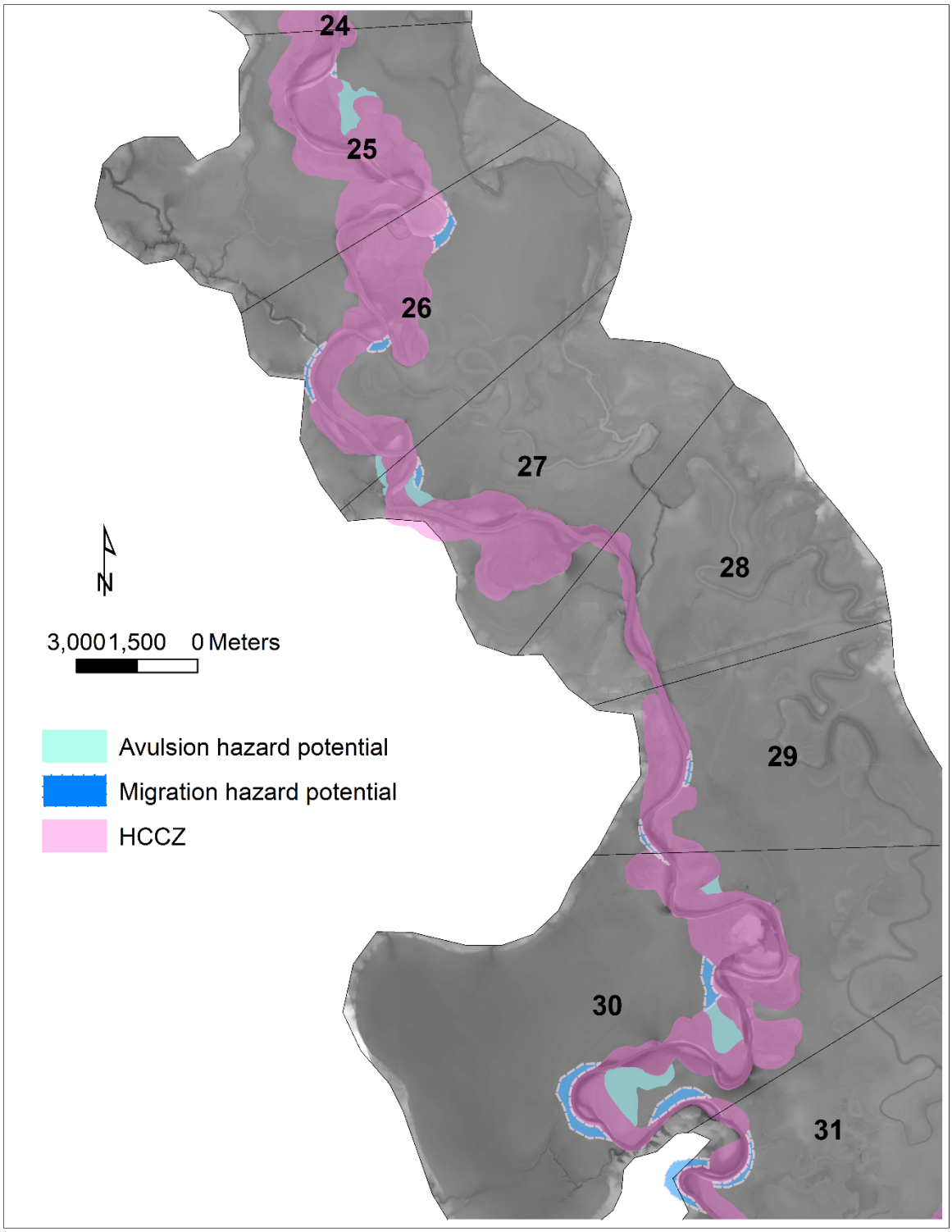

Figure (cont'd). The historical channel change zone (HCCZ) on the LBR along the floodplain sections 25-30.

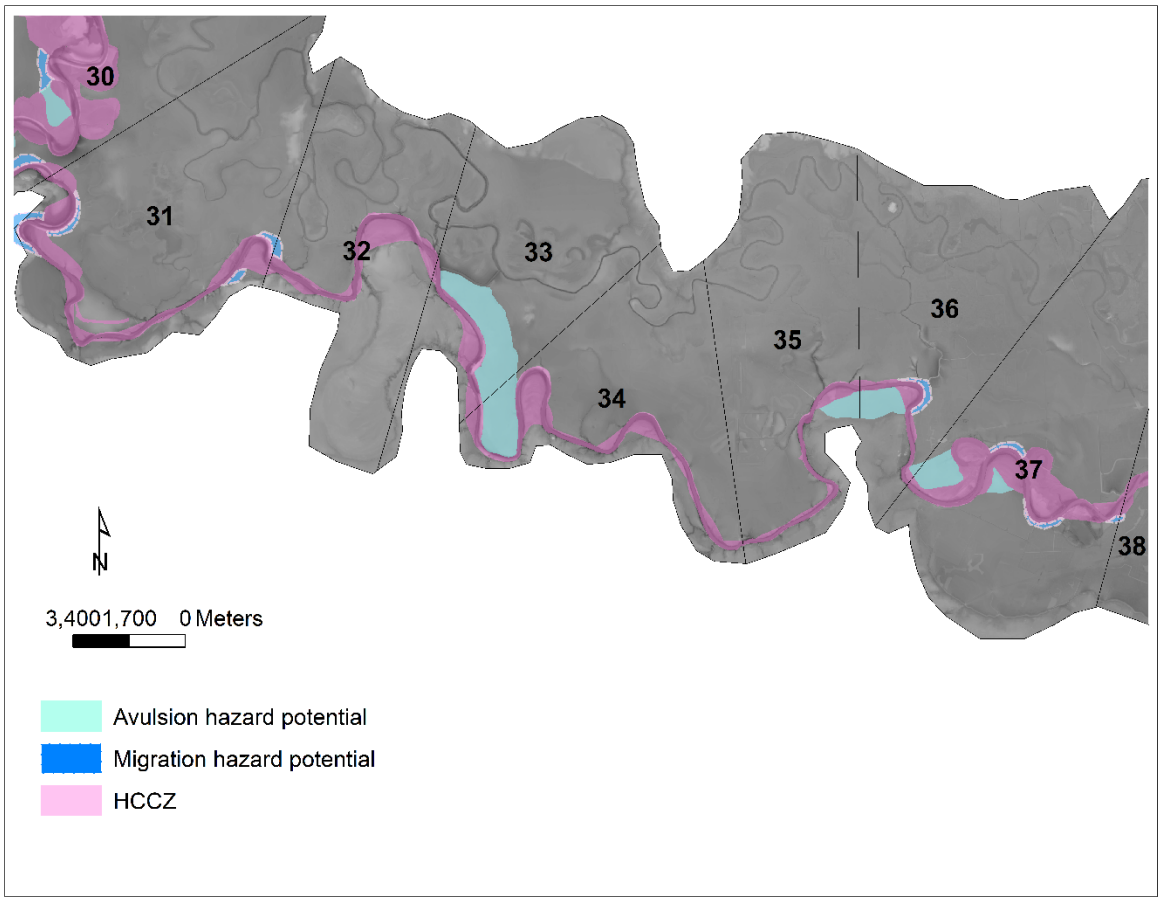

Figure 5.18 (cont'd). The historical channel change zone (HCCZ) on the LBR along the floodplain sections 31-37.

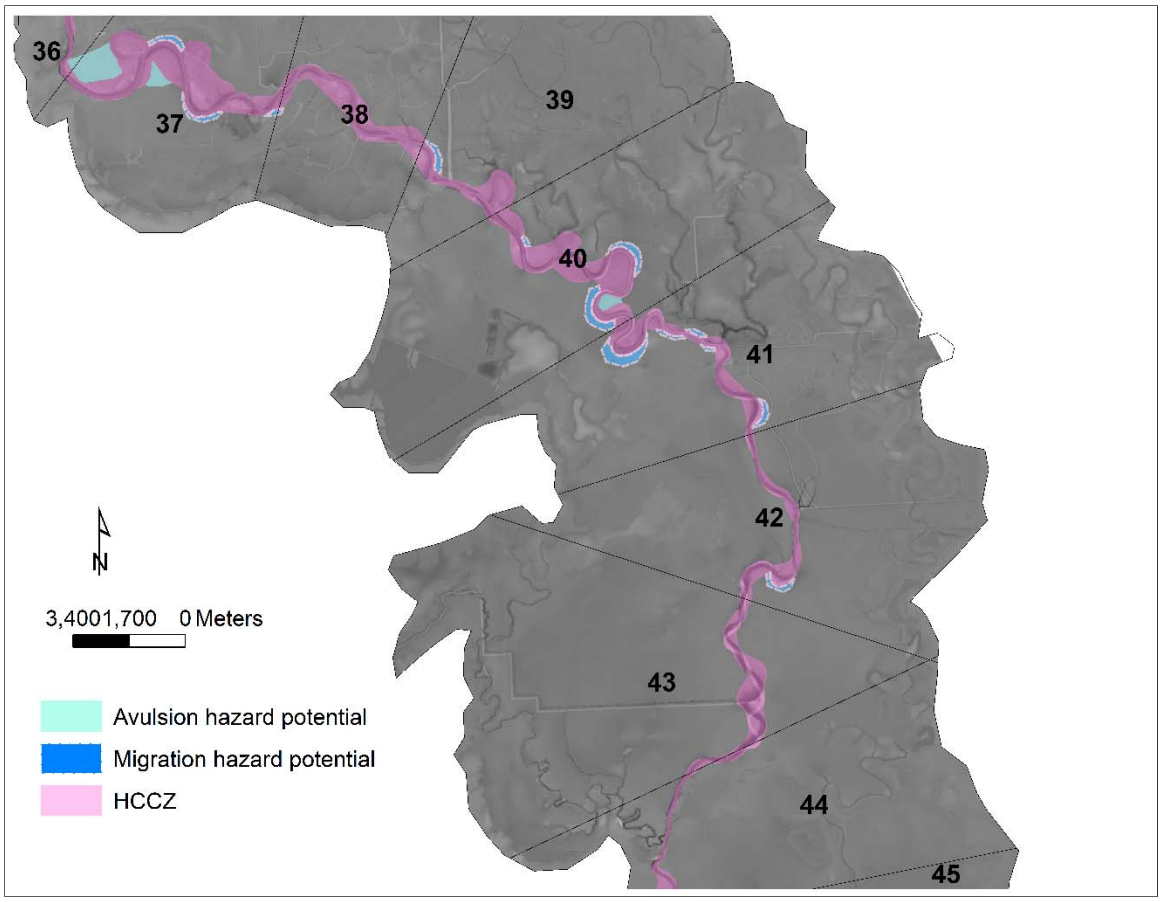

Figure 5.18 (cont'd). The historical channel change zone (HCCZ) on the LBR along the floodplain sections 38-43.

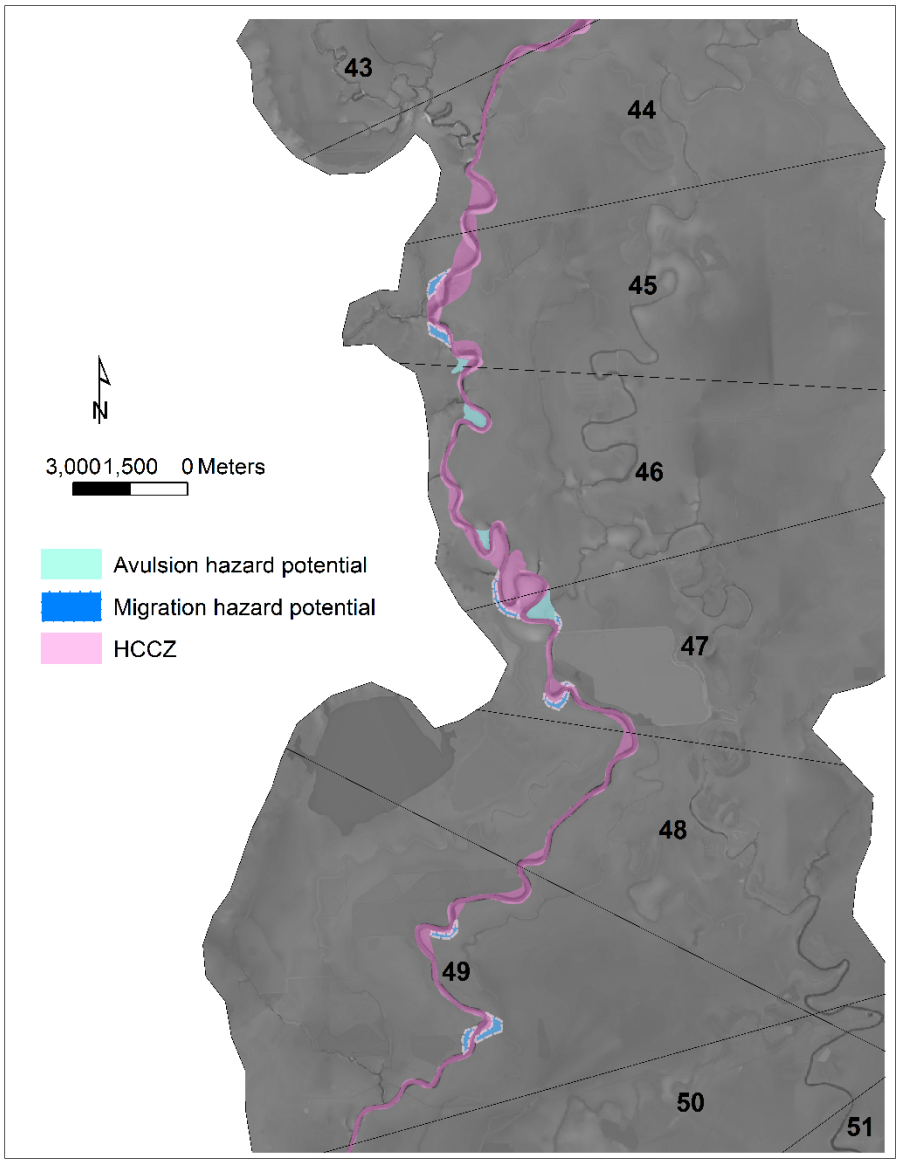

Figure 5.18 (cont'd). The historical channel change zone (HCCZ) on the LBR along the floodplain sections 44-49.

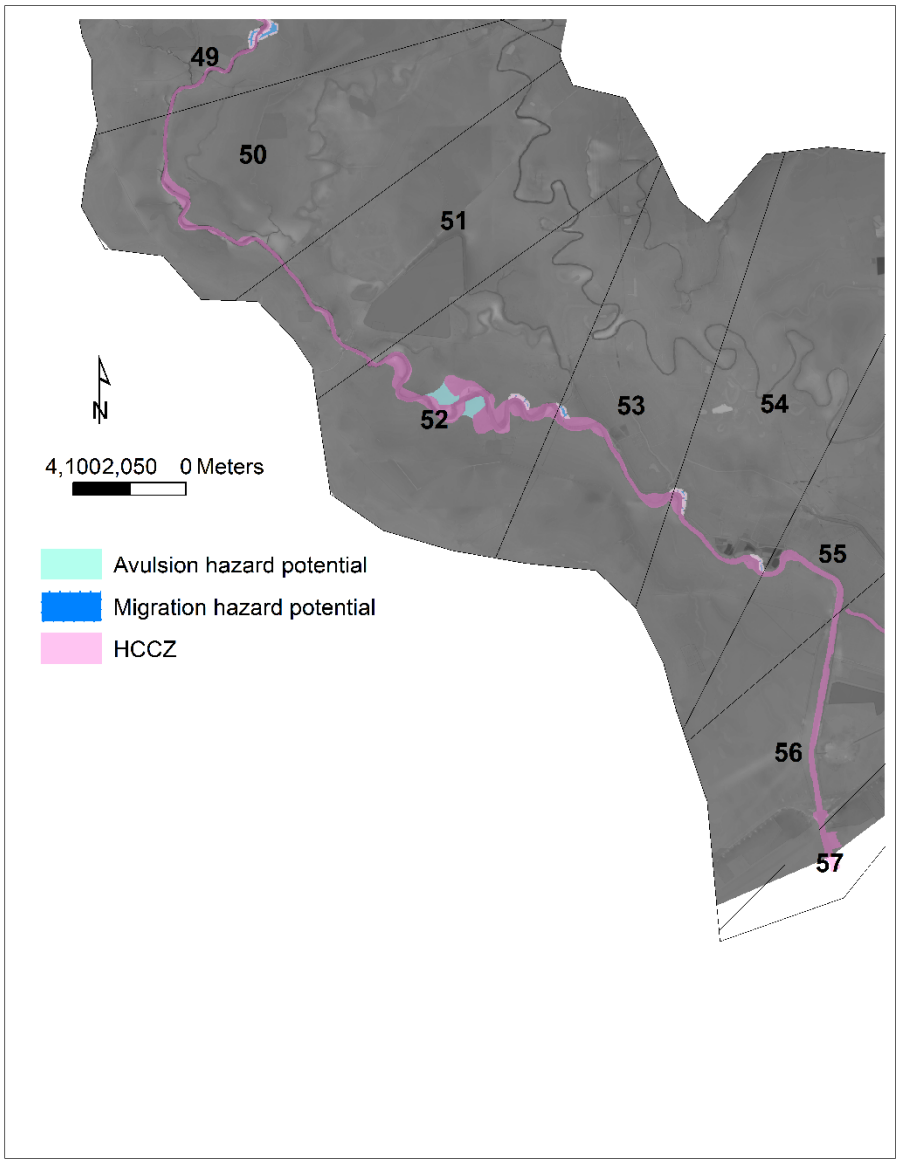

Figure 5.18 (cont'd). The historical channel change zone (HCCZ) on the LBR along the floodplain sections 50-56.

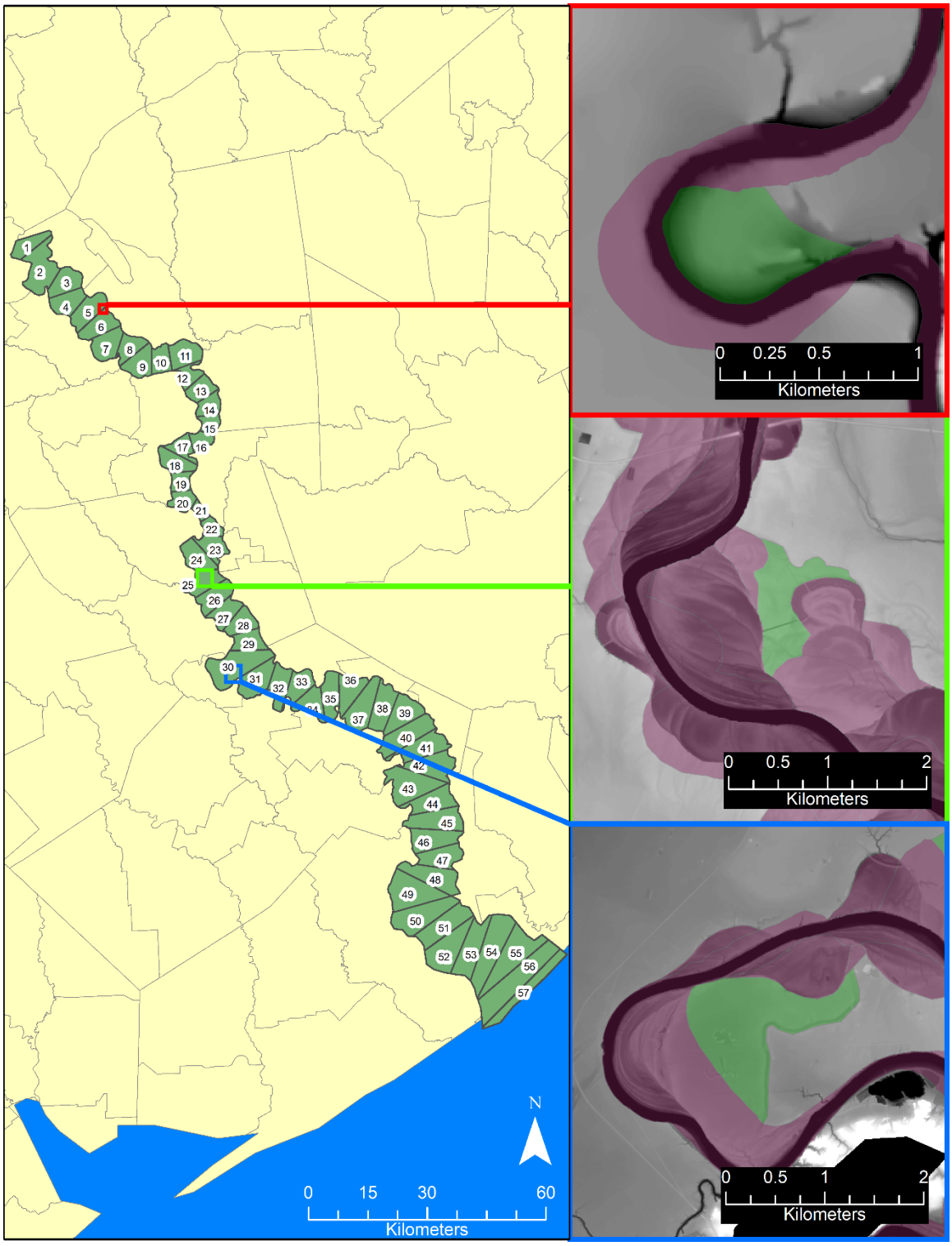

Figure 5.20. The channel change zone (CCZ) on the LBR along the floodplain sections 5, 25, and 30. The purpose area shows the HCCZ and the green area shows the addition to HCCZ representing the CCZ.

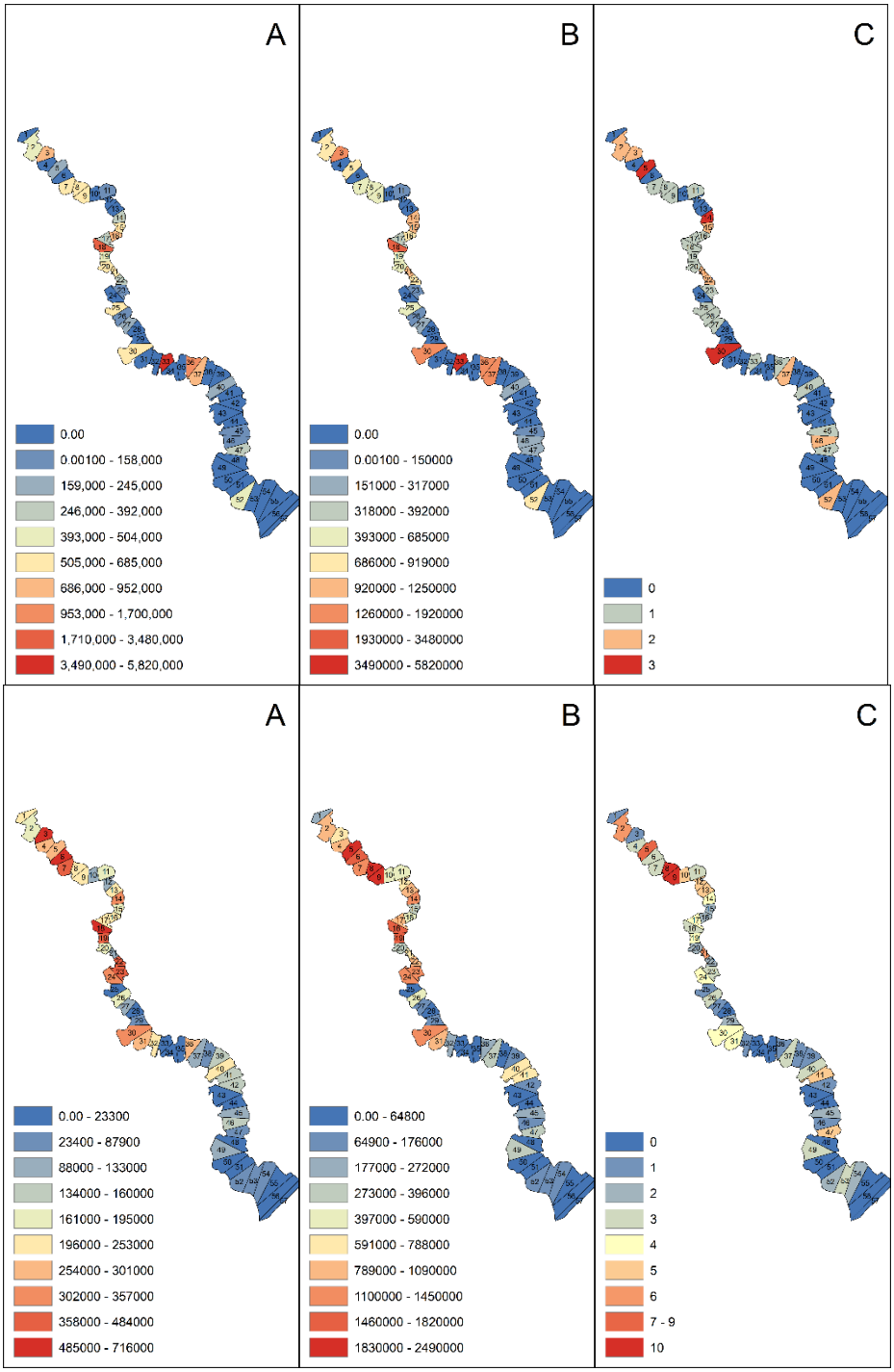

Figure 5.21: Numerical summaries of areas (m^2) occupied by avulsion hazard zones (top) and erosion hazard zones (bottom). Those numerical summaries are: A – Mean, B – Sum, and C – Count.

6. DISCUSSION

6.1. Gradient advantages

Our findings shows that scale-dependent environmental factors can be important cues for finding large gradient advantages (Phillips 2011). In terms of regional controls, we have down-valley slopes that can be attributed to basin infilling (Taha and Anderson 2008) and cross-valley slope that can be partially attributed to tectonics (Taha and Anderson 2008). Both of these factors act in ways that can either enhance the gradient advantage with a higher cross-valley slope and lower down-valley slope or vice-versa (Jones and Schumm 1999). Taking the river itself into account, there are the effects of natural levees and migration history. Furthermore, with migration history comes floodplain features—such as oxbow lakes, sloughs, crevasse splays, and abandoned channels. These features, along with steep natural levees, can interact to either increase the local cross-valley slope via abandoned oxbows and sloughs (Phillips 2011, Phillips 2014) or decrease the cross-valley slope via crevasse splays (Aslan et al. 2005) and crevasse splay complexes (Taha and Anderson 2008).

As was the case in floodplain sections 22–28—where many floodplain features that enhance the cross-valley slope as one migrates from the banks of the LBR toward the valley, and the down-valley slope of 0.0002 was relatively low compared to the two regions immediately downstream. Both of these factors worked in favor of large cross-valley slopes and small down-valley slopes—which resulted in that region having the highest gradient advantage (Figure 5.4). The coastal region, floodplain sections 46–56, despite having a low down-valley slope identical to the aforementioned region, did not have as many accessible floodplain features. This is attributable to several factors. One is the relief of the main channel's natural levee. As the channel winds its way from zone 46 to zone 56, the natural levee gradually begins to have less relief, and hence less cross-valley slope. Furthermore, there is a large urban footprint in the City of Freeport as well as the two reservoirs, the Brazoria and Harris Reservoirs. Both structures bracketed the channel with man-made levees. Also, several of the abandoned channels have high-relief natural levees—so this would act to discourage flow in the event of flooding on the main channel. These factors colluded to make a region of generally intermediate gradient advantage.

Despite the high values attributed to sections 22–28, Phillips (2011) states that floodplain depressions—depending on their context—may enhance the occurrence of crevasse breach, but not lead to successful avulsions—at least in the context of making a new channel. Most

of the floodplain features and depressions in floodplain sections 22–26 are isolated, and would most likely lead to a local avulsion event—such as chute cutoffs. However, there are several potential streams for recapture on the valley leading away from the left bank of the channel. This would be known as avulsion by annexation (Slingerland and Smith 2004, Taha and Anderson 2008). Avulsion by annexation has been a more recent occurrence in geologic time (Taha and Anderson 2008). Throughout the mid Holocene, avulsion by progradation occurred throughout the LBR, and this is attributed to delta backstepping events throughout sea level histandards during that time, which implies that there is plenty of standing of water—which the authors describe as accommodating space.

Comparing gradient advantage results obtained from the LBR with other sites, past research shows highly variable gradient advantages for different study sites. For instance, the gradient advantage for avulsions to occur was estimated to be a value of ~5 by Jones and Schumm (1999) and Slingerland and Smith (1998). Other past research also suggests values from 3 to 5 indicate a high probability of avulsion (Tornqvist and Bridge 2002). On the other hand, Aslan et al. (2005) found gradient advantages between 16 to 110, and typically greater than 30, based on their study on the lower Mississippi River. To further add weight to this variability, Phillips (2007a) found gradient advantages as small as 2.54 and over 65 for his selected sites on the Brazos River. Our work with gradient advantages on the LBR also fall in similar ranges of values between 2 and 135, when only the natural environment is considered. With man-made obstructions, chiefly in the form of manufactured levees, we measured gradient advantages of over 400. Issues encountered in our study of the LBR might also help shed light the true value of the gradient advantage—as the gathering of field and remotely-sensed data to support the finding of this critical factor can be standardized.

In the form of a ratio, the gradient advantage is a very useful characteristic that discusses the topographical contribution of the environment to setup avulsions (Jones and Schumm 1999). It is quite intellectually tractable, and it agrees with our generalized, although incomplete, understanding of the avulsion process itself. However, there are also issues in both the idea and in its implementation. In terms of the idea, the principle component missing appears to be that of scale (Hajek and Wolinsky 2012). As has been found by other researchers (Aslan et al. 2005, Phillips 2011, Phillips 2014), there are local features on the floodplain that serve to add heterogeneity to a valley's topography. These features can profoundly affect the flow as it breaches alluvial ridges or natural levees. However, at what scale—relatable to the river channel itself—is a given feature significant enough to possibly

alter the gradient advantage for that reach of the main channel? This seems to be an unanswered question with respect to our understanding of avulsion (Hajek and Wolinsky 2012).

When it comes to implementation, the most common manner to measure the gradient advantage is via the cross-section or transect. As used in our work, cross-valley profiles are derived from transects that are sampled on 5 meter LiDAR DEMs. By studying and analyzing these profiles, we found a multitude of local factors, natural and urban, that can contribute to a wide range of slope advantages or make calculating them meaningless—as it prevents the channel from overflowing its banks. However, the effect of these elements on avulsive setup on the channel banks cannot be taken and fully understood from the transect/profile alone. As our rubric in the methods suggest—we actively look at the elevation data to see if a given 'spike' is or 'pit' prismatic with the channel. If not, it is ignored. Therefore, we are innately using three-dimensional knowledge on an inherently two-dimensional analysis. Based on our experience, a three-dimensional approach would be more efficient and more easily standardized.

Therefore, the gradient advantage has the potential to have greater context and better inform researchers and stakeholders if:

- We create link valley slopes and objects on the floodplain to a scale inherent to the fluvial process—such as the river width, depth, or wavelength.
- Develop a three-dimensional implementation of the gradient advantage to evaluate avulsion setup with three-dimensional data, so that we can inherently understand a four-dimensional problem—3-d setup and trigger of avulsion with time as the 4th dimension.

6.2. Historical river channel change

Historical river-channel change analysis was conducted, with particular attention to computation and evaluation of rates of channel change. Specifically, average change rate (ACR) (m/yr) and normalized average areal change (NAAC) rates ($m^2/m^2/yr$) were calculated by floodplain section. The spatial distributions of both ACRs and NAAC rates were similar, in that higher values for both rates were concentrated in the upper ~half of the LBR, with generally distinctly lower change rates skewed toward sections in the lower half of the LBR floodplain. We then determined that there are clear associations between ACRs and linear trends in valley width, and between NAAC rates and trends in valley width. The upper portion of the LBR floodplain exhibits a relatively modest decreasing trend in valley width as

a function of distance in the downstream direction (with higher ACR and NAAC values), with a marked increasing trend further downstream in the lower half of the LBR (corresponding with lower or particularly low ACR and NAAC values).

There are various sources of potential error in the computed rates of channel change, which stem from the production of the multitemporal digital channel planforms boundaries. Such sources could have also had an effect on the locational probability analysis results. Differences in survey and map-production methods from the older to the newer maps have an effect on the accuracy or rate and/or probability calculations. Aerial photographic stereo pairs, which could enhance image interpretation during the digitization process, were not employed, and the scales of the aerial photographs used for digitization varied and were not always necessarily ideal. For example, the scale of the 1919 map is 1:62,500, whereas the scales for the 1910 maps are larger (1:31,680 and 1:24,000). The georeferencing/rectification process for the topographic maps and the aerial photographs used a basis for digitizing the river channels, as well as the interpretation digitization procedures could also be factors. Some error associated with the digital spatial representation of the river channels may be a result of multiple individuals being involved in the digitization process. This potential source of error, or variability in spatial representation of the river channels, was minimized by common training procedures among team members for aerial photograph/topographic map interpretation and digitizing of the relevant geomorphic features (Graf, 2000).

Regarding the channel change analysis in particular, we performed calculations of rates of change with the available data in each floodplain section. Some of these years entail the longest time ranges of topographic map coverage, beginning in the early 1900s (i.e., 1910 or 1919). This longer time period provides more opportunity for river planform migration, relative to a shorter time period. For the relevant sections, it is possible that some of the observed change in the river planform position could be due to potential higher spatial inaccuracies with the 1910 and/or 1919 maps (e.g., due to the mapping methods and datum used, shrink/swell of the hard-copy paper maps in storage as a function of humidity fluctuations over time; and increased difficulty of geometrically rectifying/georeferencing these older maps due to sparsity of GCPs, etc.). Any or all of these factors could have affected the variability in the widths of the computed river planform boundaries, and thus, all other analysis performed utilizing these boundaries.

6.3. Insights on potential avulsions

Moreover, the migration patterns of meandering rivers are also influenced by a range of environmental factors which include but not limited to soil erosional heterogeneity (e.g., Güneralp and Rhoads 2011, Motta et al. 2012), land use land cover (LULC) (spatially variable above- and below-ground tree biomass density (Güneralp et al. 2013), LULC change (e.g., agriculture, urbanization, mining) and water and land management practices (e.g., forest management, damming, irrigation). Some of these can cause changes in the soil erodibility while the others may alter the routing of sediment and wood and change flow regimes (Güneralp and Rhoads 2011, Jones and Grant, 1996; Konrad and Booth, 2002; Booth et al., 2004).

Thus, a comprehensive CCZ map is expected to provide insights into future gradual and abrupt changes that could result from high rates of connectivity during critical floods. The CCZ can be seen as a *first step product* for evaluating future trends in channel change in the LBR with the aim of predicting areas at risk due to fluvial processes. Understanding of the CCZ can help decrease river hazards risks associated with bank erosion and channel migration, and potentially avulsions, by guiding infrastructure and urban development along the river and on its floodplain areas based on these risk areas.

6.4. Future work

Valley-scale avulsions are abandonment of long sections of an existing meander belt in favor of a more direct route across the existing floodplain. They are common in areas where rivers aggrade relative to their floodplain. These avulsions become the dominant mechanism of river deltas and alluvial fans where channel is a common process. As the rework thick river floodplain deposits, incorporation of avulsions into the simulation models is necessary for sedimentological studies. Modeling of avulsions requires book-keeping of river elevation changes relative to its floodplain. This could be done in an *ad hoc* manner (where a constant rate of rise can be assumed or by modeling the long-valley routing of bedload and regional elevation changes; such changes may result from tectonic processes and sea-level changes.

Howard (1996) indicates that although a variety of processes and constraints may be involved in avulsions, floodplain topography is the most influential factor. Therefore, the occurrence of avulsions needs to be modelled stochastically (Mackey and Bridge 1995). Howard (1992) offers a conceptual framework which allows incorporating an avulsion

probability into the simulation model which would address the uncertainties related to relative channel-floodplain elevations, bank and natural levee height, and possibly the magnitude of the sinuosity change and individual flood heights. Howard (1992, 1996) proposes an approach similar to that used for chute cutoffs. Due to the influence environmental factors, commonly the occurrence of chute cutoffs are treated stochastically in numerical models of river planform evolution (e.g., Howard 1996). In the case of avulsions, though, the probability of a diversion would be a function of levee height and relative channel and floodplain elevations (Mohrig et al., 2000).

In this study, we examined the meander cutoffs using stability rules developed empirically for neck and chute cutoffs. As a next step, the following approach proposed by Lewis and Levin (1983) can be used for determining chute cutoffs. Chutes may occur on the inner meander bends in a range of positions and channel curvatures. Depending on the radius of curvature at the time of cutoff, the chute channel may also show some variability in its surface area compared to that of truncated point bar sediments it was associated with (Lewis and Levin 1983). In fact, the relationship of $R/(Q)^{1/2}$, where R is the critical radius of curvature and Q is discharge, is considered as another important measure for cutoff formation (Joglekar 1971). The *R* is influenced by the Q; for a small Q, the water flow will follow a sharper bend or a smaller R than it will follow with a large Q. Past research based on both field and laboratory data has also shown channel width (W) is approximately proportional to $/(Q)^{1/2}$ (Inglis (1947, Jansen 1979, Knighton 1998). The relationship $R/(Q)^{1/2}$, thus, can be rewritten as a geometric ratio of the R and W (R/W). For a given R, if the channel width W increases, then the migration rate becomes negative for small values of this ratio. This may result in occurrences of cutoffs along the inner meander bend.

Moreover, for examining neck cutoff processes, we can employ simulation models. While neck cutoff processes have been incorporated into meander migration models (e.g., Howard 1992, 1996), due to the scarcity of the observations to explain the controlling factors, chute cutoff processes are difficult to incorporate into meander-migration models. Modeling the occurrence of chute cutoffs requires taking many variables into account. Moreover, chute cutoffs are more difficult to predict. Chute cutoffs involve the development of a new channel across the floodplain and such development is strongly influenced by the floodplain conditions such as topography, soil erodibility, presence and type of vegetation and constraints to the flow, such as rocks and structures and by flow-stage variations (sequence and intensity of floods). Thus, following a stochastic approach would be highly beneficial for

both neck and chute cutoffs predictions by allowing incorporating and/or examining the sensitivity of the neck cutoffs in the river systems to range of environmental conditions (e.g., changing discharge, sediment rates, soil erodibility due to human activities etc.).

7. CONCLUSIONS

In this study, we examined the setup potential of both the valley-scale and local-scale avulsions on the Lower Brazos River (LBR). In examining the potential of valley-scale avulsions, we focused on the concept of gradient advantage. In examining the local-scale avulsions, namely, meander cutoffs and those that can results from channel migration, we analyzed the channel migration over a period of 1910-2010. Based on our findings we conclude that:

- Hazards that involve fluvial processes consist of multiple factors, and these factors must be considered within context. Furthermore, these factors rarely are collinear—in that they do not often tend to increase or decrease in unison. Hence, an optimal scenario is to find means in which to weight these factors appropriately.

- The LBR valley is a tapestry of large and small-scale processes that work to affect meander evolution. In addition to its natural uniqueness, there are several human habitations next to the LBR, such as the communities of Rosenberg, Richmond, Sugarland, and Freeport. In response, humans have built structures—such as levees—to protect their assets. This has a tendency to reduce the potential of a river to fully evolve in the dynamic floodplain environment. Although our results from the analysis of gradient advantages suggest that very high slope ratio values are attributed to levees (> 300), it is not quite certain how a breach of one of these levees would affect the rest of the channel or floodplain—given that the other side of many of these levees are paved roads and human habitations.

- By measuring exclusively natural features on a river channel, we obtain gradient advantage values that range from 2 to 135, and this range is in agreement with the findings of past research, such as the work of Aslan et al. (2005) on the Mississippi River and that of Phillips (2007a) on the LBR. However, these ranges are much greater in the face of human development. It is unknown to the authors how factors similar to the human impact that we experience on the LBR would interact to alter gradient advantages for other study areas.

- The gradient advantage, as implemented with transects, is not sufficient to reliably determine the setup potential for a given environment. There is a tendency for profiles to capture smaller scale avulsion setup—such as chute or neck cutoffs (Gay, Gay, and Gay, 1998; Hooke, 1995).
- The portion of the study area at the floodplain sections 22–28 faces the largest potential for an avulsion event in the southern half of our study area (floodplain sections 22–56). However, that event cannot be guaranteed to result in a valley-scale avulsion, as its assessment is strictly by looking at the patchiness of floodplain depressions. Hence, it is up for analyst interpretation. Our analytical tool, the gradient advantage has no way to distinguish between the potential for a given avulsion type or style.
- Channel change zones (CCZ), which combines historical channel changes with the potential channel changes in the future can give us an analytical tool for determining which areas could be under risk from fluvial processes that are primarily expressed in catastrophic events—such as large floods.

8. REFERENCES

Abbe, T.B., Montgomery, D.R. 1996. Large woody debris jams, channel hydraulics, and habitat formation in large rivers. *Regulated Rivers: Research & Management* 12:201-221.

Alford, J.J., Holmes, J.C. 1985. Meander scars as evidence of major climate change in southwest Louisiana. *Annals of the Association of American Geographers* 75, 395-403.

Allen, J.R.L. 1965, A review of the origin and characteristics of recent alluvial sediments, *Sedimentology*, 5(2), 89–191.

Amoros, C., Bornette, G. 2002. Connectivity and biocomplexity in waterbodies of riverine floodplains. *Freshwater Biology*, 47(4): 761-776.

Arnaud-Fassetta, Gilles, et al. 2009. Fluvial geomorphology and flood-risk management. *Geomorphologic-Relief Processes Environment*, V2. pp. 109-128.

Aslan, A., Blum, M.D. 1999. Contrasting styles of Holocene avulsion, Texas Gulf Coastal Plain, USA. In Smith, N.D., Rogers, J., eds., *Fluvial Sedimentology VI*. Special Publication, International Association of Sedimentology. Oxford, Blackwell, p. 193-209.

Aslan, A., Autin, W.J., Blum, M.D. 2005. Causes of river avulsion: insights from the late Holocene avulsion history of the Mississippi River, U.S.A. *Journal of Sedimentary Research*, 75 (4): 650-664.

Blum, M.D., Price, D.M. 1998. Quaternary alluvial plain construction in response to glacio-eustatic and climatic controls, Texas Gulf Coastal Plain. In Shanley, K., McCabe, P., eds., *Relative Role of Eustasy, Climate, and Tectonism in Continental Rocks*. Tulsa, OK, Society for Sedimentary Geology, SEPM spec. publ. 59, 31-48.

Blum, M.D., Aslan, A. 2006. Signatures of climate vs. sea-level change within incised valley-fill successions: Quaternary examples from the Texas Coastal Plain. *Sedimentary Geology* 190, 177-211.

Blum, M.D., Morton, R.A., Durbin, J.M. 1995. "Deweyville" terraces and deposits of the Texas Gulf coastal plain. *Gulf Coast Association of Geological Societies Transactions* 45, 53-60.

Bridge, J.S., Smith, N.D., Trent, F., Gabel, S.L., Bernstein, P. 1986. Sedimentology and morphology of a low-sinuosity river: Calamus River, Nebraska Sand Hills. *Sedimentology*, 33: 851–870.

Camporeale, C., Perona, P., Porporato, A., Ridolfi, L. 2005. On the long-term behavior of meandering rivers, *Water Resources Research*, 41(12), 1-13.

Constantine, J.A., Dunne, T. 2008. Meander cutoff and the controls on the production of oxbow lakes. *Geology*, 36(1): 23-26.

Constantine, J.A., McLean, S.R., Dunne, T. 2010. A mechanism of chute cutoff along large meandering rivers with uniform floodplain topography. *Bulletin of the Geological Society of America*, 122(5-6): 855-869.

Collins, B.D., Montgomery, D.R. 2011. The legacy of Pleistocene glaciation and the organization of lowland alluvial process domains in the Puget Sound region: *Geomorphology*, v. 126, p. 174–185.

Collins, B.D., Montgomery, D.R., Sheikh, A.J. 2003. *Reconstructing the historical riverine landscape of the Puget lowland: Restoration of Puget Sound Rivers*. University of Washington Press, Seattle, WA, p. 79–128.

Collins, B.D., Montgomery, D.R., Fetherston, K.L., Abbe, T.B. 2012. The floodplain large-wood cycle hypothesis: A mechanism for the physical and biotic structuring of temperate forested alluvial valleys in the North Pacific coastal ecoregion: *Geomorphology*, v. 139-140, p. 460–470, doi: 10.1016/j.geomorph.2011.11.011.

Crosato, A. 2008. *Analysis and Modelling of River Meandering*. Published PhD thesis, Delft University of Technology. IOS Press: Amsterdam.

Dunn, D.D., Raines, T.H. 2001. *Indications and Potential Sources of Change in Sand Transport in the Brazos River, Texas*. U.S. Geological Survey Water-Resources Investigations Report 01-4057.

Erskine, W., McFadden, C. Bishop, P. 1992. Alluvial cutoffs as indicators of former channel conditions. *Earth Surface Processes & Landforms*, 17(1): 23-37.

Ethridge, F.G., Skelly, R.L., Bristow, C.S. 1999. Avulsion and crevassing in the sandy, braided Niobrara River: complex response to base-level rise and aggradation. In: Smith, N.D., Rogers, J., *Fluvial Sedimentology VI*. Special Publication of the International Association of Sedimentologists 28, Blackwell, Oxford, pp. 179–191.

Friedkin, J.F. 1945. *A Laboratory Study of the Meandering of Alluvial Rivers*. U.S. Army Corps Eng., Waterways Exp. Stn., Vicksburg, 40 pp.

Gay, G.R. et al., 1998. Evolution of cutoffs across meander necks in Powder River, Montana, USA. *Earth Surface Processes and Landforms*, 23(7): 651-662.

Gibling, M.R., Tandon, S.K., Sinha, R., Jain, M. 2005. Discontinuity-bounded alluvial sequences of the southern Gangetic Plains, India: Aggradation and degradation in response to monsoonal strength, *Journal of Sedimentary Research*. 75, 369–385, doi:10.2110/jsr.2005.029

Gillespie, B.M., Giardino, J.R. 1997. The nature of channel planform change —Brazos River, Texas. *Texas Journal of Science*, 49, 108-142.

Gilvear, D., Winterbottom, S. Sichingabula, H. 2000. Character of channel planform change and meander development: Luangwa River, Zambia. *Earth Surface Processes and Landforms*, 25(4): 421-436.

Graf, W. L. 2000. Locational probability for a pammed, urbanizing stream: Salt River, Arizona, USA. *Environmental Management* 25(3):321-335.

Güneralp, İ., Rhoads, B.L. 2009. Empirical analysis of the planform curvature-migration relation of meandering rivers, *Water Resources Research*, *45*(9).

Güneralp, İ., Rhoads, B.L. 2010b. Spatial autoregressive structure of meander evolution revisited, *Geomorphology*, *120*(3-4), 91-106.

Güneralp, İ., Rhoads, B.L. 2011. Influence of floodplain erosional heterogeneity on planform complexity of meandering rivers. *Geophysical Research Letters*, 38(14).

Güneralp, İ., Filippi, A.M., Hales, B. 2013. River-flow boundary delineation from digital aerial photography and ancillary images using Support Vector Machines. *GIScience & Remote Sensing*, 50(1), 1-25, doi:10.1080/15481603.2013.778560.

Hajek, E.A., Wolinsky, M.A. 2012. Simplified process modeling of river avulsion and alluvial architecture: connecting models and field data. *Sedimentary Geology*. 257-260: 1-30.

Harwood, K., Brown, A.G. 1993. Fluvial processes in a forested anastomosing river: flood partitioning and changing flow patterns. *Earth Surface Processes and Landforms*. 18(8): 741–748.

Hickin, E.J. , Nanson, G.C. 1975. Character of channel migration on Beatton River, Northeast British-Columbia, *Canada. Geol. Soc. Am. Bull.*, 86(4): 487-494.

Hooke, J. M. 1980. Magnitude and distribution of rates of river bank erosion, *Earth Surface Processes*, *5*(2), 143-157.

Hooke, J.M. 1995. River channel adjustment to meander cutoffs on the River Bollin and River Dane, northwest England. *Geomorphology*, 14(3): 235-253.

Hooke, J.M. 2004. Cutoffs galore!: Occurrence and causes of multiple cutoffs on a meandering river. *Geomorphology*, 61(3-4): 225-238.

Hooke, J.M., Harvey, A.M. 1983. Meander changes in relation to bend morphology and secondary flows (River Dane, Cheshire). In: J.D. Collinson and J. Lewin (Editors), *Modern and ancient fluvial systems*. Blackwell Scientific; International Association of Sedimentologists, Special Publication 6, pp. 121-132.

Howard, A.D. 1992. Modeling Channel Migration and Floodplain Sedimentation in Meandering Streams, in *Lowland Floodplain Rivers: Geomorphological Perspectives*, edited by P. A. Carling and G. E. Petts, John Wiley & Sons Ltd.

Howard, A.D. 1996. Modelling Channel Evolution and Floodplain Morphology in *Floodplain Processes*, edited by M. G. Anderson, D. E. Walling and P. D. Bates, John Wiley & Sons Ltd.

Hudson, P.F., Mossa, J. 1997. Suspended sediment transport effectiveness of three large impounded rivers, US Gulf Coastal Plain, *Environmental Geology* 32 (4), 263-273.

Hudson, P.F., Kesel, R.H. 2000. Channel migration and meander-bend curvature in the lower Mississippi River prior to major human modification. *Geology* 28(6): 531-534

Hudson, P.F., Kesel, R.H. 2006. Spatial and temporal adjustment of the Lower Mississippi River channel to major human impacts. *Zeitschrift fur Geomorphologie*, Supplementband(143): 17-33.

Hudson, P.F., Middelkoop, H., Stouthamer, E. 2008. Flood management along the Lower Mississippi and Rhine Rivers (The Netherlands) and the continuum of geomorphic adjustment. *Geomorphology*, 101(1-2): 209-236.

Ikeda, S., Parker, G. (Editors). 1989. *River Meandering*. Water resources monograph, 12. American Geophysical Union, Washington, D.C., 485 pp.

Jensen, J.R. 2016. *Introductory Digital Image Processing: A Remote Sensing Perspective*. 4th Edition, Glenview, IL: Pearson Education, Inc., 623 p.

Joglekar, D.V. 1971. *Manual on river behaviour, control and training*, Central Board of Irrigation and Power, New Delhi, India.

Jones, L.S., Schumm, S.A. 1999. Causes of avulsion: an overview. In: Smith, N.D., Rogers, J., *Fluvial Sedimentology VI*. Special Publication of the International Association of Sedimentologists 28, Blackwell, Oxford, pp. 171-178.

Jones, J.L. 2006. Side channel mapping and fish habitat suitability analysis using LiDAR topography and orthophotography. *Photogrammetric Engineering and Remote Sensing*. 72: 1202.

Jones, J.A., Grant, G.E. 1996. Peak flow responses to clear-cutting and roads in small and large basins, western Cascades, Oregon, *Water Resources Research*, *32*(4), 959-974.

Karl, T.R., Melillo, J.M., Peterson, T.C. 2009. *Global Climate Change Impacts in the United States*. U.S. Global Change Research Program. Cambridge University Press: New York, NY, 196 pp.

Kenward, T., Lettenmaier, D., Wood, E., Zoin, M. 1996. *Vertical Accuracy of Elevation Models, in: Vertical accuracy of digital elevation models (DEM)*. Available from: http://www.hydro.washington.edu/Lettenmaier/Publications/Effect_of_DEM_Accuracy_and_Scale_on_Hydrological_Modeling/agu_post.htm (Accessed 25 February 2010)

King, W.A., Martini, I.P. 1984. Morphology and recent sediments of the lower anastomosing reaches of the Attawapiskat River, James Bay, Ontario, Canada. *Sedimentary Geology* 37: 295–320.

Knighton, D. 1998. *Fluvial forms and processes: a new perspective*: Arnold, Hodder Headline, PLC.

Konrad, C.P. 2012. Reoccupation of floodplains by rivers and its relation to the age structure of floodplain vegetation: *Journal of Geophysical Research*, v. 117, doi: 10.1029/2011JG001906.

Konrad, C.P., Booth, D.B. 2002, Hydrologic trends associated with urban development for selected streams in western Washington: *U.S. Geological Survey Water-Resources Investigations Report* 02-4040, 40 p.

Lewis, G. W., Lewin, J. 1983. *Alluvial cutoffs in Wales and the Borderlands*. In Collinson and Lewin (1983), pages 145–154.

Mackey, S.D., Bridge, J.S. 1995. Three-dimensional model of alluvial stratigraphy: theory and application. *Journal of Sedimentary Research*. B65: 7-31.

Makaske, B. 2001. Anastomosing Rivers: a review of their classification, origin, and sedimentary products. *Earth Science Reviews*. 53: 149-196.

Makaske, B., Smith, D.G., Berendsen, H.J.A. 2002. Avulsions, channel evolution and floodplain sedimentation rates on the anastamosing upper Columbia River, British Columbia. *Sedimentology* 49, 1049-1071.

Maynard, J.R. 2006. Fluvial response to active extension: evidence from 3D seismic data from the Frio formation (Oligo-Miocene) of the Texas Gulf of Mexico Coast, USA. *Sedimentology* 53, 515–536.

McCarthy, T.S., Ellery, W.N., Stanistreet, J.G. 1992. Avulsion mechanisms on the Okavango fan, Botswana: the control of a fluvial system by vegetation. *Sedimentology* 39, 779–795.

Meybeck, M. 2003. Global analysis of river systems: from Earth system controls to Anthropocene syndromes. *Philosophical Transactions of the Royal Society B-Biological Sciences*, 358(1440), 1935–1955.

Micheli, E.R., Kirchner, J.W., Larsen, E.W. 2004. Quantifying the effect of riparian forest versus agricultural vegetation on river meander migration rates, Central Sacramento River, California, USA. *River Research and Applications*, 20(5): 537-548.

Micheli, E.R., Larsen, E.W. 2011. River channel cutoff dynamics, Sacramento River, California, USA. *River Research and Applications*, 27(3): 328-344.

Milliman, J.D., Syvitski, J.P.M. 1992. Geomorphic/tectonic control of sediment discharge to the ocean: the importance of small mountainous rivers. *Journal of Geology* 100, 525–544.

Mohrig, D., Heller, P.L., Paola, C., Lyons, W.J. 2000. Interpreting avulsion process from ancient alluvial sequences: Guadalope-Matarranya system (Northern Spain) and Wasatch formation (Western Colorado), *Bulletin of the Geological Society of America*, *112*(12), 1787-1803.

Morozovo, G.S., Smith, N.D., 1999. Holocene avulsion history of the lower Saskatchewan fluvial system, CumberlandMarshes, Saskatchewan–Manitoba, Canada. *Fluvial Sedimentology VI*, Spec. Publs. Int.Ass. Sediment, vol. 28. Blackwell Science,Oxford, pp. 231–249.

Morton, R.A., Blum, M.D., White, W.A. 1996. Valley fills of incised coastal plain rivers, southeastern Texas. *Transactions of the Gulf Coast Association of Geological Societies* 46, 321-331.

Motta, D., Abad, J., Langendoen, E., Garcia, M. 2012. The effects of floodplain soil heterogeneity on meander planform shape. *Water Resources Research* 48.

Nanson, G.C. 1980. Point bar and floodplain formation of the meandering Beatton River, northeastern British Columbia, Canada. *Sedimentology*. 27(1): 3-29.

Nanson, G.C., Croke, J.C. 1992. A genetic classification of floodplains, *Geomorphology*, *4*(6), 459-486.

Nyerges, T.L. 1990. Locational referencing and highway segmentation in a geographic information system. *ITE Journal, 60*(3), 27-31.

Leopold, L.B., Wolman, M.G., Miller, J.P. 1964. *Fluvial Processes in Geomorphology*, W. H. Freeman:San Francisco, California, 522pp.

O'Connor, J.E., Jones, M.A., Haluska, T.L. 2003. Flood plain and channel dynamics of the Quinault and Queets Rivers, Washington, USA. *Geomorphology* 51:31-59.

Olson, P.L., Legg, N. T. , Abbe, T. B., Reinhart, M. A., Radloff, J. K. 2014. *A Methodology for Delineating Planning-Level Channel Migration Zones*, 83 pp, Washington State Department of Ecology, Publication no. 14-06-025.

Overton, I C., Siggins, A., Gallant, J C., Penton, D., Byrne, G. 2009. Flood Modelling and Vegetation Mapping in Large River Systems, in *Laser Scanning for the Environmental Sciences* (eds G. L. Heritage and A. R. G. Large), Wiley-Blackwell, Oxford, UK.

Paine, J.G., Morton, R.A. 1989. *Shoreline and vegetation-line movement, Texas Gulf Coast, 1974 to 1982*. Bureau of Economic Geology, Austin, TX.

Palmer, M.A., Lettenmaier, D.P., Poff, N.L., Postel, S.L., Richter, B., Warner, R. 2009. Climate Change and River Ecosystems: Protection and Adaptation Options. *Environmental Management*, 44(6), 1053–1068.

Peakall, J., Leeder, M., Best, J., Ashworth, P. 2000. River response to lateral ground tilting: a sysnthesis and some implications for the modeling of alluvial architecture in extensional basins. *Basin Research* 12, 413–424.

Peakall, J., Ashworth, P., Best, J. 2007. Meander-bend evolution, alluvial architecture, and the role of cohesion in sinuous river channels: A flue study, *Journal of Sedimentary Rsearch*., 77, 1–16

Phillips, J.D., 2006. *Geomorphic Context, Constraints, and Change in the Lower Brazos and Navasota Rivers, Texas*. Texas Water Development Board. Report. Austin, TX, 79 pp.

Phillips, J.D. 2007a. *Geomorphic Equilibrium in Southeast Texas Rivers*. Texas Water Development Board. Report. Austin, TX, 114pp.

Phillips, J.D. 2007b. *Field data collection in support of geomorphic classification of the Lower Brazos and Navasota Rivers*. Texas Water Development Boards. Report. Austin, TX, 98pp.

Phillips, J.D. 2009. Avulsion regimes in southeast Texas rivers, *Earth Surface Processes and Landforms*, 34(1), 75–87.

Phillips, J.D. 2011. Universal and local controls of avulsions in southeast Texas Rivers. *Geomorphology*. 130: 17-28.

Phillips, J.D. 2012. Log-jams and avulsions in the San Antonio River Delta, Texas, *Earth Surface Processes and Landforms*, 37(9), 936-950.

Phillips, J.D. 2014. Anastomosing Channels in the lower Neches River valley, Texas. *Earth Surface Processes and Landforms*, 39, 1888-1899.

Phillips, J.D., Lutz., J.D. 2008. Profile convexities in bedrock and alluvial streams. *Geomorphology*, 102, 554-566.

Pinter, N., Jemberie, A.A., Remo, J.W.F., Heine, R.A., Ickes, B.S. 2010. Cumulative impacts of river engineering, Mississippi and lower Missouri Rivers, *River Research and Applications*, 26(5), 546–571.

Rapp, C.F., Abbe, T.B. 2003, *A framework for delineating channel migration zones*. Washington Department of Ecology Publication 03-06-027.

Richter, B.D., Baumgartner, J.V., Wigington, R., Braun, D.P. 1997. How much water does a river need? *Freshwater Biology*, 37(1), 231–249.

RSI (Research Systems, Inc.), *ENVI User's Guide*. ENVI Vers. 4.1. 2004. Boulder, CO: RSI.

Schumann, R.R., 1989. Morphology of Red Creek, Wyoming, an arid-region anastomosing channel system. *Earth Surface Processes and Landforms*, 14, 277–288.

Schumm, S.A. 1977. *The fluvial system*. John Wiley and Sons: New York, 338 p.

Schumm, S.A. 2005. *River Variability and Complexity*. Cambridge. University Press: Cambridge, UK, 234 p.

Schumm, S.A., Erskine, W.D., Tilleard, J.W. 1996. Morphology, hydrology, and evolution of the anastomosing Ovens and King Rivers, Victoria, Australia. *Geological Society of America Bulletin*, 108: 1212–1224.

Schumm, S.A.., Spitz, W.J. 1996. Geological influences on the Lower Mississippi River and its alluvial valley, *Engineering Geology*, 45(1-4), 245-261.

Slingerland, R., Smith, N.D. 1998. Necessary conditions for a meandering-river avulsion. *Geology*, 26: 435-438.

Slingerland, R., Smith, N.D. 2004. River avulsions and their deposits. *Annual Reviews: Earth Planetary Sciences*, 32: 257-285.

Smith, N.D., Cross, T.A., Dufficy, J.P., Clough, S.R. 1989. Anatomy of an Avulsion. *Sedimentology*, 36: 1-23.

Stouthamer, E. 2001. Sedimentary products of avulsions in the Holocene Rhine-Meuse Delta, The Netherlands, *Sedimentary Geology*, *145*(1-2), 73-92.

Sun, T., Meakin, P., Jøssang, T., Schwarz, K. 1996. A simulation model for meandering rivers, *Water Resources Research*, *32*(9), 2937-2954.

Sylvia, D.A., Galloway, W.E. 2006. Morphology and stratigraphy of the late Quaternary lower Brazos valley: Implications for paleo-climate, discharge and sediment delivery, *Sedimentary Geology*, *190*(1-4), 159-175.

Taha, Z.P. 2006. *Fluvial Response to Base Level Change: A Case Study of the Brazos River, East Texas, U.S.A.*, Ph.D. Dissertation, Rice University, Houston, TX, 156 pp.

Taha, P.Z., Anderson, J.B. 2008. The influence of valley aggradation and listric normal faulting on styles of river avulsion: a case study of the Brazos River, Texas USA. *Geomorphology*, 95: 429-448.

Tooth, S., Rodnight, H., Duller, G.A.T., McCarthy, T.S., Marren, P.M., Brandt, D. 2007. Chronology and controls of avulsion along a mixed bedrock-alluvial river. *Geol. Soc. Am. Bull.,* 119 (2007), pp. 452–461

Tooth, S., Rodnight, H., McCarthy, T.S., Duller, G.A.T., Grundling, A.T. 2009. Late Quaternary dynamics of a South African floodplain wetland and the implications for assessing recent human impacts, *Geomorphology*, *106*(3-4), 278-291.

Törnqvist, T.E. 1994. Middle and late Holocene avulsion history of the River Rhine (Rhine-Meuse delta, Netherlands), *Geology*, *22*(8), 711-714.

Törnqvist, T.E., Bridge, J.S. 2002. Spatial variation of overbank aggradation rate and its influence on avulsion frequency, *Sedimentology*, *49*(5), 891-905.

Törnqvist, T.E., Bridge, J.S. 2006. Causes of river avulsion: Insights from the late Holocene avulsion history of the Mississippi River, U.S.A. - Discussion, *Journal of Sedimentary Research*, *76*(6), 959.

Vörösmarty, C.J., McIntyre, P.B., Gessner, M.O., Dudgeon, D., Prusevich, A., Green, P., Glidden, S., Bunn, S.E., Sullivan, C.A., Liermann, C.R., Davies, P.M. 2010. Global threats to human water security and river biodiversity. *Nature*, 467(7315), 555–561.

Ward, J.V., Tockner, K., Arscott, D.B. Claret, C. 2002. Riverine landscape diversity. *Freshwater Biology*, 47(4): 517-539.

Waters, M.R., Nordt, L.C. 1995. Late Quaternary floodplain history of the Brazos River in east-central Texas. *Quaternary Research*, 43, 311-319.

APPENDIX A:
IMAGE-PROCESSING ALGORITHMS

The objective of this portion of the project was to develop and study tools that could be used to either increase the degree of automation of river-feature extraction from various types of remote-sensing images (e.g., aerial photographs and other multi-band/multi-spectral remote-sensing data sets, etc.), or enhance the manual boundary delineation/feature extraction process via digitization. River-boundary extraction or digitization is a very common and important task (Nath and Deb 2010) that must be performed for various hydrologic/riverine studies (e.g., change detection, channel-migration studies, floodplain mapping, habitat classification, hydraulic modeling, and hydraulic-geometry relationship studies). Typically, this step is completed manually, and aerial photographs are often used (Merwade 2007).

Manual on-screen digitization is usually time-consuming, particularly if a large number of images needs to be processed; this is a typical characteristic of multi-site/multi-temporal river-change analyses. Manual methods are also subjective and can be influenced by human error. New types of image-enhancement products can potentially assist the human analyst when visually/manually interpreting and digitizing images. If image-processing algorithms can generate image products that enhance manual on-screen digitization, digitization/feature-extraction errors can potentially be reduced. As for semi-automated or automated methods for river-boundary/feature extraction, studies of this nature have been quite limited in the research literature (Merwade 2007; Güneralp et al. 2013, 2014). Image-enhancement algorithms can be used in conjunction with classification algorithms in an effort to increase classification accuracy, for example; enhanced images can serve as input data layers.

This appendix provides an overview of a particular and potentially quite useful supervised classification method for riverine feature extraction (i.e., support vector machine (SVM)) (Güneralp et al. 2013, 2014), as well as edge detection- and Kalman filter-based methods for image enhancement. All of these methods were used in some capacity in other parts of this project—either to enhance manual digitization and visualization or semi-automated classification. Vector-boundary smoothing is also discussed.

It should be noted that, to-date, we have published two journal articles on an aspect of the general topic of this appendix (Appendix A), which were made possible via funding from TWDB under this contract: Güneralp et al. (2013); and Güneralp et al. (2014). The former article was the most read and downloaded article in *GIScience & Remote Sensing* for several consecutive years.

River-Boundary/Feature Extraction

Several methods for enhancing the extraction of river boundaries and other floodplain features are detailed here, which were effectively employed in other project components, in manual or semi-automated feature-extraction capacities. General meandering-river examples are given in this appendix.

Support Vector Machines (SVMs)

In a supervised classification, human analysts have knowledge of the classes of interest and know sample locations in the study site that are representative of each class. The goal is to assign each spatial unit (i.e., pixel) in the study area to a known class. Training sites must be representative of the specific classes of interest. Actual locations identifying the known class locations are called the training samples (Jensen 2005).

Support Vector Machine (SVM) is a relatively recent supervised classification technique developed by Vapnik and his group at AT&T BELL Laboratories (Vapnik 1995, Cortes and Vapnik 1995). The main idea of SVM is to separate the classes with a hyperplane surface so as to maximize the margin among them. In this research, SVM is described as general case, since the rivers meander without any particular linear pattern though they are linear features. For a general case, the training data appear in the optimization problem in the form of dot products, one first maps the feature vectors to a higher-dimensional Euclidean space by mapping (Song and Civco 2004):

$$\Phi : R^d \alpha H \ .$$

Then, the optimization problem can be obtained in the space H replacing $x_i \cdot x_j$ by $\Phi(x_i) \cdot \Phi(x_j)$. Therefore the kernel function K is

$$K(x_i, x_j) = \Phi(x_i) \cdot \Phi(x_j),$$

then we only need to compute $K(x_i, x_j)$ in the training process. The decision function is

$$f(x) = sign(\sum_{i=1}^{l} y_i \lambda_i K(x_i, x_j) + b) .$$

In this research, the kernel function employed was the Multi-Layer Perceptron (MLP) with value of θ:

$$K(x_i, x_j) = \tanh(x \cdot x_i - \theta) .$$

Based on this algorithm, the input should consist of multiband/multispectral images. Input data sets are classified into single-featured images based on regions of interest. In the figures below, original/input images and the corresponding SVM classification results are given.

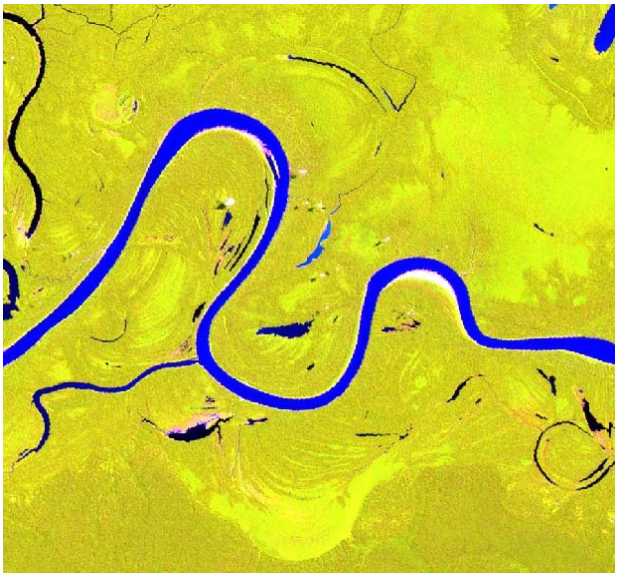

Figure A-1. Original Landsat TM image.

Figure A-2. Result of SVM algorithm.

Edge Detection-Based Boundary Extraction

This river boundary-extraction method includes three groups of image-processing algorithms: pre-segmentation, segmentation, and post-segmentation. The pre-segmentation algorithms suppress image noise and enhance edge elements in the images. The segmentation algorithms use edge-detection filter to run across the image, then use the edge-detection results as further inputs to classify image into water/non-water regions. The post-segmentation algorithms differentiate the river boundary from other object edges.

In the pre-segmentation phase, noise-removal method based on Gaussian filter is used to remove image noise. An anisotropic diffusion algorithm (Perona and Malik 1990) is used to enhance strong edges along the river boundary and suppress the weak edge.

The segmentation is to filter image by edge-detection algorithms, like Canny and Sobel algorithms. The border pixel segmented water/non-water regions can be delineated as the river boundary. Canny edge detector uses a filter based on the first derivative of Gaussian, since it is susceptible to noise present on raw unprocessed image data, so begin with, the raw image is convolved with a Gaussian filter (Canny 1986). The result is a slightly blurred version of the original which is not affected by a single noisy pixel to any significant degree. An edge in an image may point in a variety of directions, so the Canny algorithm uses four filters to detect horizontal, vertical, and diagonal edges in the blurred image. The edge-detection operator (Roberts, Prewitt, Sobel for example) returns a value for the first derivative in the horizontal direction (Gy) and the vertical direction (Gx) (Parker 1997). From this, the edge gradient and direction can be determined:

$$G = \sqrt{G_x^2 + G_y^2}\,,$$

$$\Theta = \arctan(\frac{G_y}{G_x})\,.$$

After finding the intensity gradient of the image, a search is then carried out to determine if the gradient magnitude assumes a local maximum in the gradient direction. This is worked out by passing a 3 × 3 grid over the intensity map. Then the algorithm traces edges through the image.

The figures below give the original Landsat image and the result of Canny edge detection.

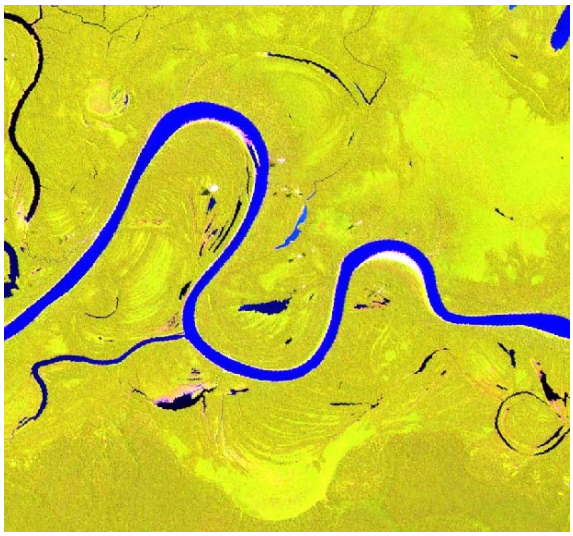

A-3. Original Landsat TM image.

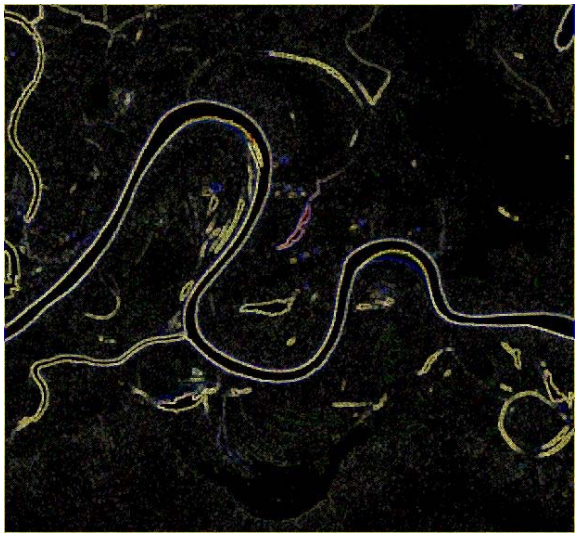

A-4. Result of Canny filter.

Then the Canny-filtered result is applied as one band in the classification method. The image below shows the result from the ISODATA unsupervised classification algorithm (Jensen 2005) integrated with the Canny algorithm.

A-5. Result of ISODATA algorithm integrated with Canny filter.

We also applied Sobel algorithm in the segmentation phase. Mathematically, Sobel operator uses two 3×3 kernels which are convolved with the original image to calculate approximations of the derivatives - one for horizontal changes, and one for vertical. If A is defined as the source image, G_x and G_y are two images which at each point contain the horizontal and vertical derivative approximations (Engel *et al.*, 2006). It can be computed as:

$$G_y = \begin{bmatrix} -1 & -2 & -1 \\ 0 & 0 & 0 \\ +1 & +2 & +1 \end{bmatrix} * A, \; G_x = \begin{bmatrix} -1 & 0 & +1 \\ -2 & 0 & +2 \\ -1 & 0 & +1 \end{bmatrix} * A,$$

where * denotes the 2-dimensional convolution operation. The image below shows the result of Sobel algorithms and the ISODATA algorithm- integrated Sobel filter.

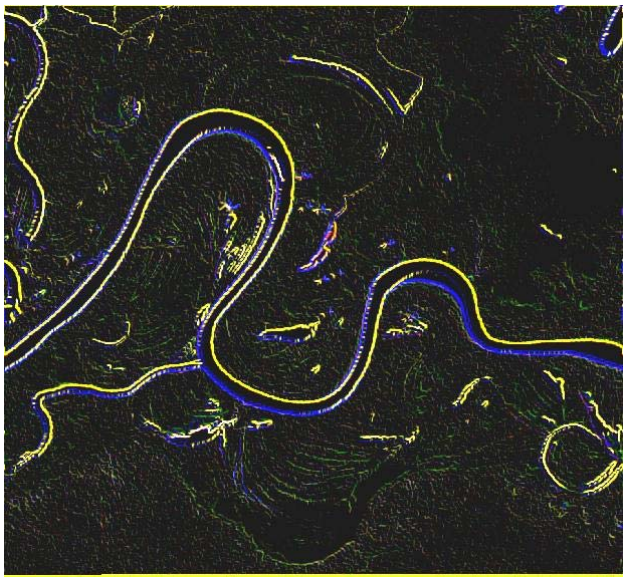

A-6. Result of Sobel filter.

A-7. Result of ISODATA algorithm integrated with Sobel filter.

At the post-segmentation-processing phase, river pixels in the segmented image are grouped into individual image objects, and the other small objects are removed. Then in the ArcGIS software package, the raster river features are converted into vector features. Because the resultant vector features are jagged in some portions following conversion, a smoothing algorithm based on the Bezier curve is applied. The Bezier curve of degree n can be generalized as follows. Given points $P_0, P_1, ..., P_n$, the Bezier curve is

$$
\begin{aligned}
&B(t) \\
&= \sum_{i=0}^{n} \binom{n}{i} (1-t)^{n-i} t^{i} P_i \\
&= (1-t)^{n} P_0 + \binom{n}{1} (1-t)^{n-1} t P_1 + \ldots + \binom{n}{n-1} (1-t) t^{n-1} P_{n-1} + t^{n} P_n, t \in [0,1]
\end{aligned}
$$

where $\binom{n}{i}$ is the binomial coefficient (Farin 1997).

Based on the algorithm, we obtain the smoothed river boundary. The images below show the jagged river boundary and smoothed river boundary.

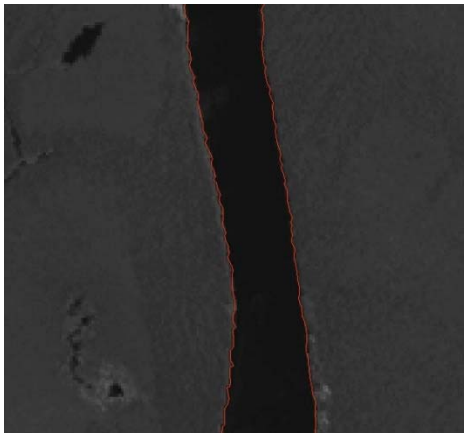

A-8. Jagged river boundary, following raster-to-vector conversion.

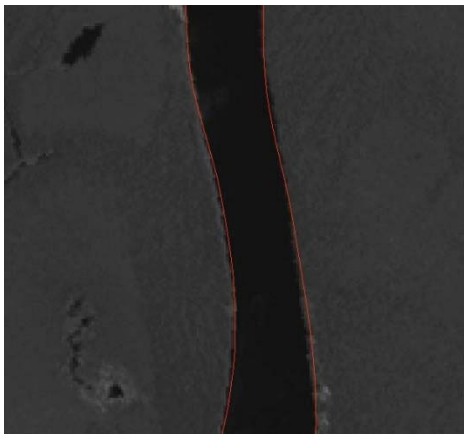

A-9. Smoothed river boundary.

Kalman Filter

Kalman filter is an optimal recursive data-processing algorithm. The Kalman filter model assumes the true state at time k is evolved from the state at $(k-1)$ according to

$$x_k = F_k x_{k-1} + B_k u_k + w_k ,$$

where F_k is the state transition model which is applied to the previous state x_{k-1}; B_k is the control-input model which is applied to the control vector u_k; w_k is the process noise which is assumed to be drawn from a zero mean multivariate normal distribution with covariance Q_k (Tekalp et al. 1989).

The Kalman filter is a recursive estimator. This means that only the estimated state from the previous time step and the current measurement are needed to compute the estimate for the current state (Azimi-Sadjadi et al. 1999). We could take advantage of this feature of the Kalman filter to process 2-D images. The key is to obtain covariance space K_k, and then calculate x_k.

Therefore, Kalman observation is $H_k = \dfrac{\varepsilon'_k C_k^T}{C_k \varepsilon'_k C_k^T + R_k}$.

Invariants is $\varepsilon_k = (1 - H_k C_k)\varepsilon'_k$, and the optimal prediction is

$$S_k = A_k S_{k-1} + H_k (x_k - C_k A_k S_{k-1}) .$$

Based on this principle, we could use Kalman filter to sharpen the edge between river water and non-water regions. In order to improve the signal-to-noise ratio (SNR) relative to traditional Kalman filter, two-dimensional (2D) Fractional Kalman Filter was applied in this research (Wang 2008, Zuo et al. 2010).

Consider the traditional 2D linear discrete model,

$$s(m,n) = \sum_{k,l \in w} A_{kl} s(m-k, n-l) + Bu(m,n) + w(m,n) \text{ and } r(m,n) = Cs(m,n) + v(m,n) \quad (1),$$

where $s(m,n)$ and $r(m,n)$ are system state and observation values; $u(m,n)$ is the control input; $w(m,n)$ is system noise; and $v(m,n)$ is observation noise. $A_{kl}s$ is system coefficient matrix, and C is transform matrix.

According to the definition of Grunwald-Letnikv (G-L) fractional calculus (Oldham et al. 1974), order a fractional difference status function can be obtained:

$$A_{kl}s(m-k,n-l) = \sum_{j=0}^{m-1-k,n-1-k} A_{kl}^{j}s(m-1-k-j,n-1-l-j) \quad (2)$$

in which $A_{kl}^{0} = A_{kl}$, when $j=0$; $A_{kl}^{j} = \begin{cases} diag\left[-(-1)^{j+1}\binom{a_i^{mn}}{j+1}\right], & k=l; \\ diag\left[-(-1)^{j+1}\binom{a_i^{m}}{j+1}\right], & k>l; \\ diag\left[-1(-1)^{j+1}\binom{a_i^{n}}{j+1}\right], & k<l; \end{cases}$, when $j>0$;

$$\binom{a_i^z}{j} = \frac{a_i^z(a_i^z-1)\cdots(a_i^z-j+1)}{j!}, \quad j=1,2,3,\cdots$$

Here, $a_i^z \in R^{*+}(z=m,n,mn)$ is the fractional order of $s_i(m,n)$, and j is the length of the data sequence.

If we merge equation (2) and (1), we obtain the 2D linear discrete fractional difference model:

$$\begin{aligned} s(m,n) &= \sum_{k,l=0}^{W}\sum_{j=0}^{m-1-k,n-1-k} A_{kl}^{j}s(m-1-k-j,n-1-l-j) + Bu(m,n) + w(m,n) \\ r(m,n) &= Cs(m,n) + v(m,n). \end{aligned} \quad (3)$$

Based on equation (3), we note the 2D Fractional Kalman Filter algorithm:

$$\hat{s}(m,n) = \tilde{s}(m,n) + K(m,n)[r(m,n) - C\tilde{s}(m,n)] \quad (4a)$$

$$\hat{s}(m,n) = \sum_{k,l=0}^{W}\sum_{j=0}^{m-1-l,n-1-l} A_{kl}^{j}\hat{s}(m-1-k-j,n-1-l-j) + Bu(m,n) \quad (4b)$$

$$K(m,n) = \tilde{P}(m,n)C^{T}[C\tilde{P}(m,n)C^{T} + R_{m,n}]^{-1} \quad (4c)$$

$$P(m,n) = [I - K(m,n)C]\tilde{P}(m,n) \quad (4d)$$

$$\tilde{P}(m,n) = \sum_{k,l=0}^{W} \sum_{j=0}^{m-1-l,n-1-l} A_{kl}^{j} P(m-k,n-l) A_{kl}^{jT} + \sum_{k,l=0}^{W} \sum_{j=0}^{m-1-l,n-1-l} A_{kl}^{j} Cov(\breve{s}(m-1-k-j,n-1-l-j)\breve{s}(m-1-k-j,n-1-l-j)) A_{kl}^{j'} + Q_{m,n} \quad (4e)$$

Here $K(m,n)$ is the Gain matrix; $R_{m,n}$ is the observation noise difference; and $Q_{m,n}$ is the process noise difference.

To apply 2D linear discrete fractional difference model to enhance images and reduce noise, we need to obtain the length L and the order a. Then the original 2D status equation needs to be converted to 2D linear discrete fractional difference status model, and then it can be applied to image processing.

The commonly-used Non-Sysmmetric Half-Plane model is applied to describe a given image, and neighborhood range $W = 3$. Therefore, the status model is

$$\begin{aligned} s(m,n) = {} & A_{0,0} s(m-1,n-1) + A_{1,1} s(m-2.n-2) \\ & + A_{2,2} s(m-3,n-3) + A_{1,0} s(m-2,n) \\ & + A_{2,0} s(m-3,n) + A_{2,1} s(m-3,n-1) \\ & + A_{0,1} s(m,n-2) + A_{0,2} s(m,n-3) \\ & + A_{1,2} s(m-1,n-3) + w(m,n) \end{aligned}$$

$$r(m,n) = Hs(m,n) + v(m,n).$$

Here, A_{kl} is evaluated by Recursive Least Squares, and H is the unit matrix with appropriate orders. The length L is 10, and the order a is 0.6.

Traditional Kalman filter and two-dimensional (2D) Fractional Kalman filter were applied to the same image below; traditional Kalman filter yielded a SNR value of 6.2834 dB, whereas the SNR value from 2D Fractional Kalman Filter is 6.7523 dB. This result demonstrates that the 2D Fractional Kalman filter can produce a higher SNR relative to traditional Kalman filter.

The image below shows the original TM image and the sharpened river-boundary result.

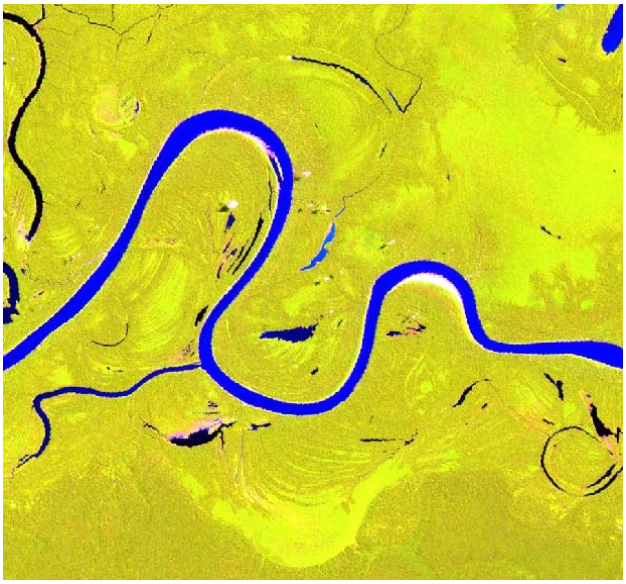

A-10. Original Landsat TM image.

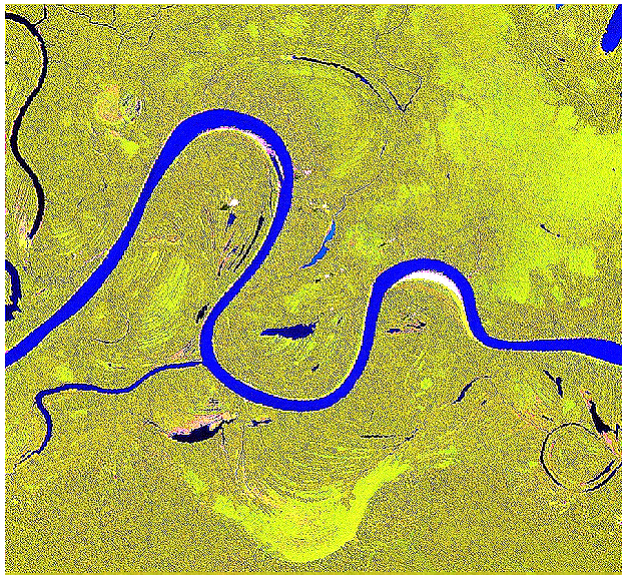

A-11. Result of 2D Fractional Kalman filter.

The figure below shows the classification result based on the 2D Fractional Kalman filter result.

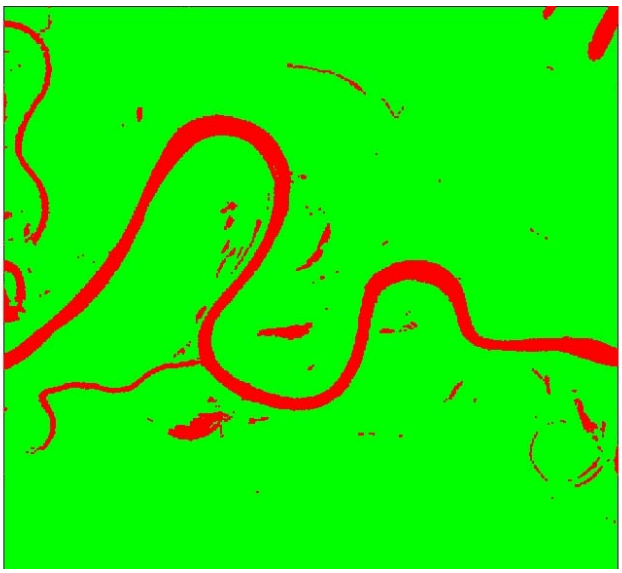

A-12. Result of ISODATA algorithm integrated with 2D Fractional Kalman filter.

REFERENCES

Azimi-Sadjadi, M. R., Xiao, R., and Yu, X. (1999), Neural Network Decision Directed Edge-Adaptive Kalman Filter for Image Estimation. *IEEE Transaction on Image Processing*, 8(4), 589-592.

Canny, J. (1986), A computational approach to edge detection. *IEEE Transactions on Pattern Analysis and Machine Intelligence*, 8, 679–698.

Cortes, C., and Vapnik, V. (1995), Support Vector Networks. *Machine Learning*, 20, 1-25.

Engel, K., Hadwiger, M., Kniss, J. M., Rezk-Salama, C., Weiskopf, D. (2006), *Real-Time Volume Graphics*. Wellesley, MA: A K Peters, Ltd., pp. 112-114.

Farin, G. (1997), *Curves and surfaces for computer-aided geometric design* (4th Ed.), Elsevier Science & Technology.

Güneralp, İ., Filippi, A. M., and Hales, B. (2013), River-flow boundary delineation from digital aerial photography and ancillary images using Support Vector Machines. *GIScience & Remote Sensing*, 50(1), 1-25, doi:10.1080/15481603.2013.778560.

Güneralp, İ., and Filippi, A. M., and Hales, B. U. (2014), Influence of river channel morphology and bank characteristics on water surface boundary delineation using high-resolution passive remote sensing and template matching. *Earth Surface Processes and Landforms*, 39(7), 977-986, doi: 10.1002/esp.3560.

Jensen, J. R. (2005), *Introductory Digital Image Processing: A Remote Sensing Perspective*, 3rd Ed., Upper Saddle River, NJ: Prentice-Hall, 544 p.

Merwade, V. M. (2007), An automated GIS procedure for delineating river and lake boundaries. *Transactions in GIS*, 11(2), 213-231.

Nath, R. K., and Deb, S. K. (2010), Water-body area extraction from high resolution satellite images--An introduction, review, and comparison. *International Journal of Image Processing*, 3(6), 353-372.

Oldham, K. B., and Spanier, J. (1974) *The Fractional Calculus*, New York and London: Academic Press, pp 5-96.

Parker, J. R. (1997), *Algorithms for Image Processing and Computer Vision*, New York: John Wiley & Sons.

Perona, P., and Malik, J. (1990), Scale-space and edge detection using anisotropic diffusion. *IEEE Transactions on Pattern Analysis and Machine Intelligence*, 12, 629-639.

Song, M., and Civco, D. (2004), Road extraction using SVM and image segmentation. *Photogrammetric Engineering & Remote Sensing*, 70(12), 1365-1371.

Tekalp, A. M., Kaufman, H., and Woods, J. W. (1989), Result of ISODATA Algorithm Integrated with Sobel Filter. *IEEE Trans.Acoust., Speech, Signal Processing*, 37, 892-899.

Vapnik, V. N. (1995), *The Nature of Statistical Learning Theory*, Spring-Verlag, New York, 188.

Wang, T (2008) Application of Kalman filter in image processing. *Science & Technology Information*, 32, 229-231.

Zuo, K., Sun, T. J., Li, Z. H., and Tao, L. (2010) 2D Fractional Kalman filter and its application to image processing. *Journal of Electronics & Information Technology*, 32(12), 3027-3031.

APPENDIX B:
DATA PROCESSING FOR HISTORICAL RIVER CHANNEL CHANGE ANALYSIS

Generation of multitemporal aerial photograph mosaics

Image mosaics of respective sets of multitemporal aerial photographs for selected river avulsion-relevant areas were produced. Aerial photographs were obtained via U.S. Geological Survey (USGS) EarthExplorer. For this research, the ideal scale of the historical aerial photographs was 1:40,000 or larger. However, smaller-scale images of otherwise acceptable quality were more available than larger-scale photographs. Of the image dates available, partial spatial coverage of the avulsion sites of interest was a frequent issue; we obtained aerial photographs in an effort to maximize spatio-temporal coverage of the study areas. For the avulsion study sites taken together, aerial photographs from the following years were acquired for mosaic production: 1953, 1968, 1977, 1979, 1981, 1983, and 1989 (Table B–1).

Raw image data were cropped in Adobe Photoshop Creative Suite 3 (CS3)®. CS3 was employed for unsupervised mosaicking due to its different blending options, as well as its unique interactive Photomerge®. Each image entailed a frame, or collar, around the perimeter the aerial photographs containing image annotation information, including roll number and acquisition date. These image-annotation areas were cropped-out of each photograph using a computationally-efficient batch method available in CS3. Each raw image was rotated to the same orientation. Once the crop script was saved for each year, the batch script ran, cropping-out the image-annotation areas in each set of images. The cropped photos were then uploaded into the Photomerge; as alluded to above, the interactive layout option was employed. The Photomerge function aligns each image based on its content; however, fine-detail alignment had to be performed manually.

Once the Photomerge process was completed, each image constituted an individual layer in Photoshop. For subsequent processing, all but two layers were visually removed at a time (i.e., the images were processed in a pairwise manner). Affine transformations were employed, and scaling was not performed to minimize introduction of additional geometric distortion. The image pairs being co-processed were rotated and cropped to fit together more precisely—i.e., to align the road intersections and river boundaries properly; the angle of rotation varied between -4° and 6°. We applied blending in a manner such that these properties of river and roads were maintained. The river took precedence over all other features during the unsupervised mosaicking process. This process was repeated for every year, across all avulsion study sites.

Geometric rectification of multitemporal aerial photograph mosaics

The resultant historical, multitemporal aerial photograph mosaics were then geometrically rectified in ENvironment for Visualizing Images® (ENVI®4.7) software (RSI (Research Systems, Inc.) 2004) in order to properly georeference the mosaics and minimize some spatial errors. The aerial photograph mosaics were geometrically rectified to a 1996 false-color infrared (CIR) digital orthophoto quarter-quadrangle (DOQQ) image base, produced by the USGS (pixel size = 1 m; coordinate system = UTM, Zone 14 North; horizontal datum = NAD83). We used a minimum of 10—though commonly more—ground control points (GCPs) (Table B–1), with affine transformations. The GCPs were all situated on roads/road intersections that could be well-distinguished on both the older aerial photo mosaics and the DOQQ image base. Old, historical prominent roads are often contemporary double-/quadruple-lane highways. GCPs were iteratively sorted by root-mean-square error (RMSE), as higher-error GCPs were iteratively corrected or removed during the process. For the various avulsion sites and years of available photographs of acceptable quality, the total RMSE (m) of each geometrically-rectified aerial photograph mosaics is given in Table B–1.

River-channel digitizing based on aerial photograph mosaics and DOQQs

Manual, on-screen digitization-based delineation of the river-channel banks was performed such that pointbars and areas of little to no vegetation near the river-water edge were considered to be within the river channel (i.e., such areas were included between the two respective bank boundaries). River banks were also included within the channel; thus, the delineated channels represent bank-full conditions. Digitizing progressed from an upstream-to-downstream direction (with right and left banks defined with respect to the downstream direction). The aerial photograph-based river-channel boundaries were used to augment the channel-boundary spatial-temporal coverage that was obtained from topographic maps, discussed below.

Geometric rectification/georeferencing of multitemporal topographic maps

We geometrically-rectified/georeferenced a series of multitemporal scanned/digital maps---topographic maps produced by U.S. Geological Survey (USGS) and tactical maps generated by the U.S. Army Corps of Engineers. The older historical maps were acquired in scanned, digital/digitized form from the University of Texas—Austin. A summary of the topographic maps employed for multitemporal LBR channel digitization, including their characteristics, such as the year of publication, the original map scale, and root-mean-squared error (RMSE) associated the geometric rectification/georeferencing step, is given in Table B–2. It should be noted that the older maps employed (i.e., 1910-1919) generally entail somewhat to markedly smaller scales (Table B–2).

River channel-boundary digitizing based on topographic maps

We then manually digitized the river-channel boundaries based on the georeferenced digital topographic maps. The methods utilized from map-based digitizing were similar to those used for aerial photography-based delineation.

Year-merging of multitemporal topographic maps

Since full topographic map (and/or aerial photography) coverage of the LBR study area was typically not afforded by the maps produced and available for a given year, we employed a year-merging rule, whereby topographic maps that were generated in a ~±2-year temporal envelope around a given map-production year were considered to be maps associated with that central year. (If the data supported it, a ±3-year temporal window could alternatively be considered.) Hence, maps within the specified temporal envelope were merged into that central year, meaning that the temporally-merged maps and the GIS products derived from those maps (e.g., river-channel polylines and polygons) were treated as being from the same year and processed together in subsequent analyses. In addition to the temporal envelope criterion, other criteria for year-merging included: observed minimal changes in map features (e.g., river-channel boundaries) between years; and that topographic map-derived channel boundaries are prioritized over aerial photo mosaic boundaries.

For this study, a summary of the years for which topographic maps and/or aerial photography is available is given below, including the years of data that were temporally merged, based on the rule noted above:

1910
1919
1943
1952, 1953, 1955 => 1953
1958, 1959, 1960, 1961, 1962 => 1960
1970, 1971, 1972 => 1971
1977
1979, 1980, 1981 => 1980
1983
1988, 1989 => 1989
1996
2004
2010

The notation "<year>, <year>…<year> => <year>" given above denotes that the map/aerial photo years on the left were merged into to the year on the right. For example, the digitized river-channel polylines and polygons from 1979, 1980, and 1981 were merged into one "1980" vector data set. Note

that or the year 1983, all maps entailed partial coverage with respect to the floodplain sections, so 1983 maps and derived GIS products were not used in this analysis. Additionally note that DOQQs were available for the entire LBR study area/reach for 1996, 2004, and 2010, and additional DOQQ image base maps are available for other recent years. Table B–3 includes an accounting of the years of available data for the LBR study area and these year-merging details, as well as types of data available by floodplain section, including the degree of spatial coverage within a given section (i.e., partial or full coverage).

Table B–1. Summary of total root-mean-square error (RMSE) (m) and resultant cell sizes (m) of geometrically-rectified multitemporal aerial photograph mosaics, by avulsion-relevant site and by year of available historical aerial photographs of acceptable quality and scale. The number of ground control points (GCPs) used in the geometric rectification of the digital aerial photograph mosaics is also indicated. The aerial photograph mosaics were geometrically rectified to a 1996 false-color infrared (CIR) digital orthophoto quarter-quadrangle (DOQQ) image base, produced by the United States Geological Survey (USGS) (pixel size = 1 m; coordinate system = UTM, Zone 14 North; horizontal datum = NAD83). Note that avulsion-relevant sites 2 and 3 are covered by the same image mosaic, for each year studied.

Avulsion Site	Year	# of GCPs	RMSE (m)	Cell Size (m)
1	1953	20	3.85	4.38
1	1977	30	6.77	5.08
1	1989	20	6.72	3.68
2_3	1953	15	2.29	4.38
2_3	1977	13	4.18	5.08
4	1953, Subset 1	20	3.38	4.38
4	1953, Subset 2	14	3.33	4.38
4	1953, Subset 3	16	2.95	4.38
4	1977, Subset 1	20	2.76	5.08
4	1977, Subset 2	20	4.31	5.08
4	1981, Subset 1	20	2.68	5.08
4	1981, Subset 2	21	2.44	5.08
4	1981, Subset 3	19	3.44	5.08
5	1977	15	6.94	0.86
5	1981	15	2.53	5.08
6	1953	10	2.97	0.86
6	1968	12	4.65	2.03
6	1983	20	1.92	3.68
7	1977	15	3.73	5.08
7	1983	15	2.37	3.68
8	1979	20	1.57	4.21
8	1989	18	1.42	3.68

Table B–2. Summary of (scanned, digitial) topographic/tactical maps employed for multitemporal LBR channel-boundary digitization that were geometric rectified/georeferenced; for each map, the year, root-mean-squared error (RMSE), output/resultant cell size, and the original map scale are given.

Quadrangle	Year	RMSE (m)	Cell Size (m)	Scale
Millican	1910	7.68793	4.135329	1:31,680
Washington	1910	8.06921	3.820025	1:24,000
Sugar Land	1915	6.85754	7.927469	1:62,500
Wallis	1919	3.6755	8.223965	1:62,500
Brazoria	1952	9.91585	3.770247	1:24,000
East Columbia	1952	7.26818	3.778383	1:24,000
Otey	1953	12.26682	3.739242	1:24,000
Thompsons	1953	7.63608	3.739093	1:24,000
Richmond	1955	13.89409	7.549246	1:62,500
Sugar Land	1955	13.41845	7.589328	1:62,500
Courtney	1958	8.7429	3.771335	1:24,000
Washington	1958	5.11311	3.725205	1:24,000
San Felipe	1960	9.90045	3.746617	1:24,000
Sunny Side	1960	7.67273	3.747572	1:24,000
Wallis	1960	10.57424	3.758238	1:24,000
Burleigh	1961	7.21996	3.761884	1:24,000
Daniels	1961	9.52536	3.766284	1:24,000
Hempstead	1961	5.77078	3.749392	1:24,000
Howth	1961	7.05893	3.754091	1:24,000
Buckhorn	1962	10.91891	3.780074	1:24,000
Lake Jackson	1963	7.44645	3.762331	1:24,000
Missouri City	1970	7.46047	3.742714	1:24,000
Sugar Land	1970	9.84137	3.736746	1:24,000
Fulshear	1971	4.54351	3.762421	1:24,000
Orchard	1971	12.44207	3.772114	1:24,000
Richmond	1971	10.24181	3.76379	1:24,000
Brazoria	1972	7.90291	3.791043	1:24,000
Lake Jackson	1974	5.23692	3.76128	1:24,000
Howth	1979	8.43488	3.7698	1:24,000
East Columbia	1980	7.80508	3.794523	1:24,000
Fulshear	1980	11.75756	3.788573	1:24,000
Hempstead	1980	6.08777	3.753487	1:24,000
Missouri City	1980	10.00287	3.747266	1:24,000
Orchard	1980	9.32714	3.755078	1:24,000

Table B–2 (cont'd). Summary of (scanned, digitial) topographic/tactical maps employed for multitemporal LBR channel-boundary digitization that were geometric rectified/georeferenced; for each map, the year, root-mean-squared error (RMSE), output/resultant cell size, and the original map scale are given.

Quadrangle	Year	RMSE (m)	Cell Size (m)	Scale
Otey	1980	10.09818	3.788346	1:24,000
Richmond	1980	11.30885	3.746503	1:24,000
San Felipe	1980	10.02967	3.764992	1:24,000
Sugar Land	1980	8.19642	3.767104	1:24,000
Sunny Side	1980	9.37524	3.757735	1:24,000
Thompsons	1980	11.98805	3.759317	1:24,000
Wallis	1980	11.95516	3.748288	1:24,000
Burleigh	1981	7.42371	3.773389	1:24,000
Washington	1988	8.99985	3.743152	1:24,000
Buckhorn	1989	9.22304	3.773528	1:24,000
Courtney	1989	9.68762	3.773142	1:24,000
Daniels	1989	9.25286	3.774526	1:24,000
Missouri City	1995	8.35614	3.763623	1:24,000

Table B–3. Spatio-temporal data availability, by LBR floodplain section, TX, USA, 1910-2010. Years of available data and year-merging details (in column header parentheses) are noted, as are data types available, by floodplain section, including degree of spatial coverage per section (i.e., partial (denoted with (*P*) and gray shading, or full). *Topo* = topographic map; *AP* = aerial photo mosaic; *Topo,AP* (with blue shading) = both Topo and AP spatial coverage and were utilized; and *DOQQ* = digital orthophoto quarter-quadrangle. Light blue shading indicates that the given topo map coverage was not used.

Floodplain section	1910	1919	1943	1953 (52,53,55)	1960 (58,59,60,61,62)	1971 (70,71,72)	1977	1980 (79,80,81)	1983	1989 (88,89)	1995	1996	2004	2010
1										Topo		DOQQ(P)	DOQQ(P)	DOQQ(P)
2					Topo(P)	Topo(P)		Topo(P)		Topo(P)		DOQQ	DOQQ	DOQQ
3					Topo	Topo		Topo				DOQQ	DOQQ	DOQQ
4					Topo	Topo		Topo				DOQQ	DOQQ	DOQQ
5					Topo	Topo		Topo				DOQQ	DOQQ	DOQQ
6					Topo	Topo(P)		Topo				DOQQ	DOQQ	DOQQ
7					Topo			Topo				DOQQ	DOQQ	DOQQ
8					Topo			Topo				DOQQ	DOQQ	DOQQ
9					Topo			Topo(P)		Topo(P)		DOQQ	DOQQ	DOQQ
10	Topo(P)				Topo			Topo(P)		Topo(P)		DOQQ	DOQQ	DOQQ
11	Topo				Topo			Topo		Topo(P)		DOQQ	DOQQ	DOQQ
12	Topo			AP(P)	Topo			Topo(P)		Topo(P)		DOQQ	DOQQ	DOQQ
13	Topo			AP	Topo		AP(P)			Topo		DOQQ	DOQQ	DOQQ
14	Topo			AP	Topo		AP			Topo		DOQQ	DOQQ	DOQQ
15	Topo	Topo(P)		AP	Topo		AP	Topo(P)		Topo,AP		DOQQ	DOQQ	DOQQ
16	Topo	Topo		AP	Topo		AP	Topo(P)		Topo,AP		DOQQ	DOQQ	DOQQ
17	Topo	Topo		AP	Topo		AP			Topo		DOQQ	DOQQ	DOQQ
18	Topo	Topo		AP	Topo		AP			Topo		DOQQ	DOQQ	DOQQ
19	Topo(P)	Topo		AP	Topo		AP			Topo		DOQQ	DOQQ	DOQQ
20		Topo		AP	Topo		AP			Topo		DOQQ	DOQQ	DOQQ
21		Topo		AP	Topo		AP	Topo(P)		Topo(P)		DOQQ	DOQQ	DOQQ
22		Topo		AP	Topo		AP	Topo				DOQQ	DOQQ	DOQQ
23		Topo		AP	Topo		AP	Topo				DOQQ	DOQQ	DOQQ
24		Topo		AP	Topo		AP	Topo				DOQQ	DOQQ	DOQQ
25		Topo		AP	Topo		AP	Topo				DOQQ	DOQQ	DOQQ
26		Topo		AP	Topo		AP	Topo				DOQQ	DOQQ	DOQQ
27		Topo		AP(P)	Topo		AP	Topo			Topo(P)	DOQQ	DOQQ	DOQQ
28		Topo			Topo		AP(P)	Topo			Topo	DOQQ	DOQQ	DOQQ
29		Topo			Topo			Topo			Topo	DOQQ	DOQQ	DOQQ

Table B–3. (cont'd) Spatio-temporal data availability, by LBR floodplain section, TX, USA, 1910-2010. Years of available data and year-merging details (in column header parentheses) are noted, as are data types available, by floodplain section, including degree of spatial coverage per section (i.e., partial (denoted with (*P*) and gray shading, or full). *Topo* = topographic map; *AP* = aerial photo mosaic; *Topo,AP* (with blue shading) = both Topo and AP spatial coverage and were utilized; and *DOQQ* = digital orthophoto quarter-quadrangle. Light blue shading indicates that the given topo map coverage was not used.

Floodplain section	1910	1919	1943	1953 (52,53,55)	1960 (58,59,60,61,62)	1971 (70,71,72)	1977	1980 (79,80,81)	1983	1989 (88,89)	1995	1996	2004	2010
30		Topo			Topo			Topo			Topo	DOQQ	DOQQ	DOQQ
31		Topo(P)		Topo(P)	Topo(P)	Topo(P)		Topo			Topo(P)	DOQQ	DOQQ	DOQQ
32				Topo		Topo		Topo				DOQQ	DOQQ	DOQQ
33				Topo		Topo		Topo				DOQQ	DOQQ	DOQQ
34				Topo		Topo		Topo				DOQQ	DOQQ	DOQQ
35				Topo		Topo		Topo				DOQQ	DOQQ	DOQQ
36				Topo		Topo		Topo				DOQQ	DOQQ	DOQQ
37				Topo		Topo		Topo	AP(P)			DOQQ	DOQQ	DOQQ
38				Topo		Topo		Topo				DOQQ	DOQQ	DOQQ
39				Topo		Topo		Topo				DOQQ	DOQQ	DOQQ
40				Topo		Topo		Topo				DOQQ	DOQQ	DOQQ
41				Topo		Topo(P)		Topo				DOQQ	DOQQ	DOQQ
42				Topo				Topo				DOQQ	DOQQ	DOQQ
43				Topo				Topo				DOQQ	DOQQ	DOQQ
44				Topo				Topo				DOQQ	DOQQ	DOQQ
45				Topo				Topo				DOQQ	DOQQ	DOQQ
46				Topo			AP(P)	Topo	AP(P)			DOQQ	DOQQ	DOQQ
47				Topo			AP(P)	Topo	AP(P)			DOQQ	DOQQ	DOQQ
48				Topo				Topo				DOQQ	DOQQ	DOQQ
49				Topo				Topo				DOQQ	DOQQ	DOQQ
50				Topo		Topo(P)		Topo(P)				DOQQ	DOQQ	DOQQ
51				Topo		Topo		AP(P)		AP(P)		DOQQ	DOQQ	DOQQ
52			Topo(P)	Topo(P)		Topo(P)		AP		AP		DOQQ	DOQQ	DOQQ
53			Topo					AP(P)		AP(P)		DOQQ	DOQQ	DOQQ
54			Topo									DOQQ	DOQQ	DOQQ
55			Topo									DOQQ	DOQQ	DOQQ
56			Topo									DOQQ	DOQQ	DOQQ
57			Topo(P)									DOQQ(P)	DOQQ(P)	DOQQ(P)

REFERENCES

RSI (Research Systems, Inc.), ENVI User's Guide. ENVI Vers. 4.1. 2004, Boulder, CO: RSI.

APPENDIX C:
HISTORICAL CHANNEL CHANGES ON THE LBR FOR THE PERIOD 1910–2010

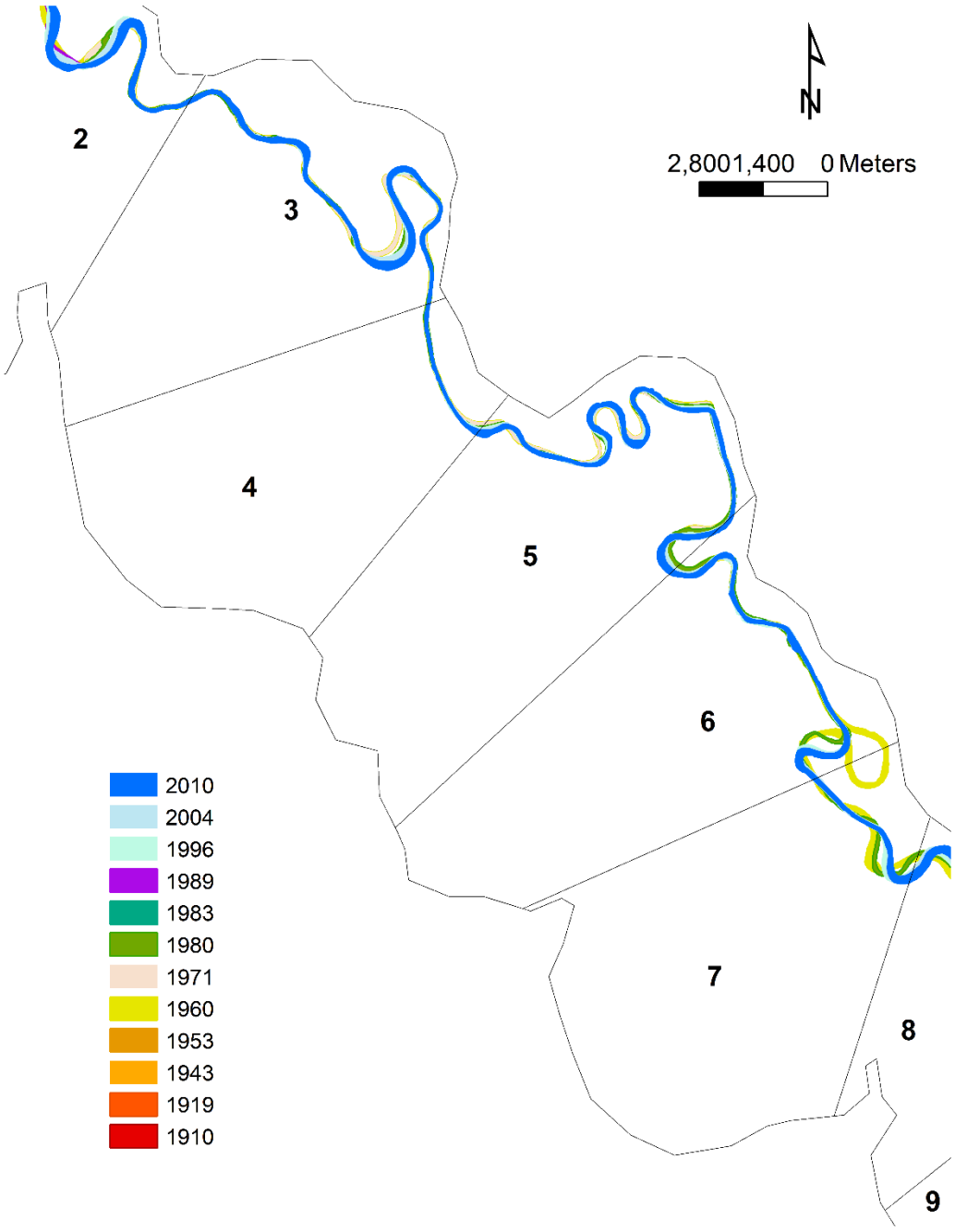

Figure C–1. Multitemporal river-channel planforms from various years, LBR, focused on floodplain sections 1–7.

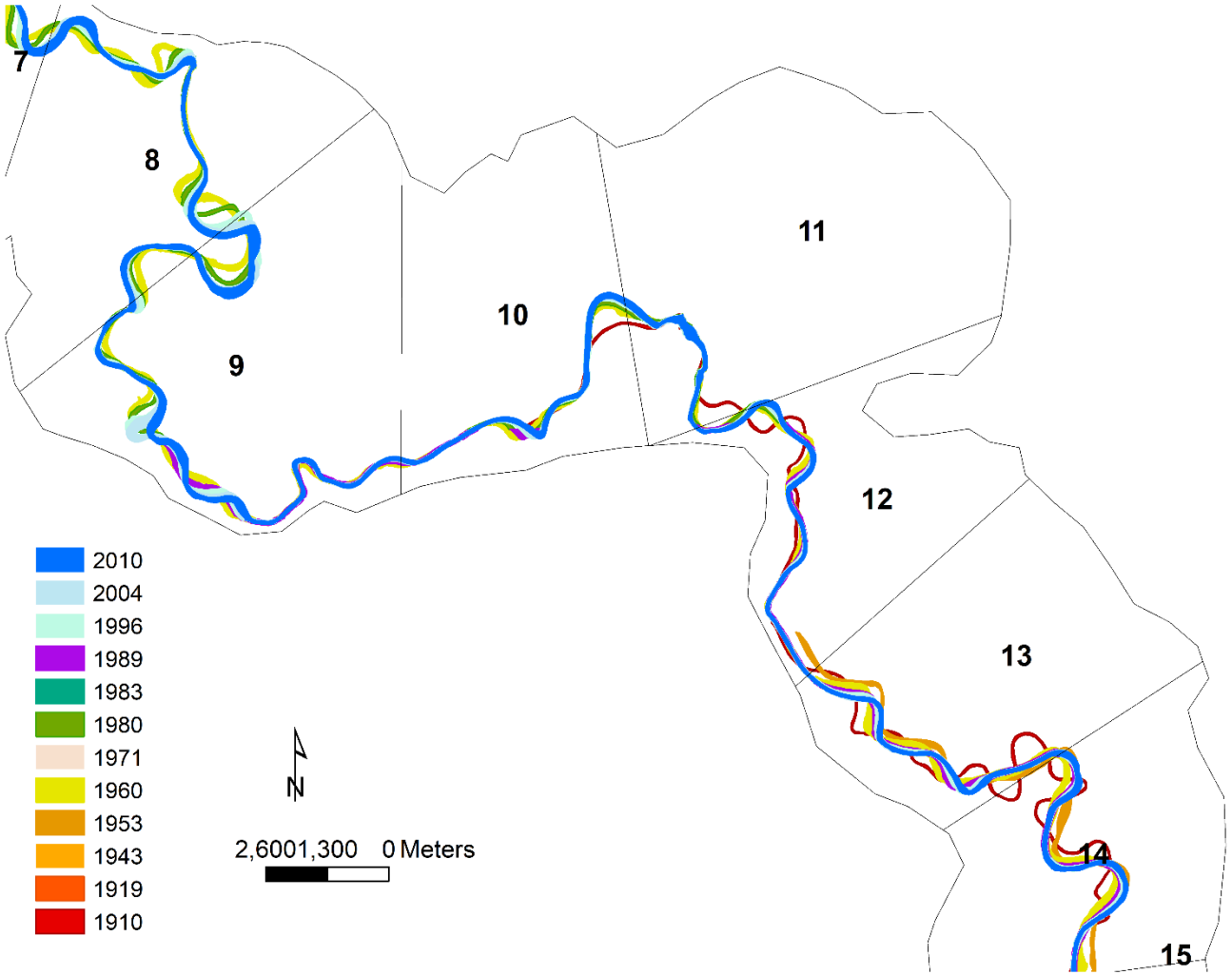

Figure C–2. Multitemporal river-channel planforms from various years, LBR, focused on floodplain sections 8–15.

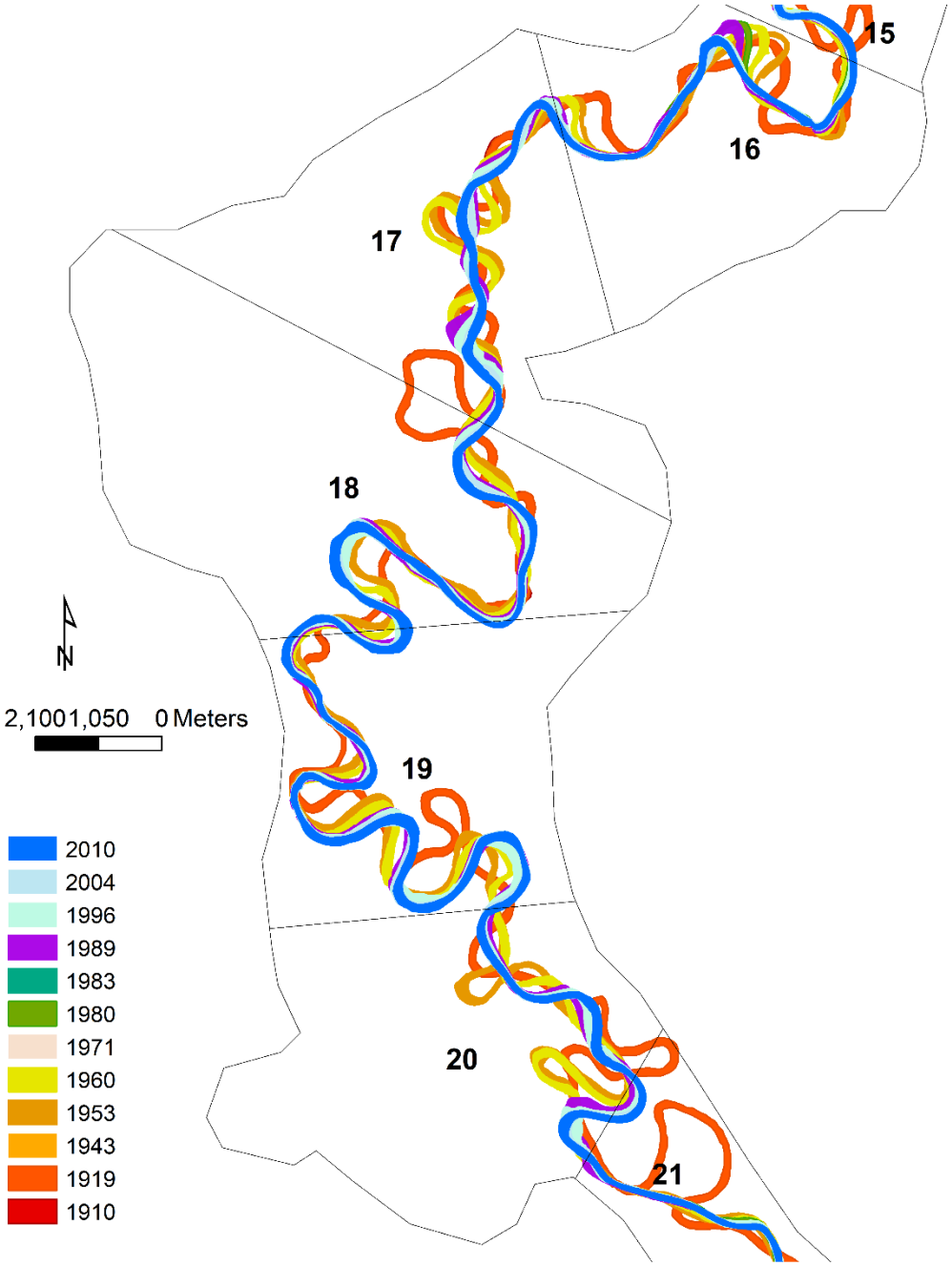

Figure C–3. Multitemporal river-channel planforms from various years, LBR, focused on floodplain sections 18–20.

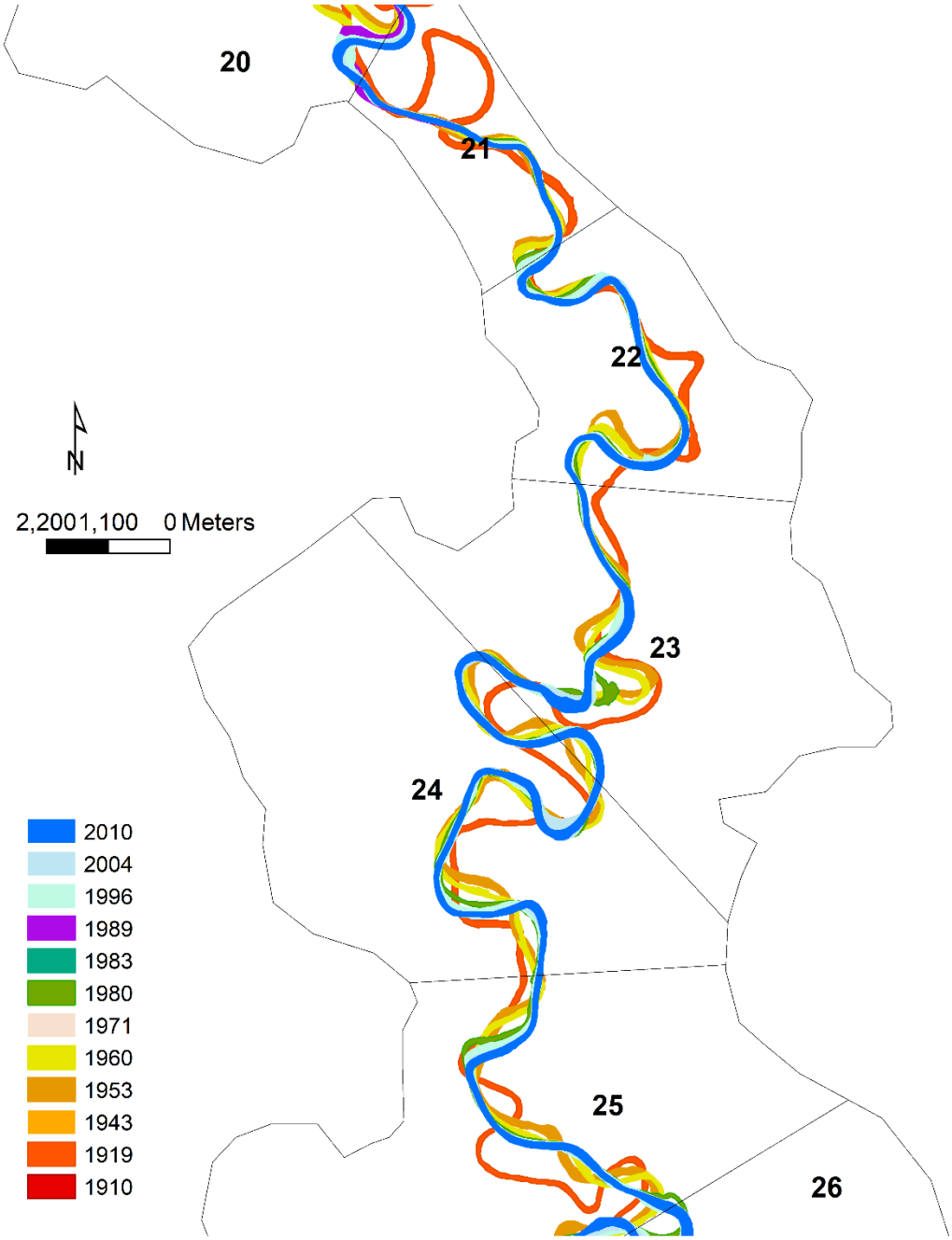

Figure C–4. Multitemporal river-channel planforms from various years, LBR, focused on floodplain sections 21-25.

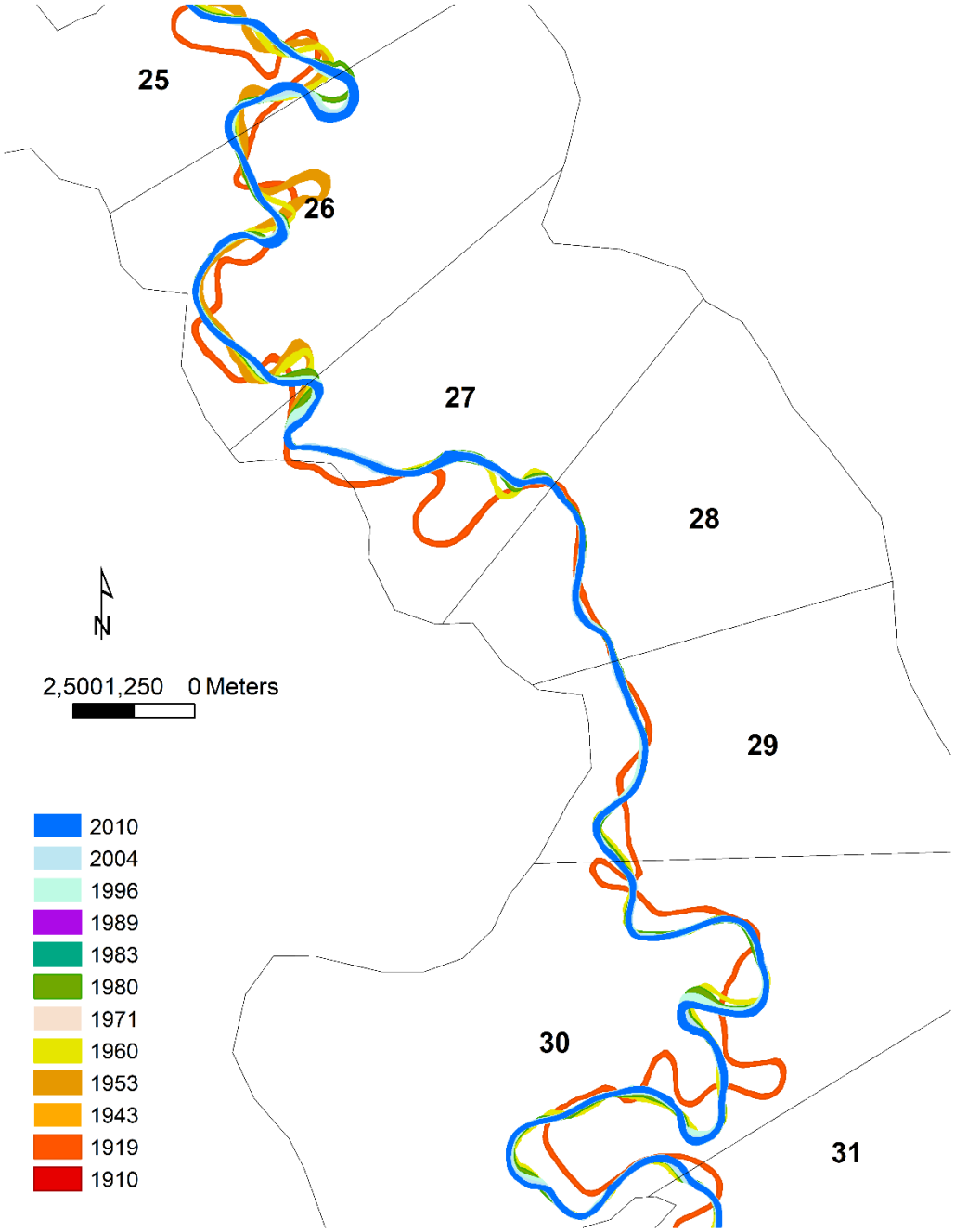

Figure C–5. Multitemporal river-channel planforms from various years, LBR, focused on floodplain sections 26-30.

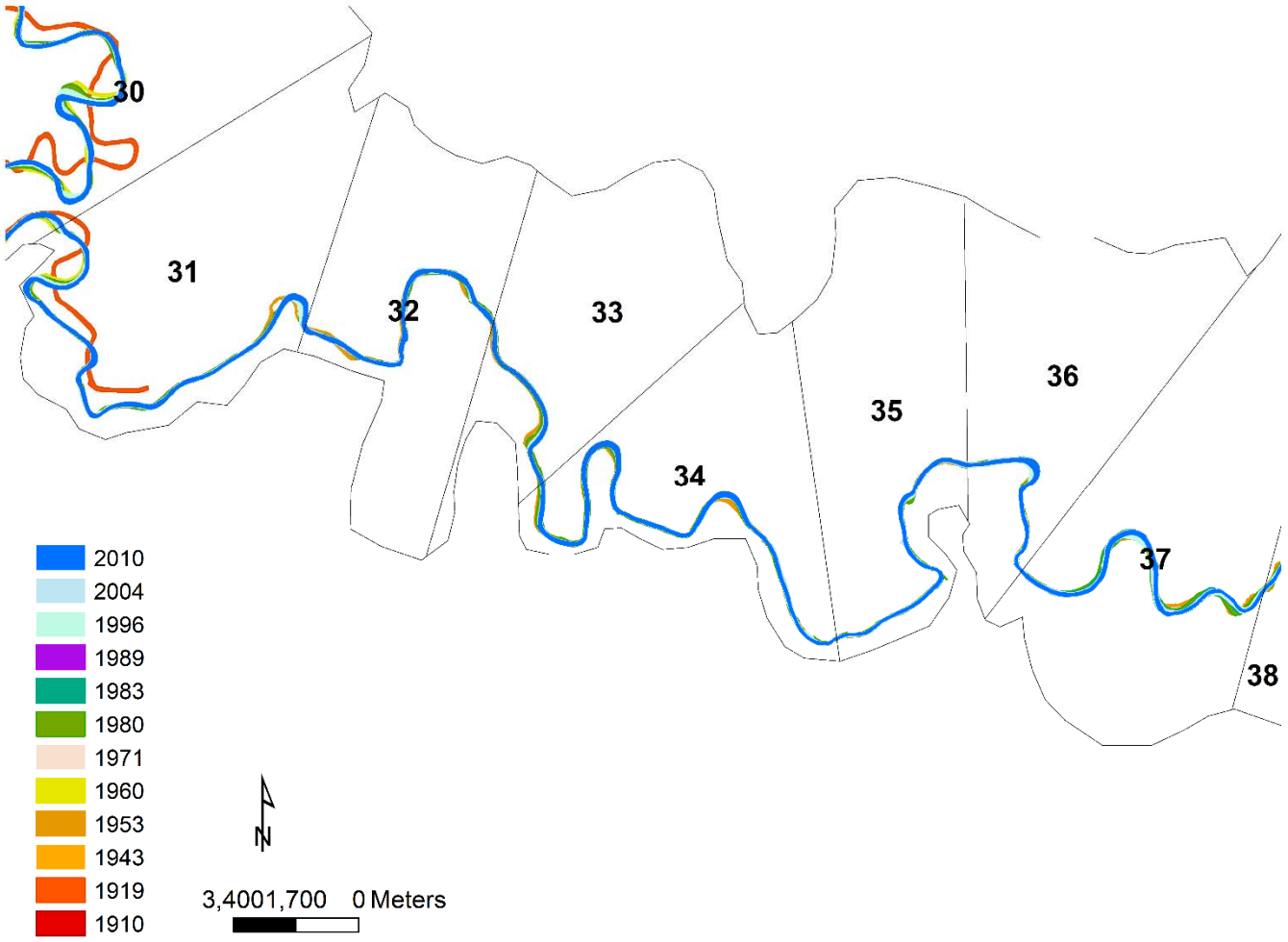

Figure C–6. Multitemporal river-channel planforms from various years, LBR, focused on floodplain sections 31-37.

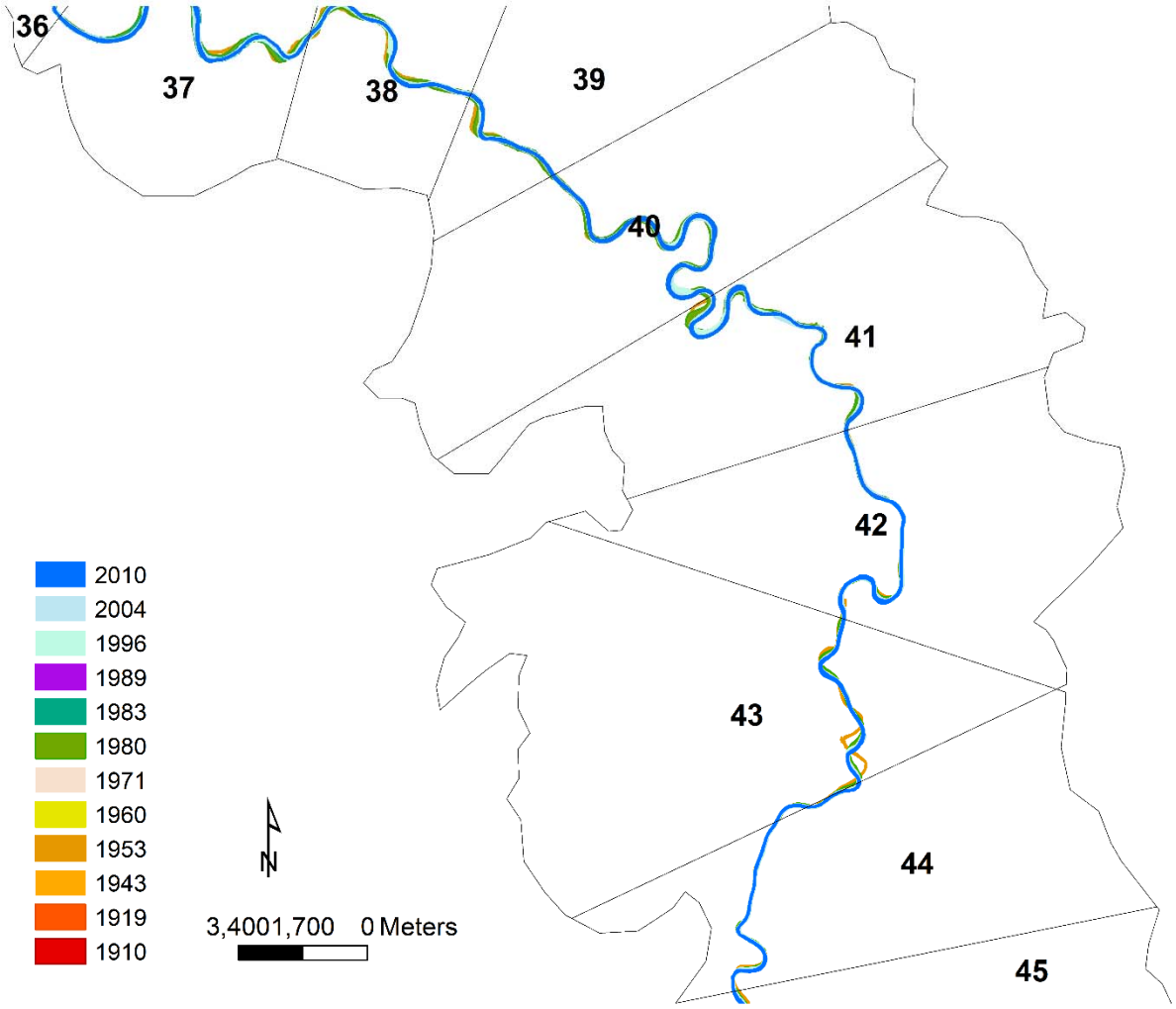

Figure C–7. Multitemporal river-channel planforms from various years, LBR, focused on floodplain sections 38-44.

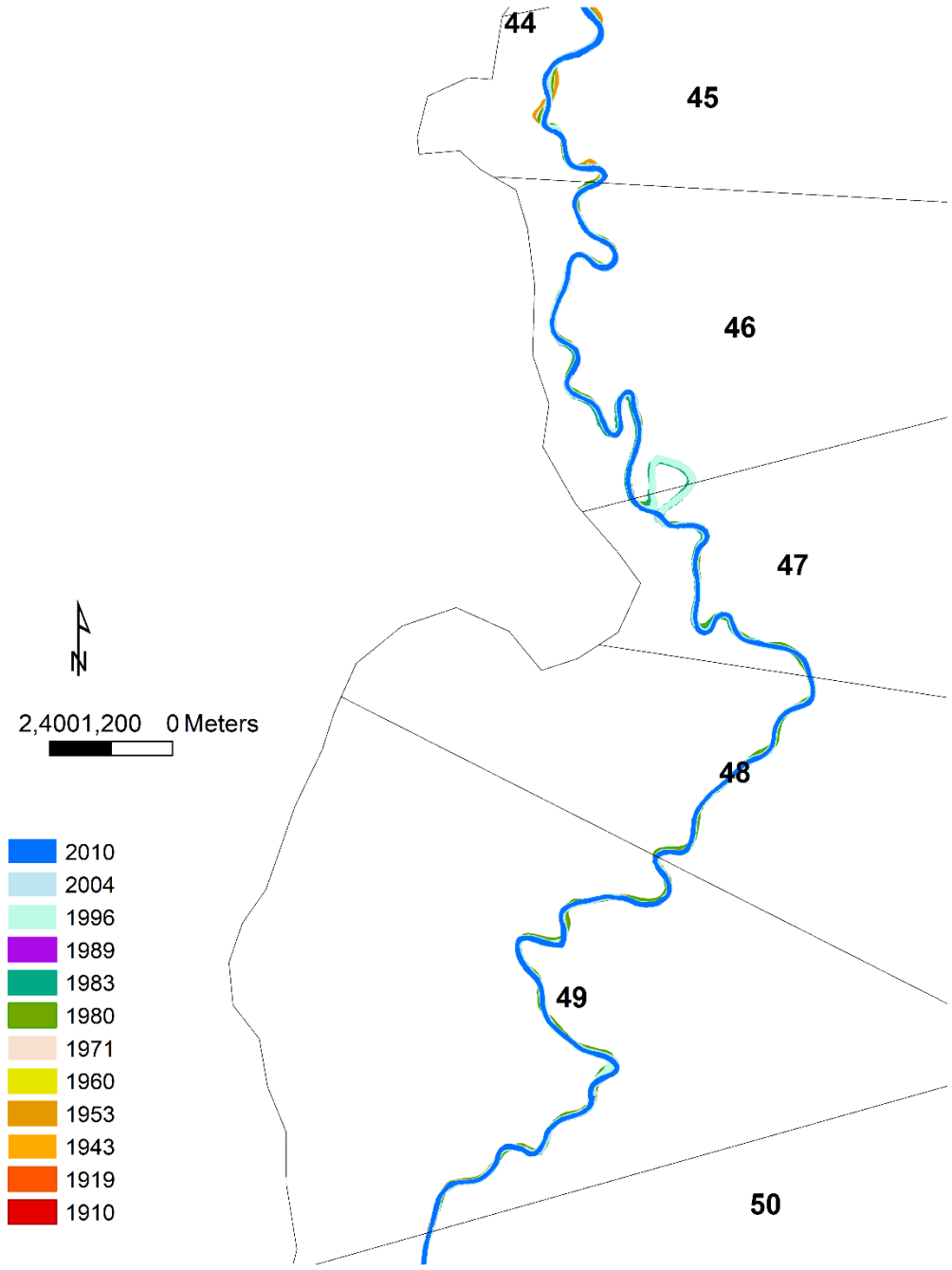

Figure C–8. Multitemporal river-channel planforms from various years, LBR, focused on floodplain sections 45-49.

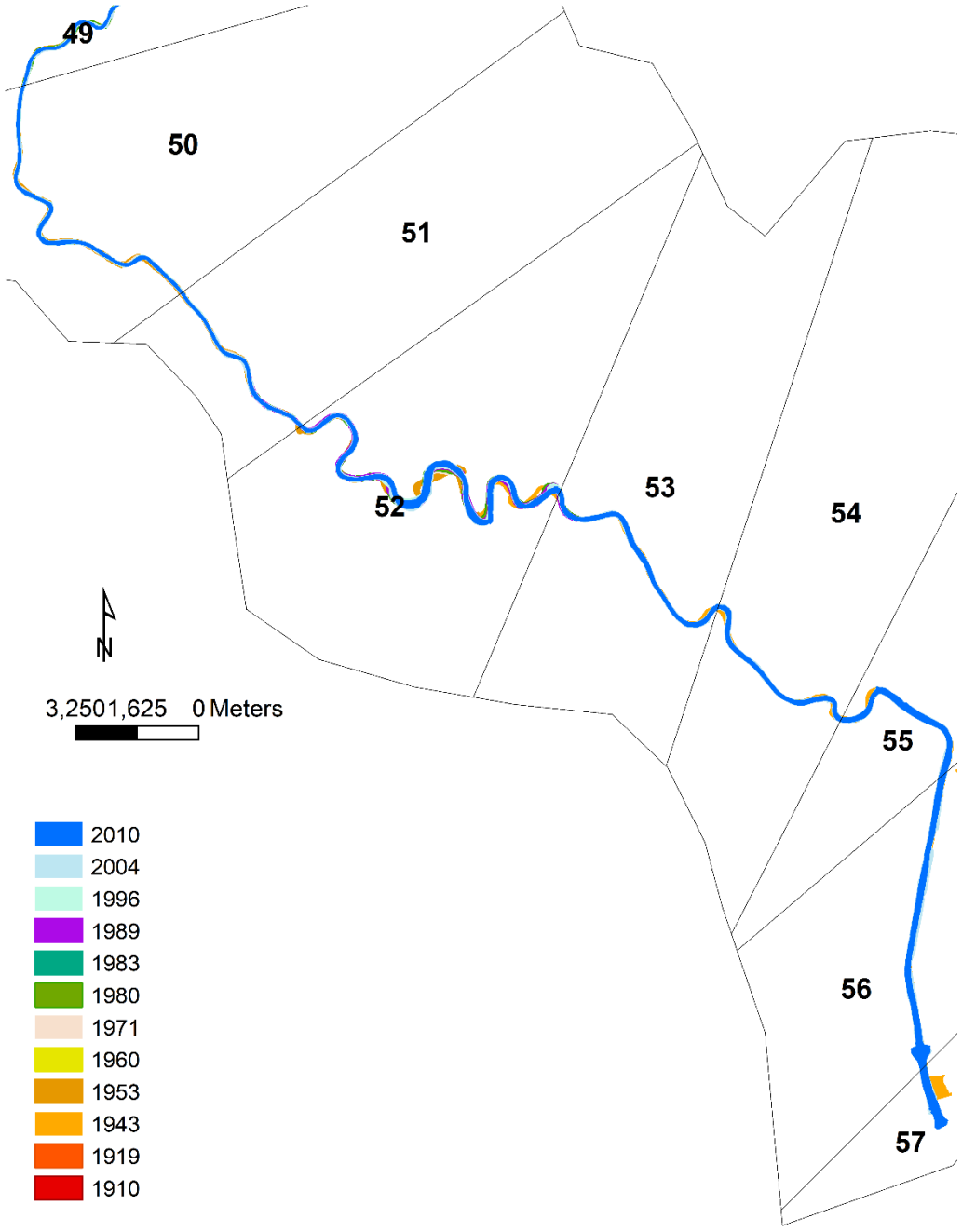

Figure C–9. Multitemporal river-channel planforms from various years, LBR, focused on floodplain sections 50-56.